ORNL/TM-2017/038

X-ray Analysis of Defects and Anomalies in AGR-5/6/7 TRISO Particles

Grant W. Helmreich
John D. Hunn
Darren J. Skitt
John A. Dyer
Austin T. Schumacher

June 2017

OAK RIDGE NATIONAL LABORATORY
MANAGED BY UT-BATTELLE FOR THE US DEPARTMENT OF ENERGY

ORNL/TM-2017/038

Fusion and Materials for Nuclear Systems Division

X-RAY ANALYSIS OF DEFECTS AND ANOMALIES IN AGR-5/6/7 TRISO PARTICLES

BWXT Coater Batches 93164 – 93172

Grant W. Helmreich
John D. Hunn
Darren J. Skitt
John A. Dyer
Austin T. Schumacher

Date Published: June 2017

Work sponsored by
US DEPARTMENT OF ENERGY
Office of Nuclear Energy
under the
Advanced Gas Reactor Fuel Development and Qualification Program

Prepared by
OAK RIDGE NATIONAL LABORATORY
Oak Ridge, TN 37831-6283
managed by
UT-BATTELLE, LLC
for the
US DEPARTMENT OF ENERGY
under contract DE-AC05-00OR22725

CONTENTS

LIST OF FIGURES

LIST OF TABLES

ACRONYMS

AGR	Advanced Gas Reactor (Fuel Development and Qualification Program)
AGR-5/6/7	Fifth/Sixth/Seventh AGR program irradiation experiments
ATR	Advanced Test Reactor
BWXT	BWX Technologies
CVD	Chemical vapor deposition
DAM	Data Acquisition Method
INL	Idaho National Laboratory
IPyC	Inner pyrolytic carbon (TRISO layer)
OPyC	Outer pyrolytic carbon (TRISO layer)
ORNL	Oak Ridge National Laboratory
PIP	Product Inspection Plan
QC	Quality control
SiC	Silicon carbide (TRISO layer)
SOG	Standard Operating Guideline
TRISO	Tristructural-isotropic (coated particles)
UCO	Uranium carbide/uranium oxide mixture (fuel kernels)
XRT	X-ray tomography

ACKNOWLEDGMENTS

This work was sponsored by the U.S. Department of Energy, Office of Nuclear Energy, through the Idaho National Laboratory Advanced Reactor Technologies Technology Development Office as part of the Advanced Gas Reactor Fuel Development and Qualification Program.

1. INTRODUCTION

Coated particle fuel batches J52O-16-93164, 93165, 93166, 93168, 93169, 93170, and 93172 were produced by Babcock and Wilcox Technologies (BWXT) for possible selection as fuel for the Advanced Gas Reactor Fuel Development and Qualification (AGR) Program's AGR-5/6/7 irradiation test in the Idaho National Laboratory (INL) Advanced Test Reactor (ATR), or may be used for other tests. Each batch was coated in a 150-mm-diameter production-scale fluidized-bed chemical vapor deposition (CVD) furnace. Tristructural isotropic (TRISO) coatings were deposited on 425-µm-nominal-diameter spherical kernels from BWXT lot J52R-16-69317 containing a mixture of 15.4%-enriched uranium carbide and uranium oxide (UCO), with the exception of Batch 93164, which used similar kernels from BWXT lot J52L-16-69316. The TRISO-coatings consisted of a ~50% dense carbon buffer layer with 100-µm-nominal thickness, a dense inner pyrolytic carbon (IPyC) layer with 40-µm-nominal thickness, a silicon carbide (SiC) layer with 35-µm-nominal thickness, and a dense outer pyrolytic carbon (OPyC) layer with 40-µm-nominal thickness. Each coated particle batch was sieved to upgrade the particles by removing over-sized and under-sized material, and the upgraded batch was designated by appending the letter A to the end of the batch number (e.g., 93164A). Secondary upgrading by sieving was performed on the upgraded batches to remove specific anomalies identified during analysis for Defective IPyC, and the upgraded batches were designated by appending the letter B to the end of the batch number (e.g., 93165B). Following this secondary upgrading, coated particle composite J52R-16-98005 was produced by BWXT as fuel for the AGR Program's AGR-5/6/7 irradiation test in the INL ATR. This composite was comprised of coated particle fuel batches J52O-16-93165B, 93168B, 93169B, and 93170B.

Samples riffled from each upgraded TRISO batch were shipped to the Oak Ridge National Laboratory (ORNL) for quality control (QC) acceptance testing and analysis. The procedures for the characterization and qualification of the particles performed at ORNL are outlined in the ORNL Product Inspection Plan for AGR-5/6/7 Coated Particle (AGR-CHAR-PIP-28, Hunn 2016). The fraction of particles with Defective IPyC was determined for two subsamples riffled from each TRISO sample. The ORNL Data Acquisition Method for Counting of TRISO Particles with Excessive Uranium Dispersion Inside SiC (AGR-CHAR-DAM-47, Hunn 2013), provides the detailed procedures and requirements for the analysis that was performed to determine the Defective IPyC fraction. Summaries of the Defective IPyC fractions measured for each batch [Hunn et al. 2017a, Hunn et al. 2017b] and in the final composite [Helmreich et al. 2017] are discussed in separate reports.

Additional analyses of the x-ray images obtained for determination of the Defective IPyC fraction were performed to identify and quantify any other obvious microstructural anomalies in the TRISO-coated particle samples. Details about these anomalies and additional images acquired by high-resolution x-ray tomography to further characterize them, as well as the uranium dispersion in the particles with Defective IPyC, are discussed in this report.

2. DEFECTIVE IPYC AND URANIUM DISPERSION

Particles with Defective IPyC are defined in the AGR-5/6/7 Fuel Specification (Marshall 2016). Several variable properties of the IPyC layer are controlled by this specification (e.g. thickness, density, and anisotropy); however, Defective IPyC is defined specifically to control particles with excessively permeable IPyC as an attribute property. Excessively permeable IPyC is of concern for reactor operation due to the potential for heavy metal dispersion in the IPyC (Petti et al. 2004, Hanson 2009). Since the permeability of the IPyC layer is difficult to measure directly, the fuel specification prescribes counting of particles with Defective IPyC based on the presence of excessive uranium dispersion into or through the buffer, where excessive dispersion is determined based on a visual standard (Scheffel and Saurwein 2003). Gaseous HCl, a byproduct of the chemical vapor deposition process used for the SiC layer, can infiltrate through permeable IPyC into the buffer region during the initial stages of SiC deposition. Once HCl infiltrates the buffer layer, it can react with the kernel to disperse uranium into the coating layers, particularly when particles are heated to 1800°C during the compact manufacturing process. While particles with Defective IPyC may generally be identified by the presence of uranium dispersion, there are other particle anomalies which may also result in uranium dispersion unrelated to the quality of the IPyC layer, such as secondary kernel fragments embedding in the buffer layer. Particles with embedded kernel fragments were observed in the AGR-5/6/7 TRISO particle batches as discussed below.

Identification of particles with Defective IPyC was completed as described in DAM-47 using the visual standard for the degree of uranium dispersion that signifies a Defective IPyC layer that is provided in the AGR-5/6/7 Fuel Specification. This procedure uses low-resolution radiographs, which are sufficient for basic defect identification but are of limited use for further analysis due to both their resolution and their nature as a singular two-dimensional projection of three-dimensional objects. Thus, high-resolution x-ray tomography (XRT) was used to better understand the morphology of particles with Defective IPyC. Individual particles identified by low-resolution radiography were selectively-removed from their Kapton tape bulk radiography mounts and transferred to 1-mm-diameter polyimide tubes for XRT. This method allowed for significantly higher throughput for the large number of particles that needed to be analyzed, compared to the typical single-particle mounts used for high-resolution x-ray tomography, at an acceptable cost of decreased image quality and increased reconstruction artifacts. Computed tomography datasets for each particle were acquired using an Xradia MicroXCT x-ray microtomography system according to the ORNL Standard Operating Guideline for the Xradia MicroXCT (ORNL-CHAR-SOG-22, Helmreich and Hunn 2017).

Uranium dispersion was observed in three general classifications. The first classification of uranium dispersion was particles in which uranium dispersed out from the kernel uniformly, terminating either partway through the buffer layer or at the buffer/IPyC interface. This type of uranium dispersion has been previously reported and is the basis of the visual standards used to determine if a particle should be deemed to have Defective IPyC [Marshall 2016, Scheffel and Saurwein 2003]. In some cases, soot inclusions were observed between the buffer and IPyC layers that were likely related to the apparent IPyC permeability, while in others there was no observable direct cause for the Defective IPyC. Of the 115 particles with uranium dispersion which were observed across all batches of material, 35 were of this type. Several examples of this uniform uranium dispersion into and through the buffer layer have been analyzed by XRT. Figure 2-1 shows a particle in which very minor uranium dispersion was observed in the buffer layer immediately adjacent to the kernel. Based on the visual standard in the AGR-5/6/7 Fuel Specification for the identification of particles with Defective IPyC using low-resolution radiography, this particle did not qualify as having excessive uranium dispersion, and thus was not counted as having Defective IPyC. Figure 2-2 shows a particle with uranium dispersed partially through the buffer, which met the visual standard for identification of Defective IPyC. Figure 2-3 and Figure 2-4 both show particles in which soot inclusions between the buffer and IPyC layers led to significant uranium

dispersion out to the buffer/IPyC interface. In Figure 2-3 a crack in the IPyC layer is evident adjacent to the primary soot inclusion, while in Figure 2-4 there is high-Z material diffused into the IPyC layer with a shape suggestive of a source from the outside of the IPyC layer. Note that in these tomographic cross-sections there are some reconstruction artifacts which give the false appearance of local image texture. These artifacts are a result of the inability of x-rays to penetrate the kernel and the limited number of projections which were acquired for each tomographic dataset.

Of the 35 particles with Defective IPyC identified as having this uniform uranium dispersion in and through the buffer layer, 10 featured uranium dispersion partially through the buffer and 25 featured uranium dispersion out to the buffer/IPyC interface. Of those 25, 16 had identifiable soot inclusions, while the remaining 9 may possibly have had soot inclusions which were not identifiable by low-resolution radiography.

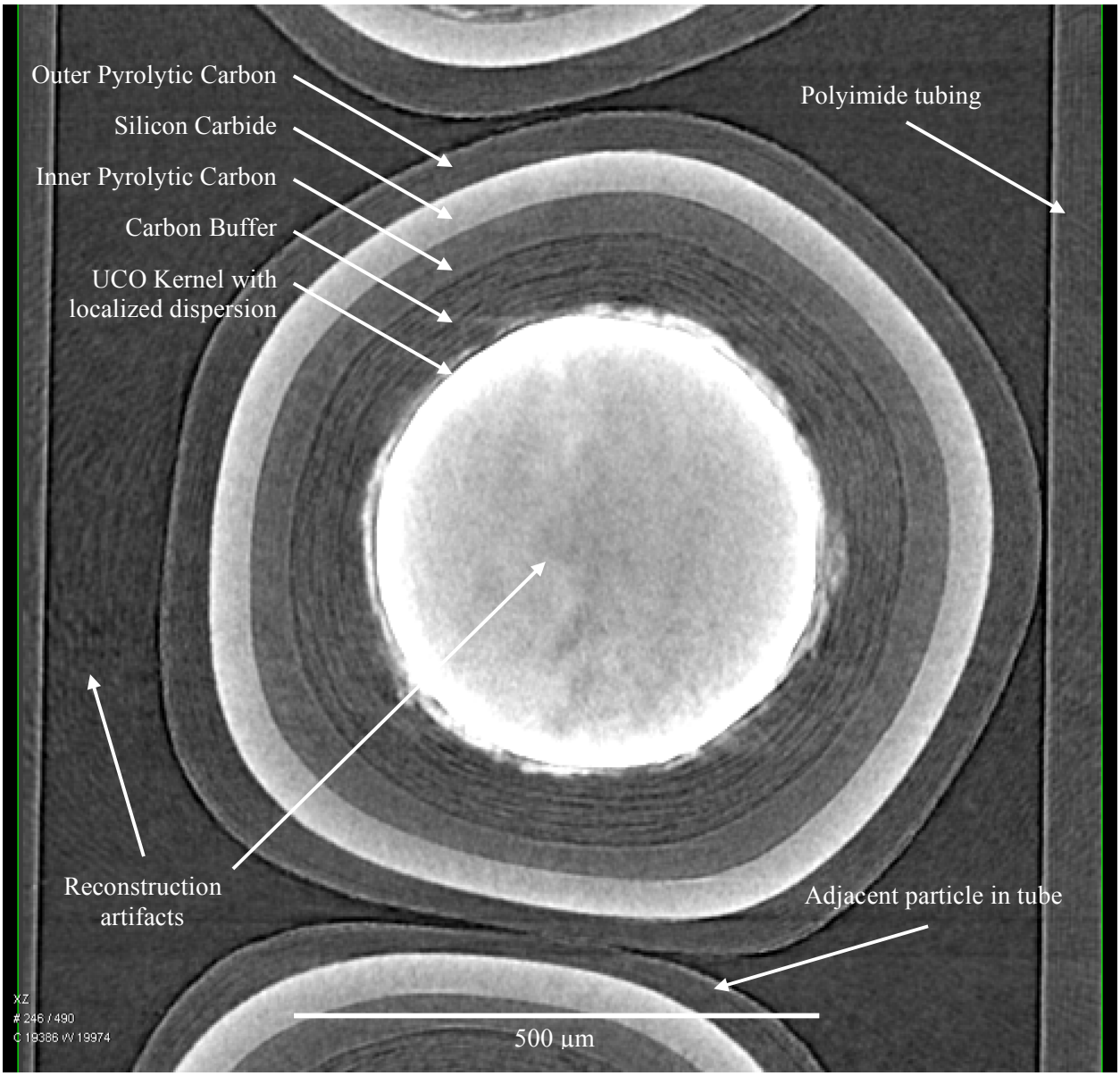

Figure 2-1. Tomographic cross-section of a particle with very minor uranium dispersion around the kernel. The radiograph of this particle was below the visual standard for identifying a particle as having Defective IPyC.

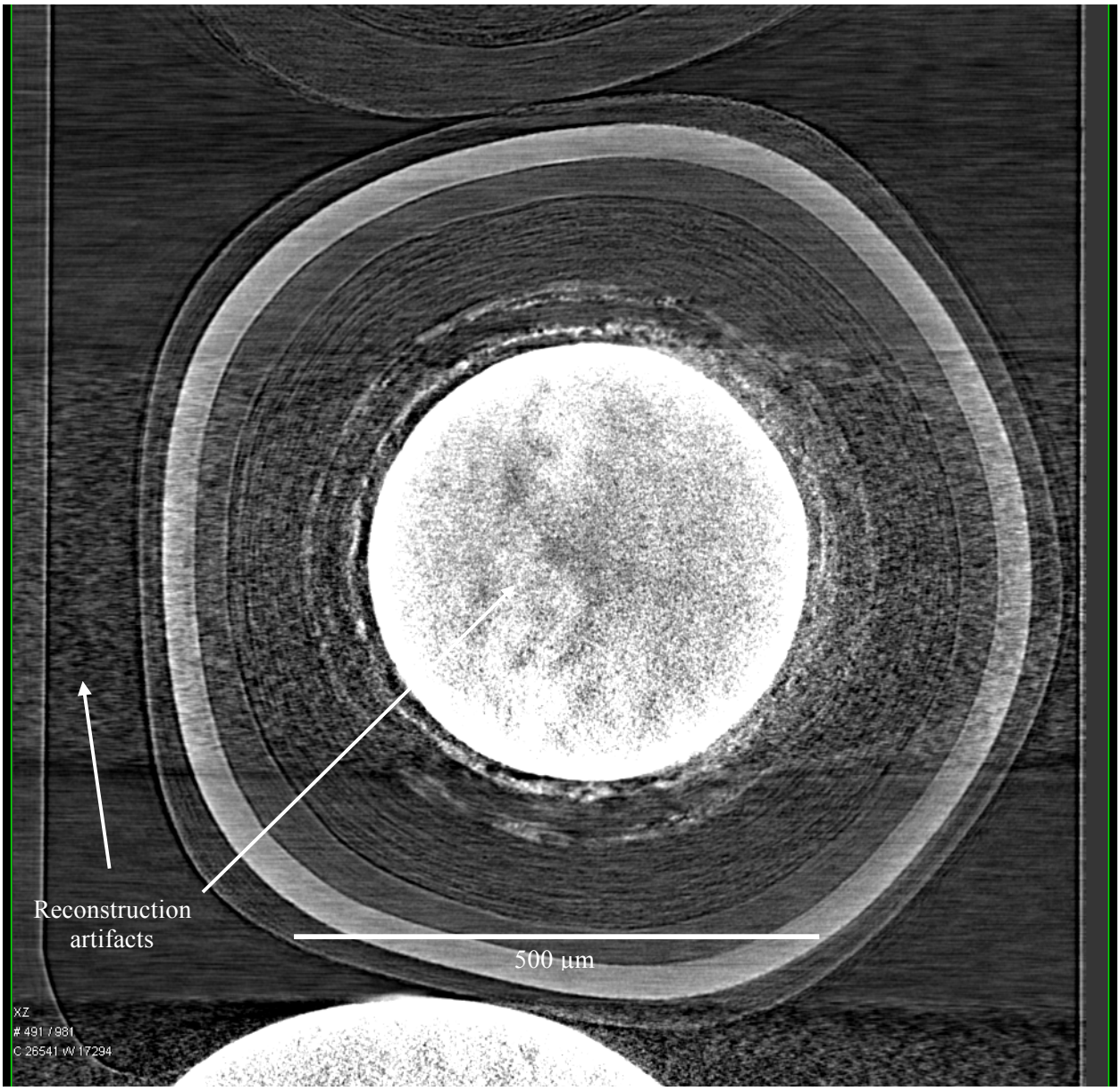

Figure 2-2. Tomographic cross-section of a particle with uranium dispersion diffused partway into the buffer layer.

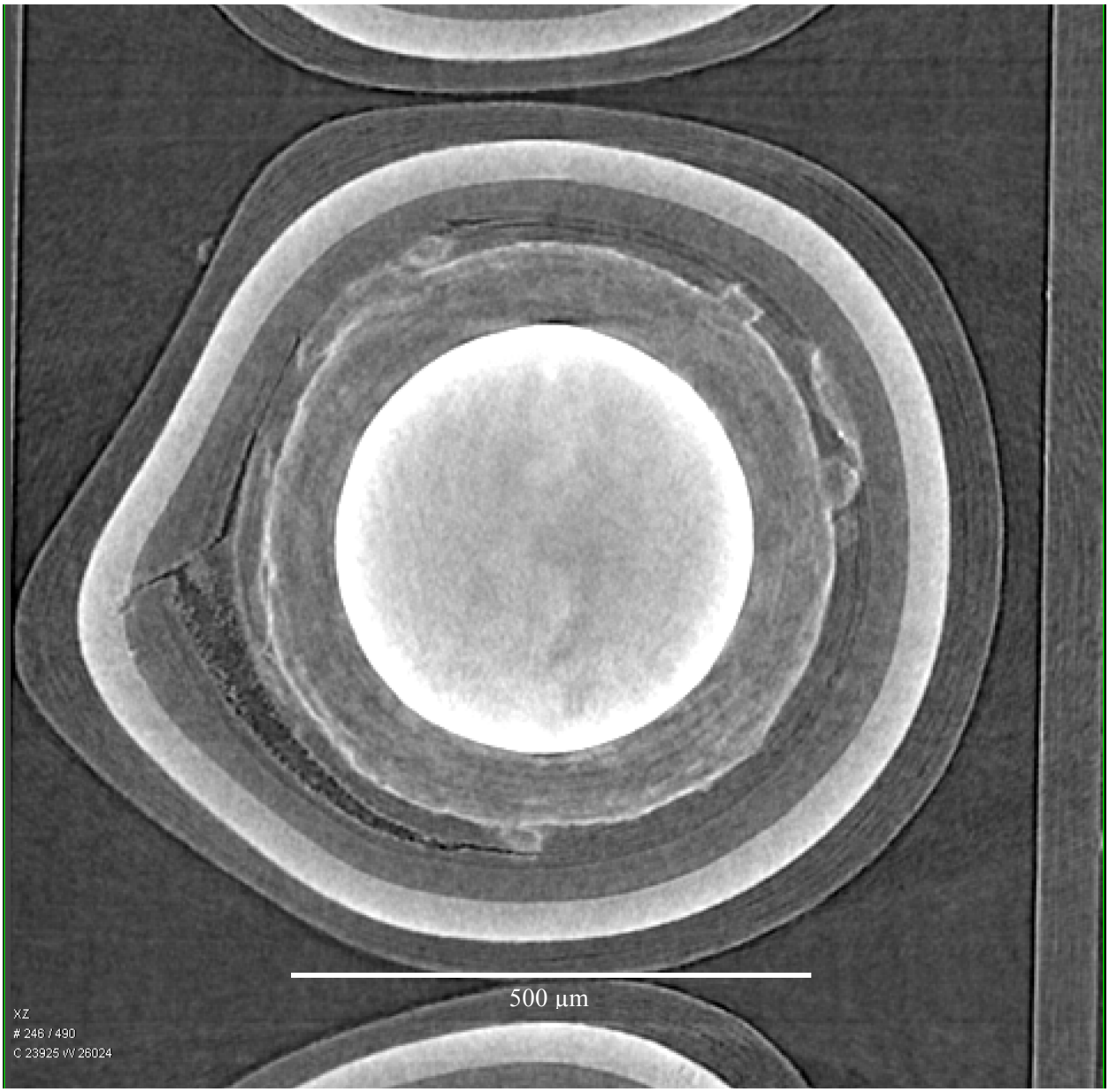

Figure 2-3. Tomographic cross-section of a particle with uranium dispersion caused by a soot inclusion between the buffer and IPyC layers. Note the crack through the IPyC layer adjoining the soot inclusion.

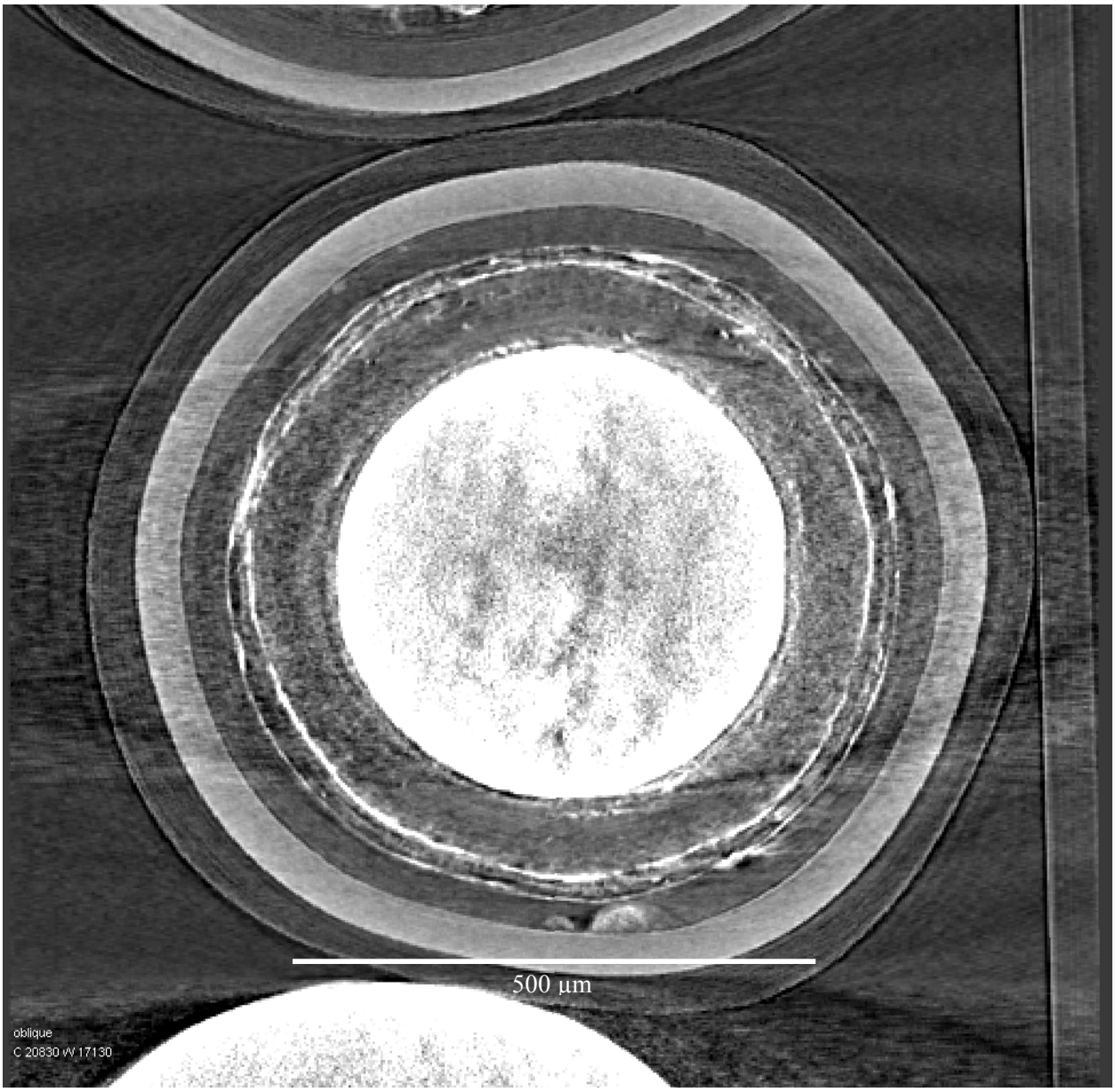

Figure 2-4. Tomographic cross-section of a particle with uranium dispersion caused by a soot inclusion between the buffer and IPyC layers. Note the high-Z material in the IPyC layer at the bottom of the particle.

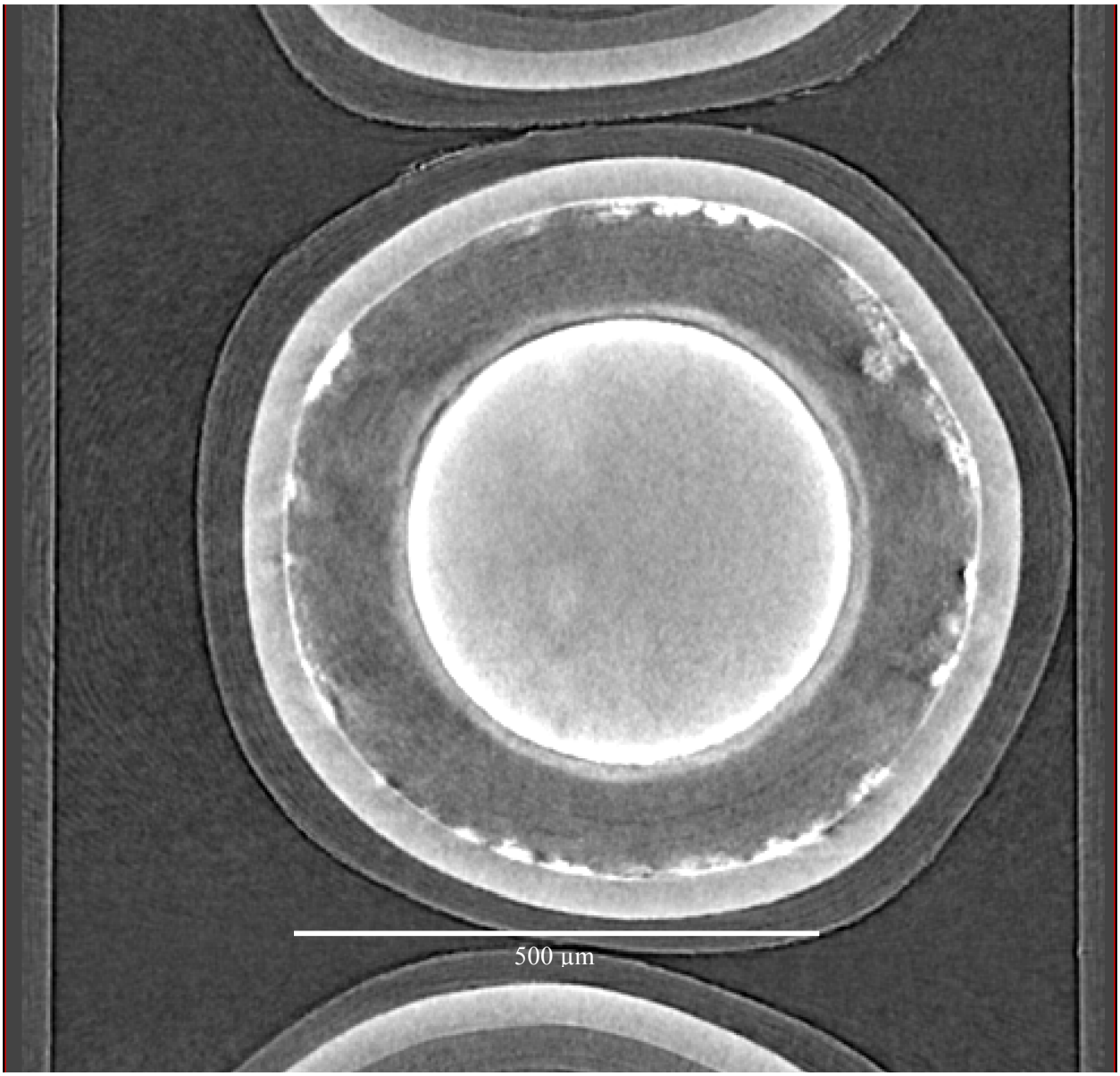

Figure 2-5. Tomographic cross-section of a particle without an IPyC layer and with uranium dispersion concentrated at the buffer/SiC interface.

The second classification of uranium dispersion was particles in which the IPyC layer was either missing or entirely compromised, resulting in uranium dispersion out to the inner edge of the SiC layer. Of the 115 particles with uranium dispersion which were observed across all batches of material, 27 were of this type. The missing IPyC layer on these particles was identified based on XRT, which showed no visually distinguishable IPyC layer and a layer thickness from the kernel/buffer interface to the inner edge of the SiC consistent with only an intervening buffer layer being present, as shown in Figure 2-5. This issue of missing IPyC layers on some particles was part of a larger observation of particles with either missing or extra layers, as is discussed in Section 4. Particles in this classification of uranium dispersion were counted as having Defective IPyC, since a missing or fully compromised IPyC layer will result in the unacceptable permeability which the Defective IPyC specification seeks to control.

Once some particles with missing IPyC were identified by XRT, further particles with missing IPyC were distinguishable from particles with uniform uranium dispersion to the buffer/IPyC interface based on low-resolution radiography. Figure 2-6 shows low-resolution radiographs for particles with uranium dispersion into the buffer or to the buffer/IPyC interface. In both cases a dark ring corresponding to the IPyC is distinguishable between the bright uranium dispersion and bright SiC layer. In contrast, Figure 2-7 shows low-resolution radiographs for particles with uranium dispersion all the way to the SiC layer, which has been confirmed by high-resolution XRT to correspond to either a missing or highly abnormal IPyC layer.

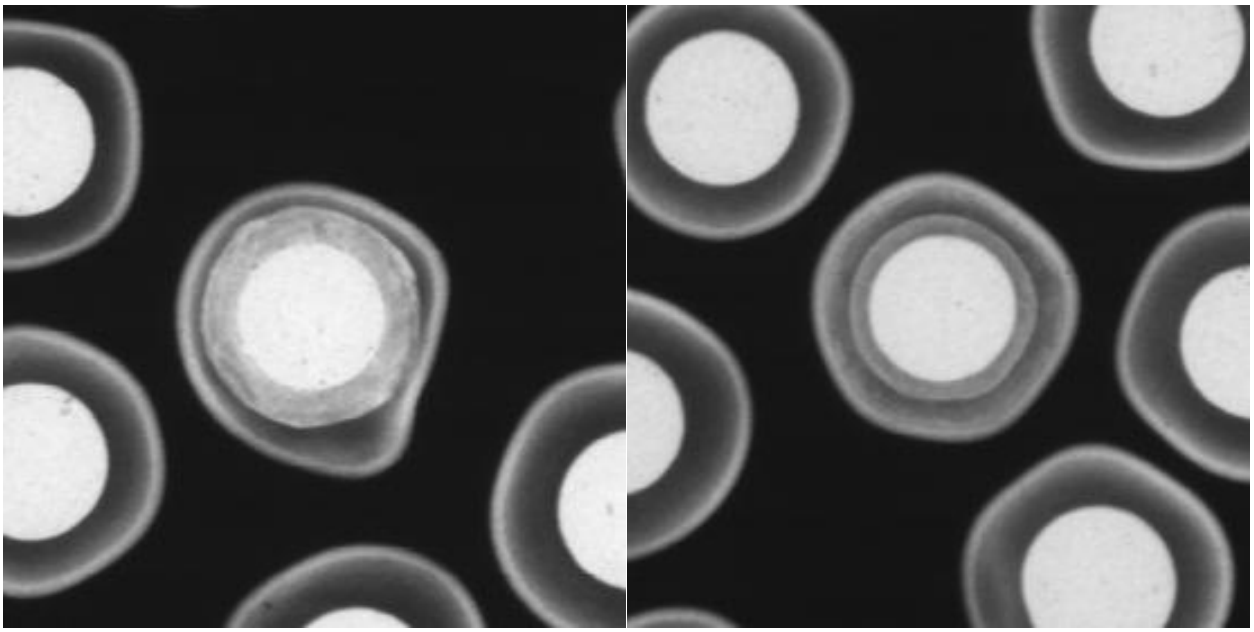

Figure 2-6. Low-resolution radiographs of particles with uranium dispersion out to the buffer/IPyC interface (left) or partially through the buffer layer (right).

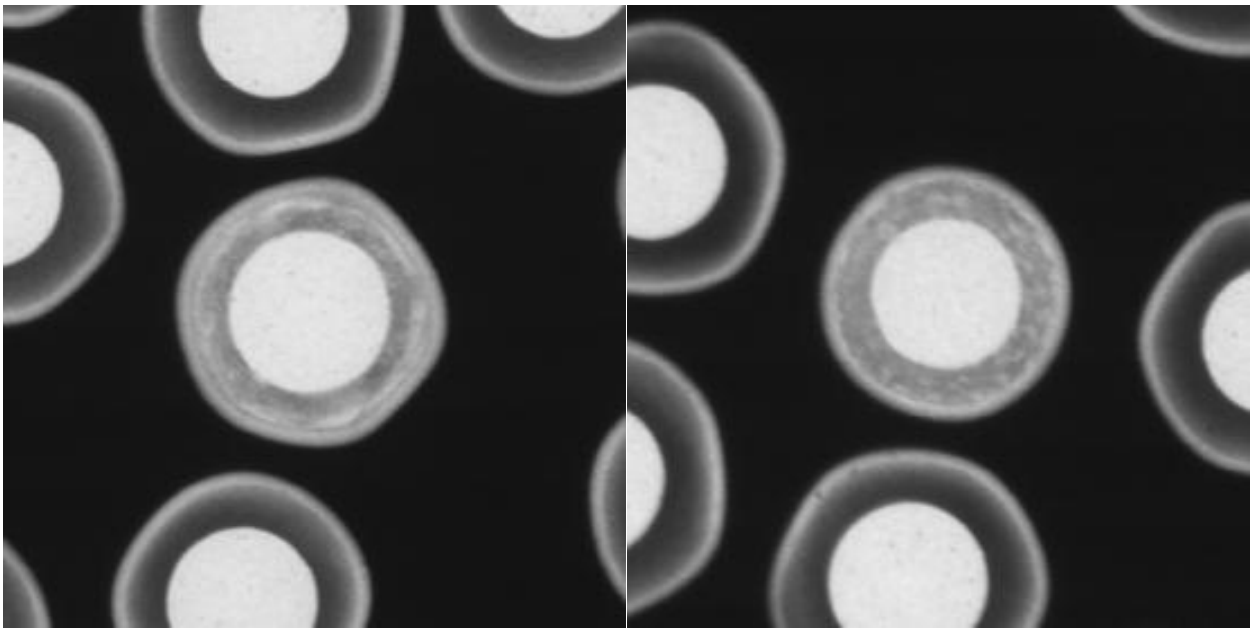

Figure 2-7. Low-resolution radiographs of particles with uranium dispersion out to the SiC layer, indicating either a missing or severely compromised IPyC layer.

While this method was accurate in distinguishing some particles with missing IPyC, the range of uranium dispersion behaviors associated with missing or highly abnormal IPyC included some particles which would not necessarily be distinguishable from normal Defective IPyC particles based on low-resolution radiography alone. For example, Figure 2-8 shows a particle with no apparent IPyC layer in which uranium dispersion proceeded only partway through the buffer layer. The distribution of uranium dispersion in this particle may be due to microstructural variations in the buffer layer. Fluctuations in particle fluidization and coating rates may have resulted in the deposition of a relatively high density ring in the buffer, which then prevented further dispersion of uranium. It is also possible that this particle had a thin buffer layer, a coating anomaly discussion in Section 4, which resulted in the deposition of a thicker and lower density IPyC layer. In this case, the uranium dispersion would mark the boundary between the IPyC and buffer layers. Technical capabilities to determine the nature of the uranium dispersion in this particle are available; however, it is beyond the scope of the current fuel qualification effort.

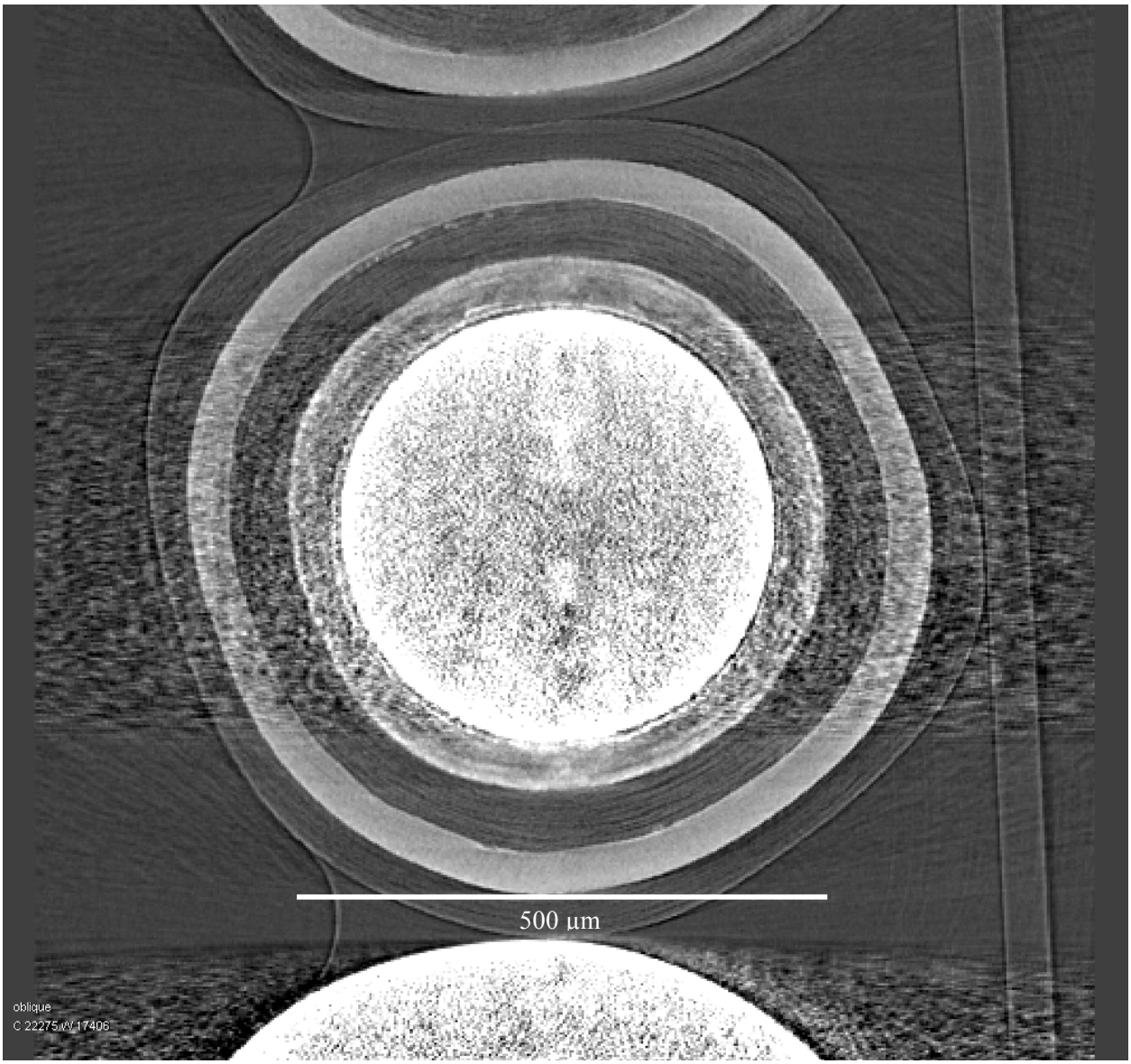

Figure 2-8. Tomographic cross-section of a particle without an IPyC layer and with uranium dispersion stopping about 60 µm from the kernel.

Figure 2-9 shows a particle in which either a soot inclusions or a highly permeable IPyC layer is present, but the layer is fully compromised and infiltrated by uranium dispersion. The nature of this abnormal IPyC layer is not fully clear from the tomographic cross-section due to the pervasive uranium dispersion; however, it appears more textured and porous than typical IPyC layers, potentially indicating that the layer is abnormally low density. Finally, Figure 2-10 shows a particle with a very thin (~10-µm-thick) IPyC layer with an intervening soot layer between the IPyC and buffer. Once again, concentration of dispersed uranium midway through the buffer layer may indicate microstructural variations within the buffer layer, but determination of such is beyond the scope of the current work.

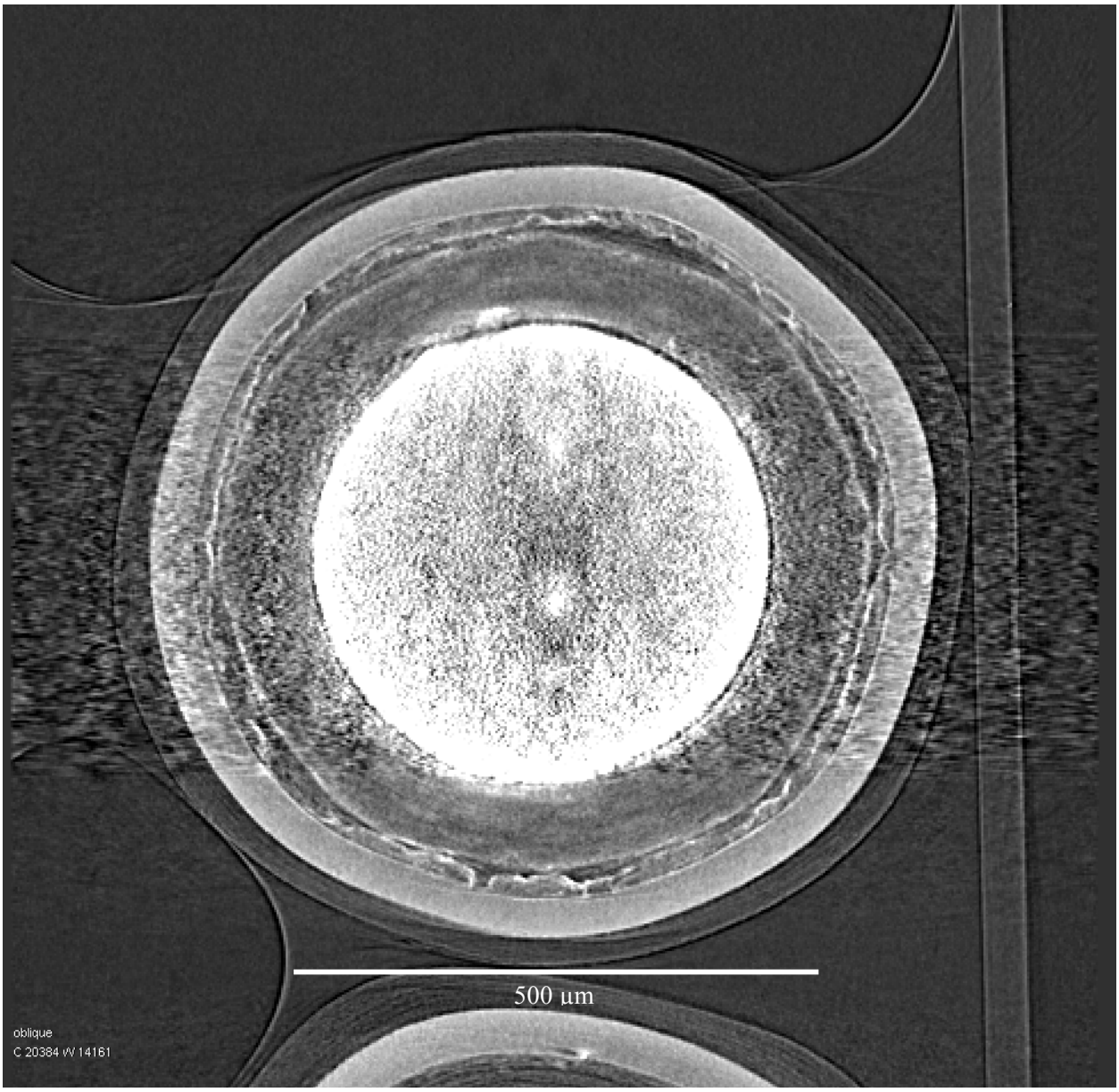

Figure 2-9. Tomographic cross-section of a particle with an entirely compromised IPyC layer (possibly mixed with a soot inclusion) that exhibits uranium dispersion out to the SiC layer.

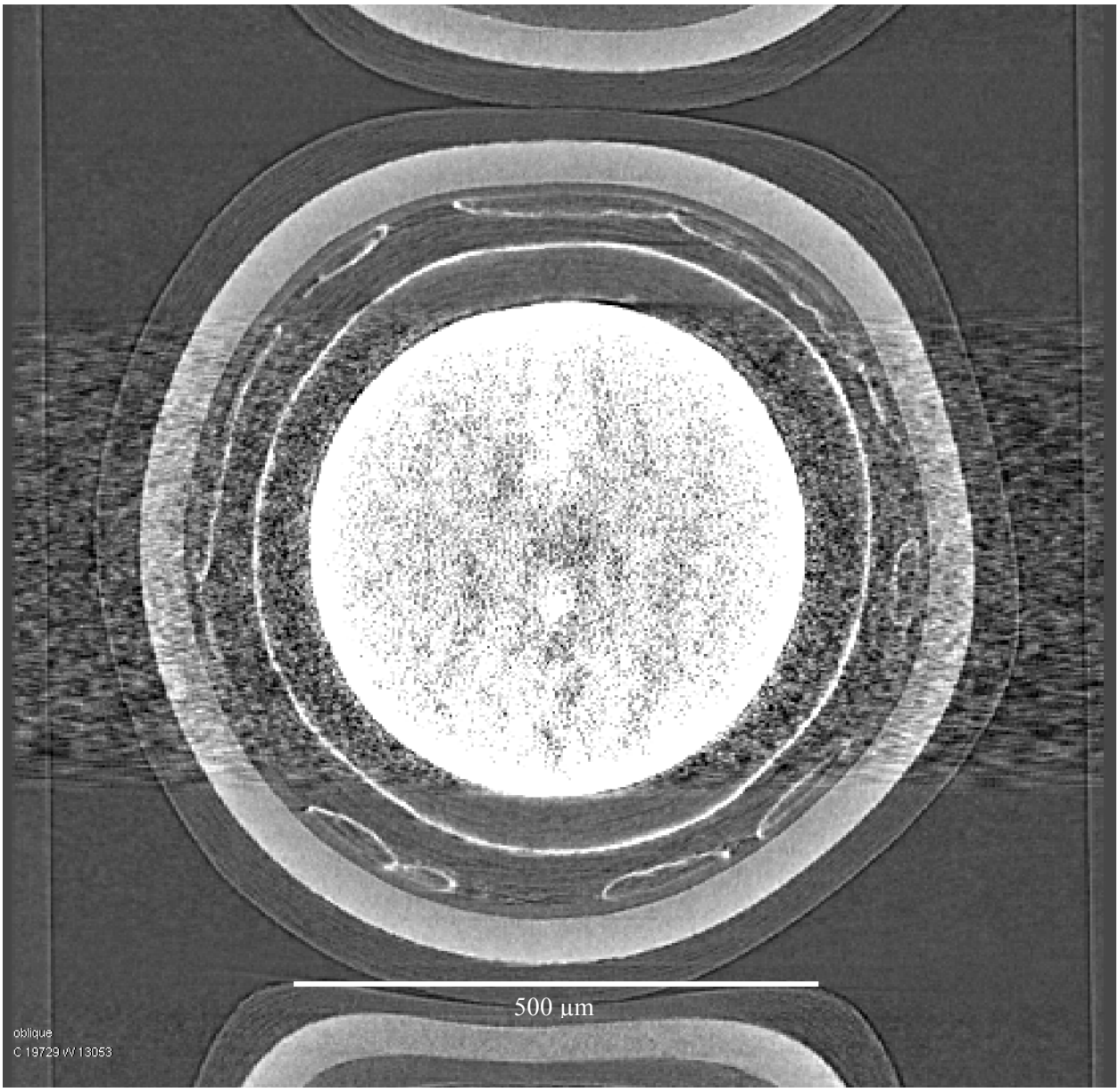

Figure 2-10. Tomographic cross-section of a particle with a very thin IPyC layer and uranium dispersion concentrated midway through the buffer layer and near the IPyC.

Finally, the third classification of uranium dispersion was particles in which the dispersion was clearly asymmetric, commonly associated with what appeared to be kernel fragments embedded in the buffer layer. Of the 115 particles with uranium dispersion which were observed across all batches of material, 53 were of this type, of which many were identified to include embedded kernel fragments or multiple kernels. Figure 2-11 and Figure 2-12 show particles in which embedded kernel fragments resulted in localized asymmetric uranium dispersion near the fragments. In Figure 2-11 the embedded fragments appear to be from an additional kernel, while in Figure 2-12 they may have fractured from the primary kernel. Figure 2-13 and Figure 2-14 show particles in which localized asymmetric uranium dispersion was observed, but no kernel fragments were observed. In these cases, it is possible that the high-Z material identified as uranium dispersion is some other foreign material; however, determination of that would require metallographic examination of the particles that is outside the scope of the current activity. The localized nature of the uranium dispersion observed in these particles indicates that a mechanism

other than IPyC permeability to HCl is likely the cause, since that would be expected to produce a more uniform dispersion of uranium into the buffer.

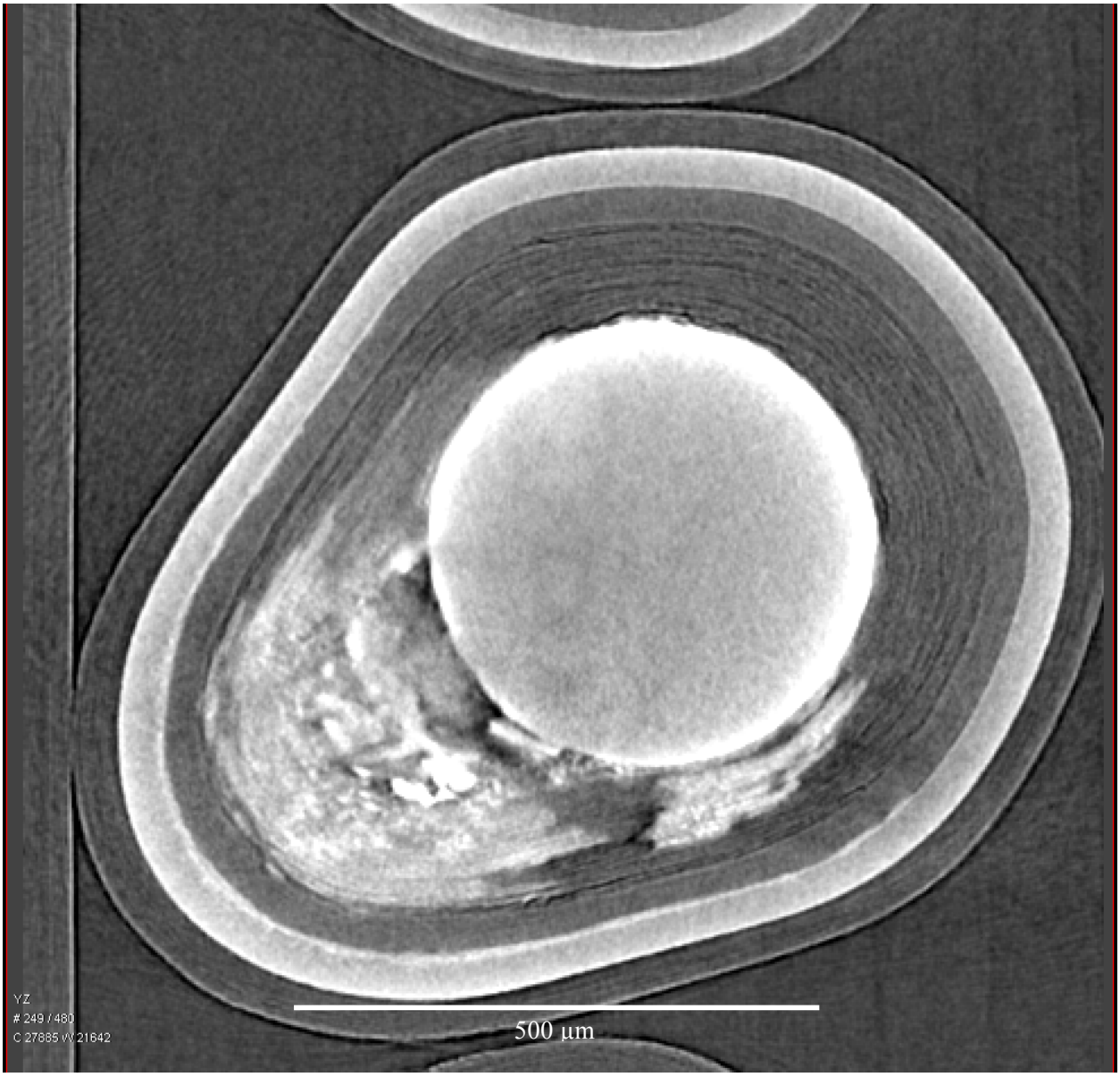

Figure 2-11. Tomographic cross-section of a particle with uranium dispersion near embedded kernel fragments.

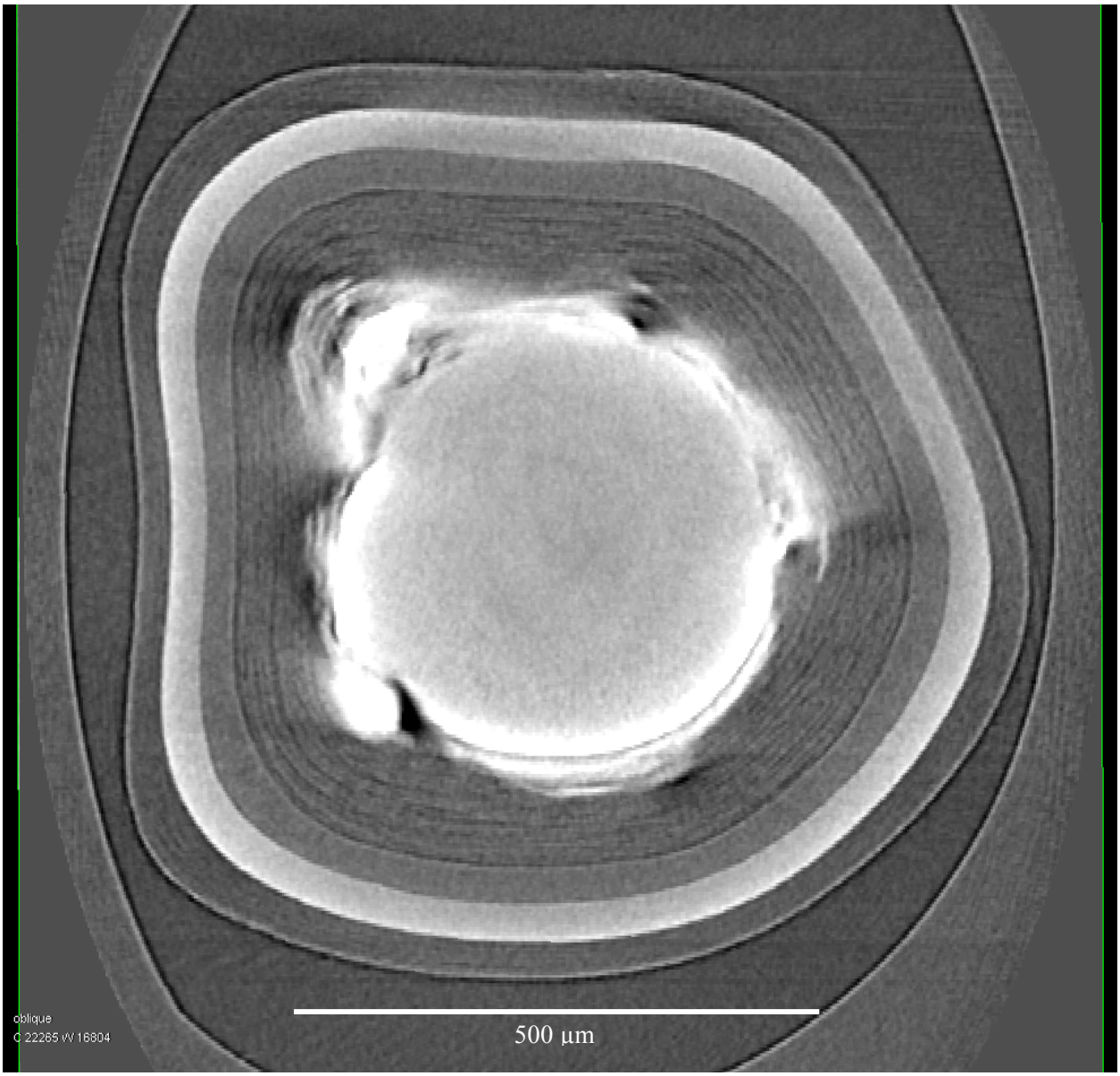

Figure 2-12. Tomographic cross-section of a particle with uranium dispersion near embedded fragments as well as the primary kernel.

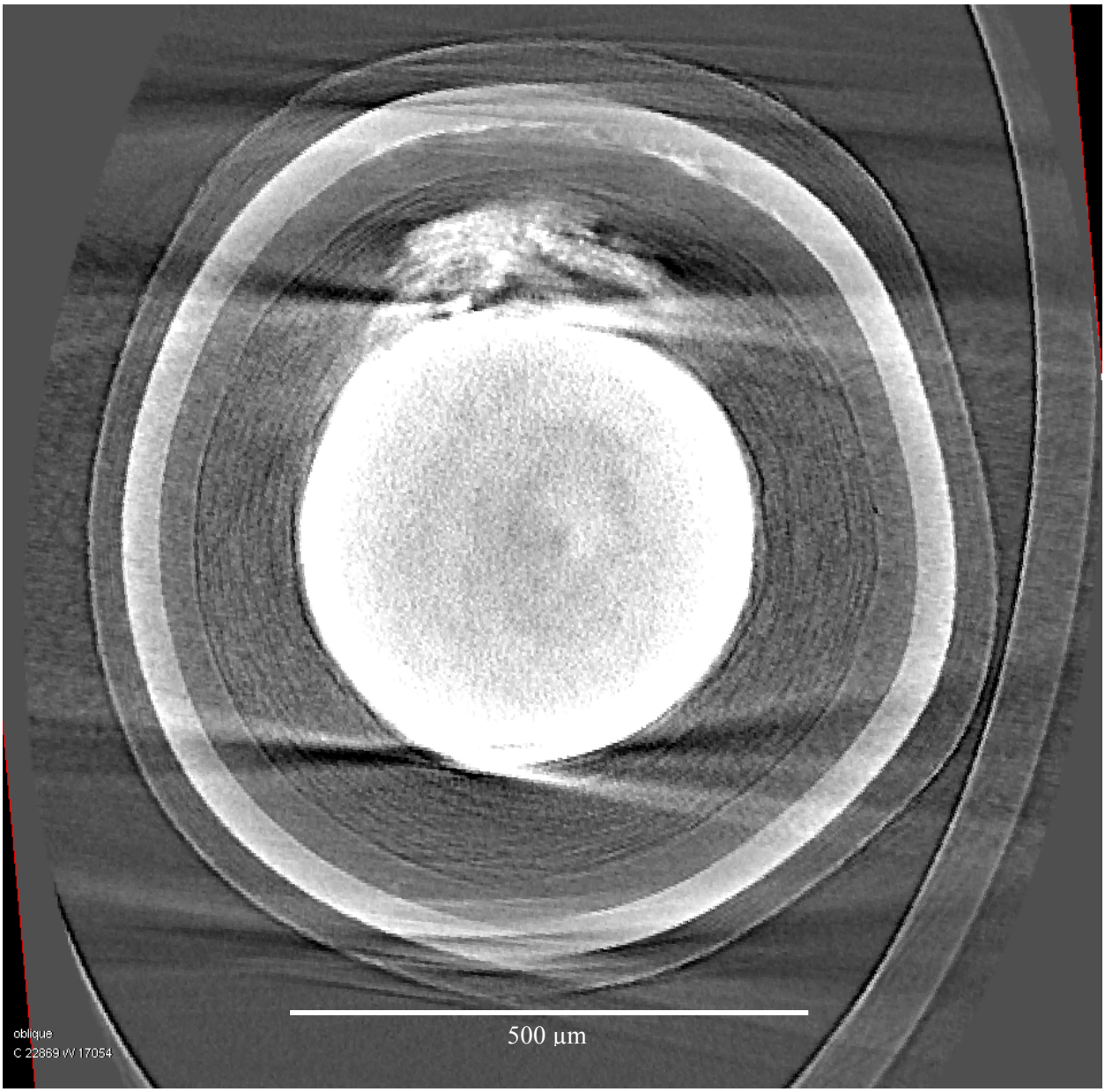

Figure 2-13. Tomographic cross-section of a particle with localized asymmetric uranium dispersion and no indication of extra kernel material.

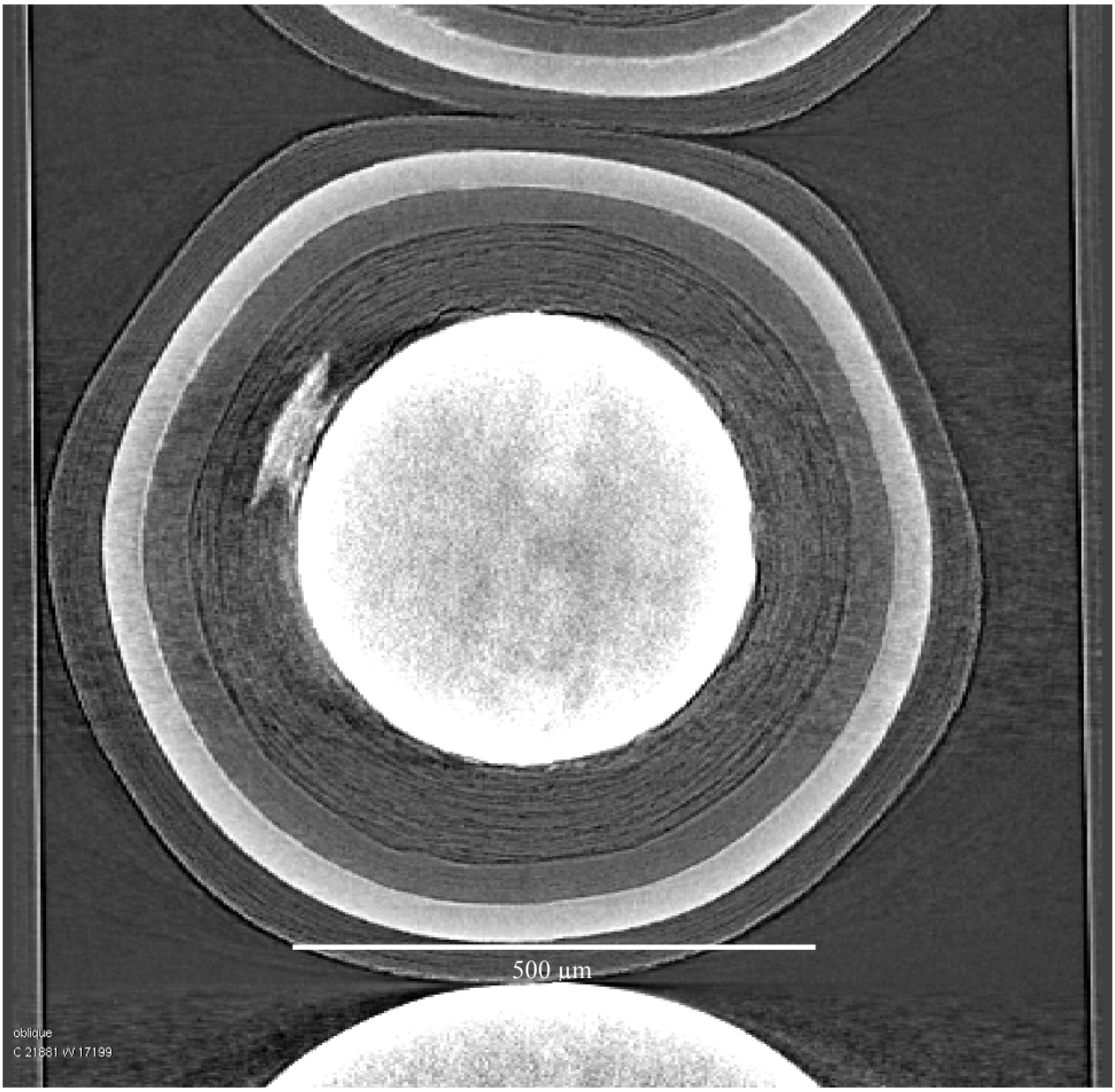

Figure 2-14. Tomographic cross-section of a particle with localized asymmetric uranium dispersion and no indication of extra kernel material.

A programmatic decision was made to not count particles with asymmetric dispersion related to kernel fracture and embedded fragments as Defective IPyC particles, based on interpretation of the intent of the AGR-5/6/7 specification. As such, the J52R-16-98005 composite was determined to satisfy the specified limits for Defective IPyC with a defect fraction of $\leq 7.6\times10^{-5}$ at 95% confidence (Helmreich et al. 2017). Including the particles with kernel fragments would have resulted in a defect fraction of $\leq 1.1\times10^{-4}$, just shy of satisfying the specification limit of 1.0×10^{-4} without increasing the sample size to reduce the binomial distribution statistical penalty. Either way, the defect population was unusually high compared to previous AGR fuel composites (Table 2-1). Irrespective of whether it is related to higher-permeability IPyC, the presence of dispersed uranium in the buffer layer may impact fuel performance and the results of this study suggest that the presence of embedded kernel fragments and other forms of uranium dispersion should be limited by the specification.

Table 2-1. Results of Defective IPyC Analysis for AGR UCO composites

Irradiation test	Fuel composite	Particles analyzed	Number of particles with Defective IPyC	Observed fraction with Defective IPyC	95% confidence limit on Defective IPyC
AGR-1	LEU01-46T	49735	0	0	$\leq 6.1\times10^{-5}$
AGR-1	LEU01-47T	49799	0	0	$\leq 6.1\times10^{-5}$
AGR-1	LEU01-48T	49555	0	0	$\leq 6.1\times10^{-5}$
AGR-1	LEU01-49T	49516	0	0	$\leq 6.1\times10^{-5}$
AGR-2	LEU06*	63724	0	0	$\leq 4.8\times10^{-5}$
AGR-2	LEU07*	63538	443	7.0×10^{-3}	$\leq 7.6\times10^{-3}$
AGR-2	LEU09	63525	0	0	$\leq 4.8\times10^{-5}$
AGR-5/6/7	98005	241822	11	4.5×10^{-5}	$\leq 7.6\times10^{-5}$

* AGR-2 Batches LEU06 and LEU07 were rejected due to high fraction of particles with exposed uranium. LEU07 was also rejected due to high Defective IPyC fraction.

While significant variation in the fraction of particles with uranium dispersion was found from batch to batch, this variation was predominantly focused on particles with localized uranium dispersion. As shown in Figure 2-15, the observed fraction of particles with missing IPyC or with symmetric uranium dispersion typical of Defective IPyC was generally uniform from batch to batch, with some variation as would be expected due to binomial sampling statistics. In contrast, the observed fraction of particles with localized uranium dispersion varied significantly more from batch to batch, indicating that there may have been differences in batch handling and production which were responsible, such as the presence of fragments from fissured kernels or other foreign contaminants.

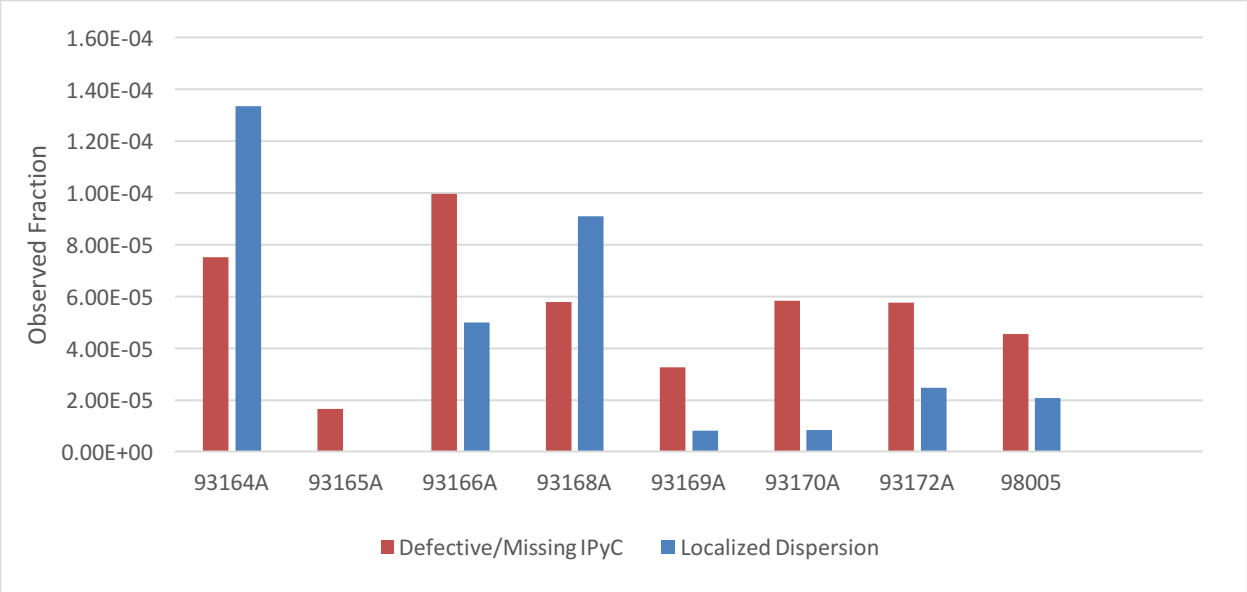

Figure 2-15. Observed fraction of particles with uranium dispersion in each batch separated by classification of uranium dispersion.

3. KERNEL ANOMALIES

While the primary objective of radiographic analysis of kernels from each batch was the determination of Defective IPyC fractions, several additional particle anomalies were identified and catalogued in the analysis process to glean additional information regarding each batch. These anomalies may be divided into two sub-categories: kernel anomalies and coating anomalies. Kernel anomalies, which are discussed in this section, were those in which there was an observation of either some irregularity in the kernel or an irregularity in the coating layers known to result from kernel irregularities which may not have been visible in the two-dimensional radiograph. Tabulation of these anomalies was complicated by the influence of operator judgement to some degree. The identification of particles with Defective IPyC relies on a well-defined visual standard, which ensures consistency across multiple operators. A similar approach was implemented for identification of anomalies; however, variations in degree along with the large numbers of anomalies identified made absolute consistency difficult in the case of kernel anomalies. As such, quantitative comparison of the fraction of kernel anomalies found in each batch of material may be of limited usefulness; however, a summary of the kernel anomalies identified in each batch of material is given in Table 3-1. Note that the Total column in Table 3-1 is a total without repetition, as some particles were identified as having multiple kernel anomalies.

Table 3-1. Summary of kernel anomalies identified in each material batch.

TRISO Batch	Sample	Total	Dimple or Facet	Severe Dimple or Facet	Notched Kernel	Irregular Kernel	Multi-Kernel
93164A	NP-C1364	2812/119944 2.34×10^{-2}	1135/119944 9.46×10^{-3}	Not Counted	1808/119944 1.51×10^{-2}	164/119944 1.37×10^{-3}	6/119944 5.00×10^{-5}
93165A	NP-C1350	1634/121032 1.35×10^{-2}	1474/121032 1.22×10^{-2}	Not Counted	78/121032 6.44×10^{-4}	82/121032 6.78×10^{-4}	0/121032
93166RA	NP-C1358	1651/120474 1.37×10^{-2}	1526/120474 1.27×10^{-2}	Not Counted	95/120474 7.89×10^{-4}	135/120474 1.12×10^{-3}	1/120474 8.30×10^{-6}
93168A	NP-C1369	3381/120819 2.80×10^{-2}	2895/120819 2.40×10^{-2}	168/120819 1.39×10^{-3}	122/120819 1.01×10^{-3}	245/120819 2.03×10^{-3}	23/120819 1.90×10^{-4}
93169A	NP-C1391	2610/122226 2.14×10^{-2}	2288/122226 1.87×10^{-2}	92/122226 7.53×10^{-4}	81/122226 6.63×10^{-4}	211/122226 1.73×10^{-3}	5/122226 4.09×10^{-5}
93170A	NP-C1402	2332/119831 1.95×10^{-2}	2135/119831 1.78×10^{-2}	56/119831 4.67×10^{-4}	60/119831 5.01×10^{-4}	129/119831 1.08×10^{-3}	2/119831 1.67×10^{-5}
93172A	NP-C1421	2098/121383 1.73×10^{-2}	1822/121383 1.84×10^{-2}	144/121383 1.19×10^{-3}	66/121383 5.45×10^{-4}	110/121383 9.09×10^{-4}	4/121383 3.31×10^{-5}
98005	NP-C1498 NP-C1504	4191/241822 1.73×10^{-2}	3806/241822 1.57×10^{-2}	166/241822 6.86×10^{-4}	113/241822 4.67×10^{-4}	149/241822 6.16×10^{-4}	6/241822 2.48×10^{-5}

Reported fractions are the number of particles observed with a kernel anomaly (numerator) over the total number of particles observed (denominator) followed by this observed fraction in scientific notation.

Most kernel anomalies involved deviations from roundness in the kernel. These could appear as a simple facet (Figure 3-1), a localized notch (Figure 3-2), or more extensive irregular shapes (Figure 3-3). Significant deviations from roundness were generally observed to result in dimples in the coating layers which ranged from ordinary (Figure 3-1) to severe (Figure 3-4), and dimples were generally observed to have a corresponding kernel anomaly. Since the low-resolution radiographs were limited to a single two-

dimensional projection of the particles, it is likely that cases in which one was observed without the other were due to the angle of the particle. As noted above, consistent classification of these defects was challenging, particularly in borderline cases (e.g., a particle with only a slight dimple). Dimples in the coating layers are a potential concern for fuel performance due to layer thinning in the center of the dimple and stress concentration points around the perimeter. The degree of both concerns will be related to the severity of the dimple, so dimples which were particularly severe were tabulated separately as they may have an impact on fuel performance. The reference for what constituted a severe dimple was based on the radiographs in Figure 3-4, in which dimples extend deeply into the particle or extend over a large area of the particle surface in an abnormal shape.

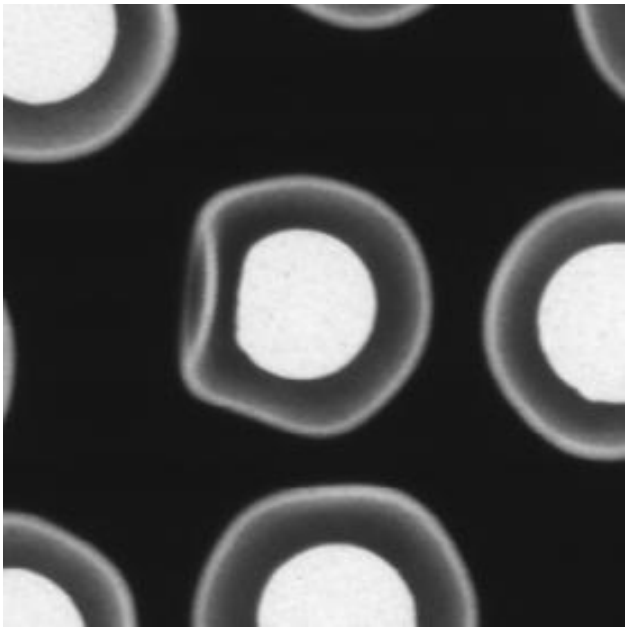

Figure 3-1. Radiograph of a particle with a faceted kernel and a corresponding dimple in the coating layers.

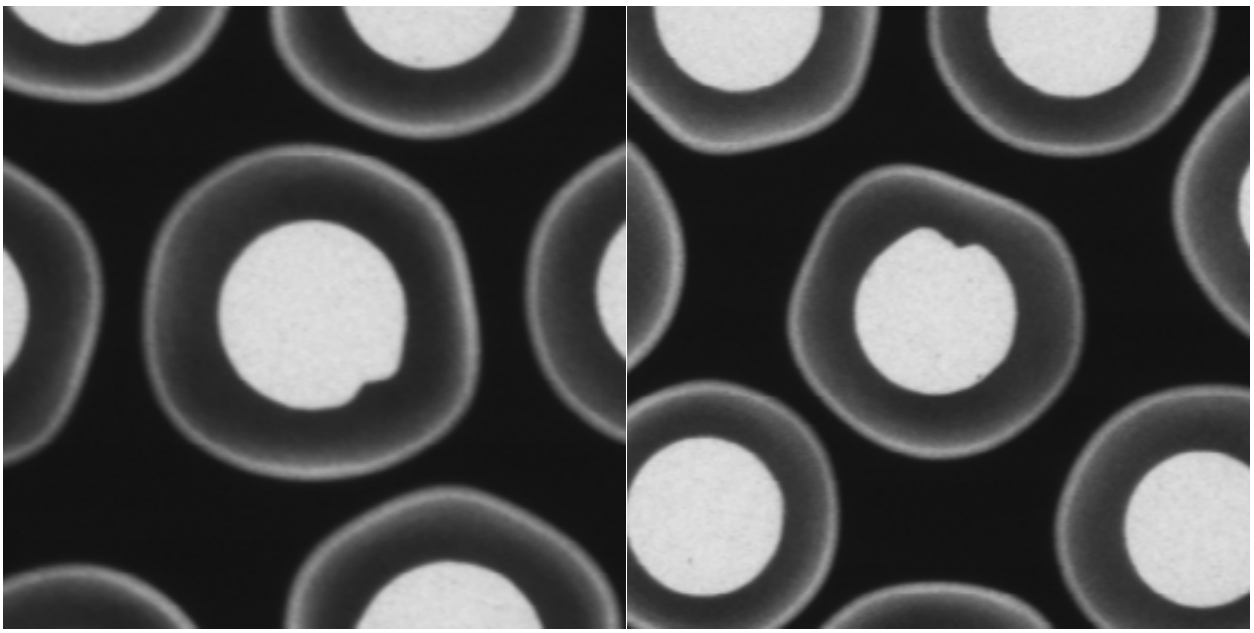

Figure 3-2. Radiographs of particles with notched kernels.

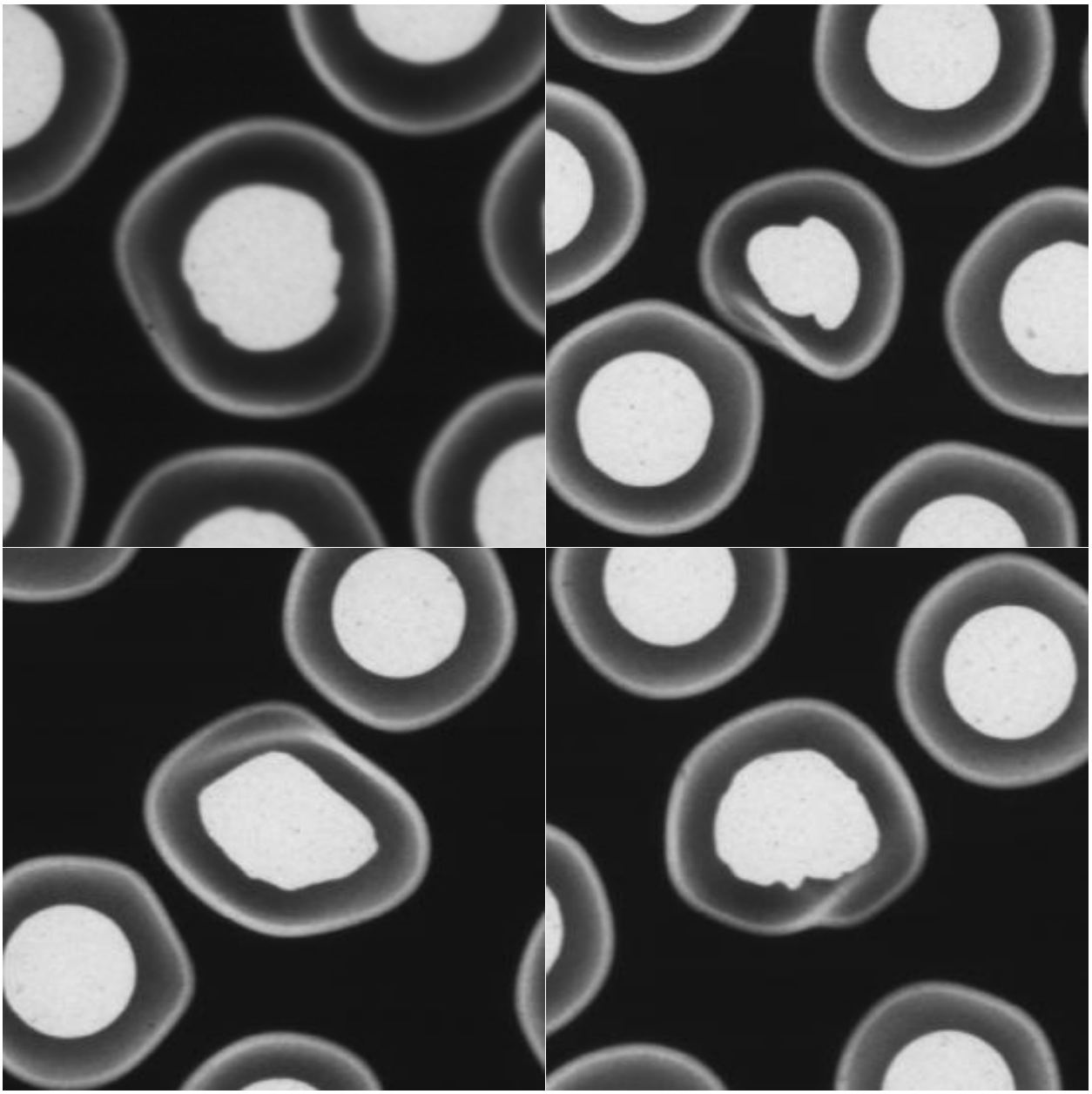

Figure 3-3. Radiographs of particles with irregular kernels.

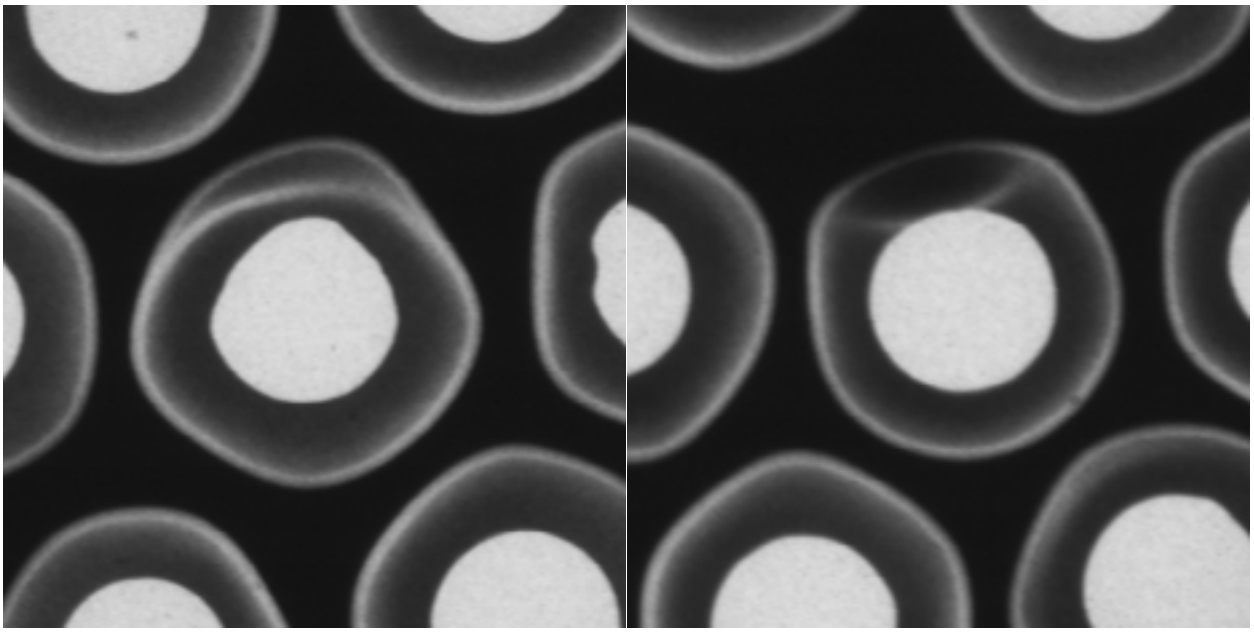

Figure 3-4. Radiographs of particles with severe dimples in their coating layers.

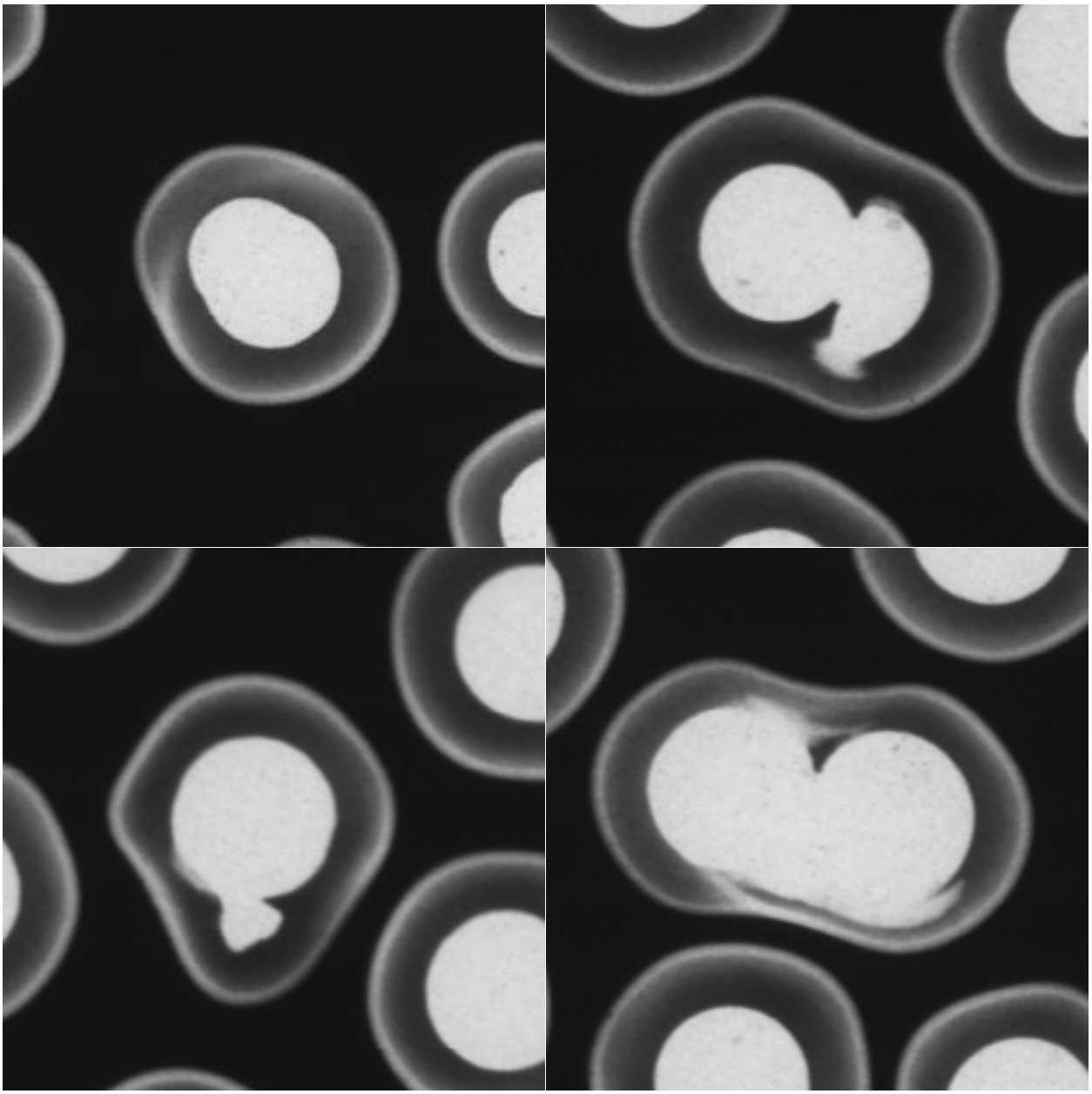

Figure 3-5. Radiographs of particles with multiple kernels.

The final classification of kernel anomalies was particles with additional kernel fragments or multiple whole kernels (Figure 3-5). As discussed in the preceding section, there were some particles in which this extra material resulted in uranium dispersion into the buffer layer; however, there were also particles in which the extra material did not result in dispersion. Particles with uranium dispersion around embedded kernel material were counted as having asymmetric uranium dispersion, while particles without uranium dispersion around embedded kernel material were not.

4. COATING ANOMALIES

While the anomalies in the preceding section may be attributed primarily to variations in the kernel, the anomalies discussed in this section are related to variations in the coating process. A summary of the coating anomalies observed for each batch of material is given in Table 4-1. In general, coating anomalies were less prevalent than kernel anomalies, and while kernel anomalies were generally related, coating anomalies were essentially unique and individual occurrences.

Table 4-1. Summary of coating anomalies identified in each material batch.

TRISO Batch	Sample	Thin or Missing Buffer	Thin or Missing SiC	Extra Layers	Missing Kernel	Kernel Migration	Bare Kernel
93164A	NP-C1364	1/119944 8.34×10^{-6}	9/119944 7.50×10^{-5}	0/119944	5/119944 4.17×10^{-5}	2/119944 1.67×10^{-5}	0/119944
93165A	NP-C1350	1/121032 8.26×10^{-6}	6/121032 4.96×10^{-5}	0/121032	2/121032 1.65×10^{-5}	0/121032	0/121032
93166RA	NP-C1358	1/120474 8.30×10^{-6}	10/120474 8.30×10^{-5}	2/120474 1.66×10^{-5}	0/120474	1/120474 8.30×10^{-6}	0/120474
93168A	NP-C1369	3/120819 2.48×10^{-5}	9/120819 7.45×10^{-5}	0/120819	0/120819	0/120819	0/120819
93169A	NP-C1391	20/122226 1.64×10^{-4}	13/122226 1.06×10^{-4}	1/122226 8.18×10^{-6}	0/122226	0/122226	0/122226
93170A	NP-C1402	25/119831 2.09×10^{-4}	25/119831 2.09×10^{-4}	1/119831 8.35×10^{-6}	0/119831	0/119831	2/119831 1.67×10^{-5}
93172A	NP-C1421	4/121383 3.30×10^{-5}	8/121383 6.59×10^{-5}	0/121383	0/121383	0/121383	0/121383
98005	NP-C1498 NP-C1504	0/241822	18/241822 7.44×10^{-5}	0/241822	0/241822	4/241822 1.65×10^{-5}	2/241822 8.27×10^{-6}

Reported fractions are the number of particles observed with a coating anomaly (numerator) over the total number of particles observed (denominator) followed by this observed fraction in scientific notation.

One notable result of the identification and analysis of other anomalies evident in the x-ray radiographs was the detection of particles with a thin or missing buffer layer. This was particularly important because, unlike some of the other observed anomalies that are also detected by other QC tests (e.g., missing SiC), missing or thin buffer is only detected by the x-ray radiography analysis done during the Defective IPyC QC test. The buffer layer is critical for fuel performance under irradiation, as it protects the IPyC from fission product recoil and accommodates fuel kernel swelling. As such, it is probable that TRISO particles without buffer layers will fail at a significantly higher rate under irradiation. Particles with missing buffer were not initially counted in the first several samples of material analyzed as the anomaly had not been identified at the time. Once significant numbers of particles exhibiting this anomaly were found in later samples, a review of particles marked as odd but unclassifiable in the initial sample sets revealed some particles without buffer. High-resolution x-ray tomography was performed on some of the particles without buffer, showing that some of these particles in fact had a very-thin buffer layer (Figure 4-1), while others had no buffer layer at all (Figure 4-2). After identification of this anomaly in the production fuel batches, an additional sieving step was performed on batches 93165A, 93168A, 93169A, and 93170A using a 760µm sieve to remove particles without a full buffer layer. These batches were then blended to form Composite 98005. As shown in Table 4-1, no particles with thin or missing buffer were

found in the composite, indicating that the additional sieving step was very effective in removing this anomaly.

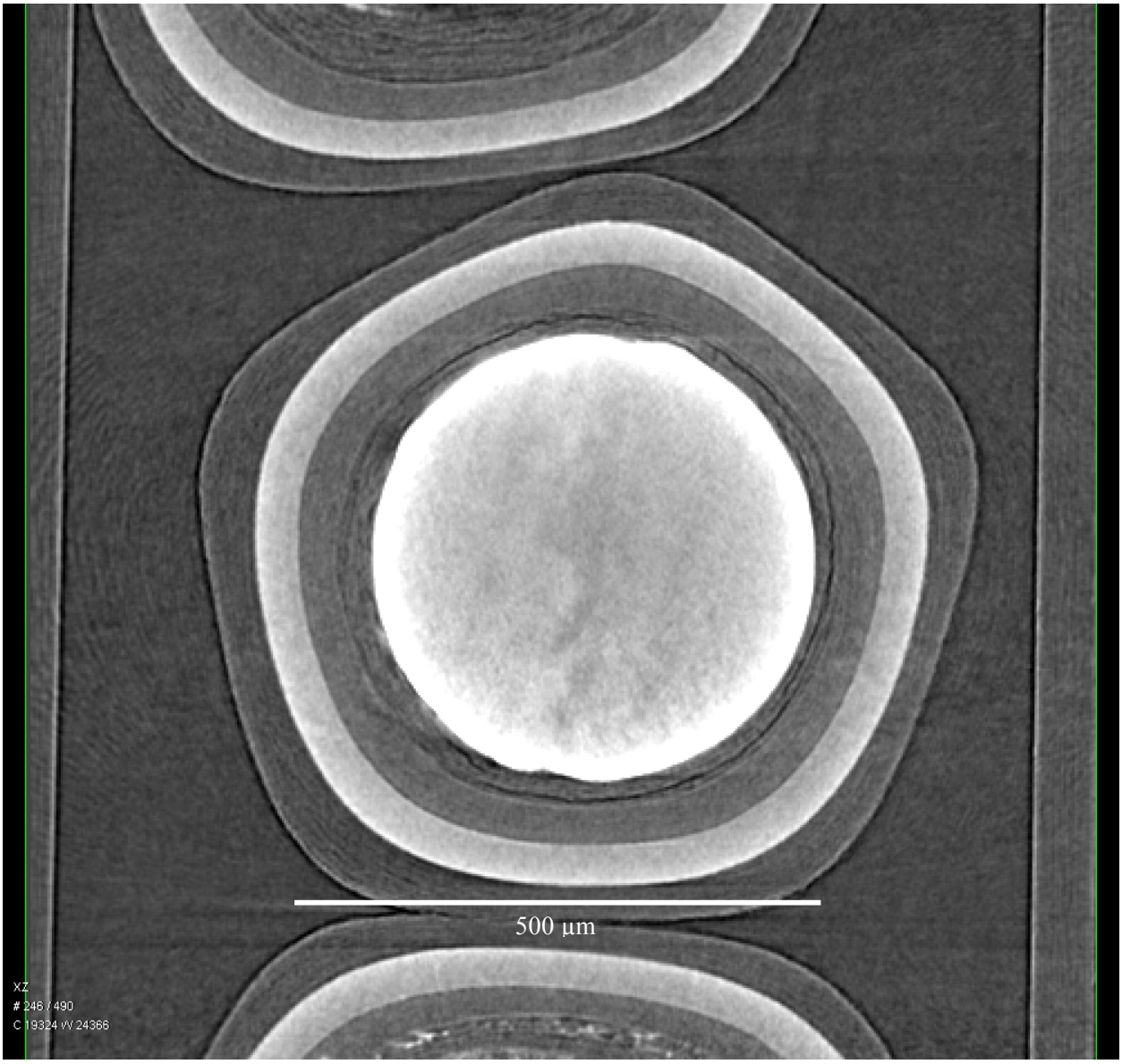

Figure 4-1. Tomographic cross-section of a particle with a very-thin buffer layer.

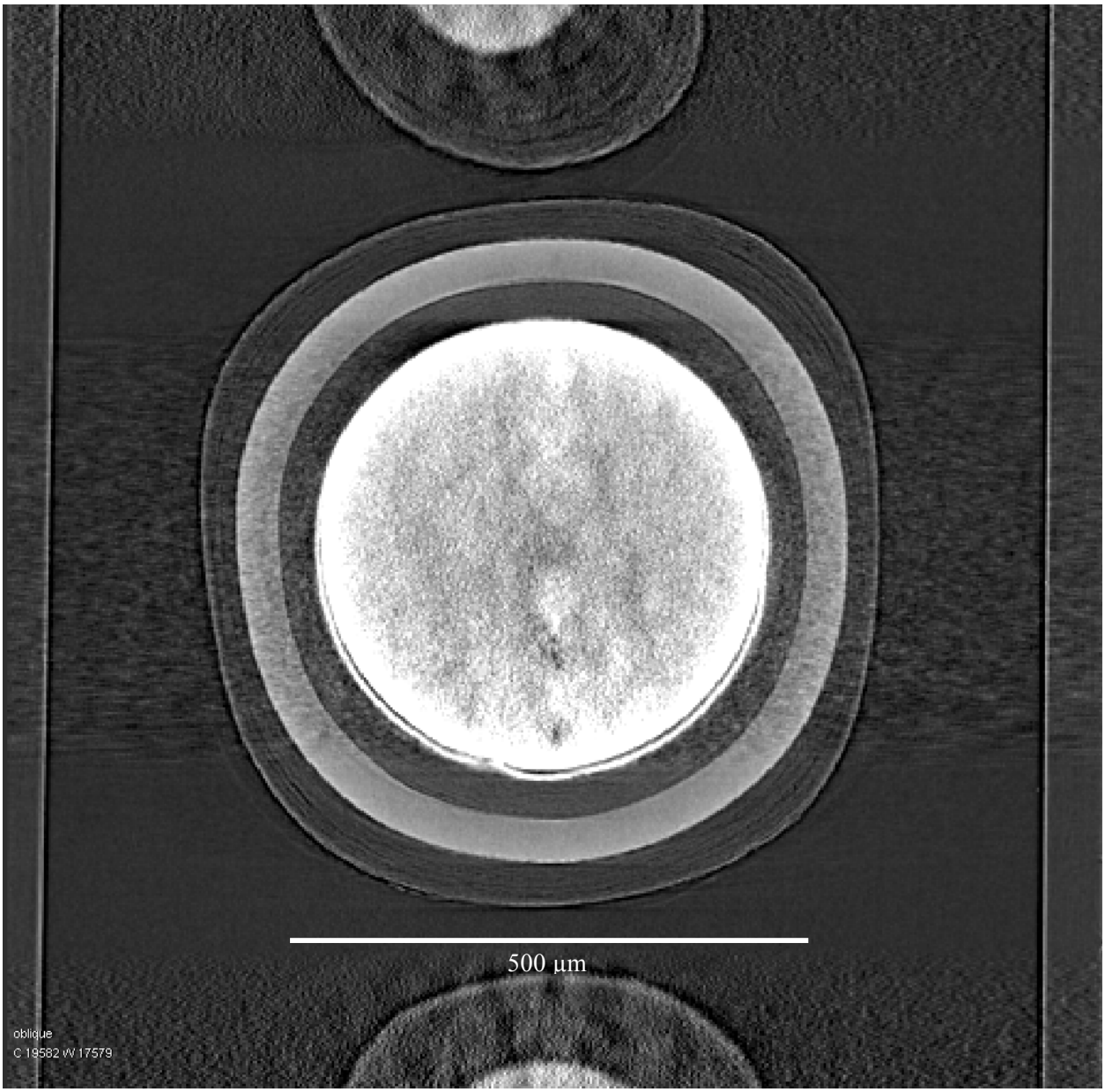

Figure 4-2. Tomographic cross-section of a particle with no buffer layer.

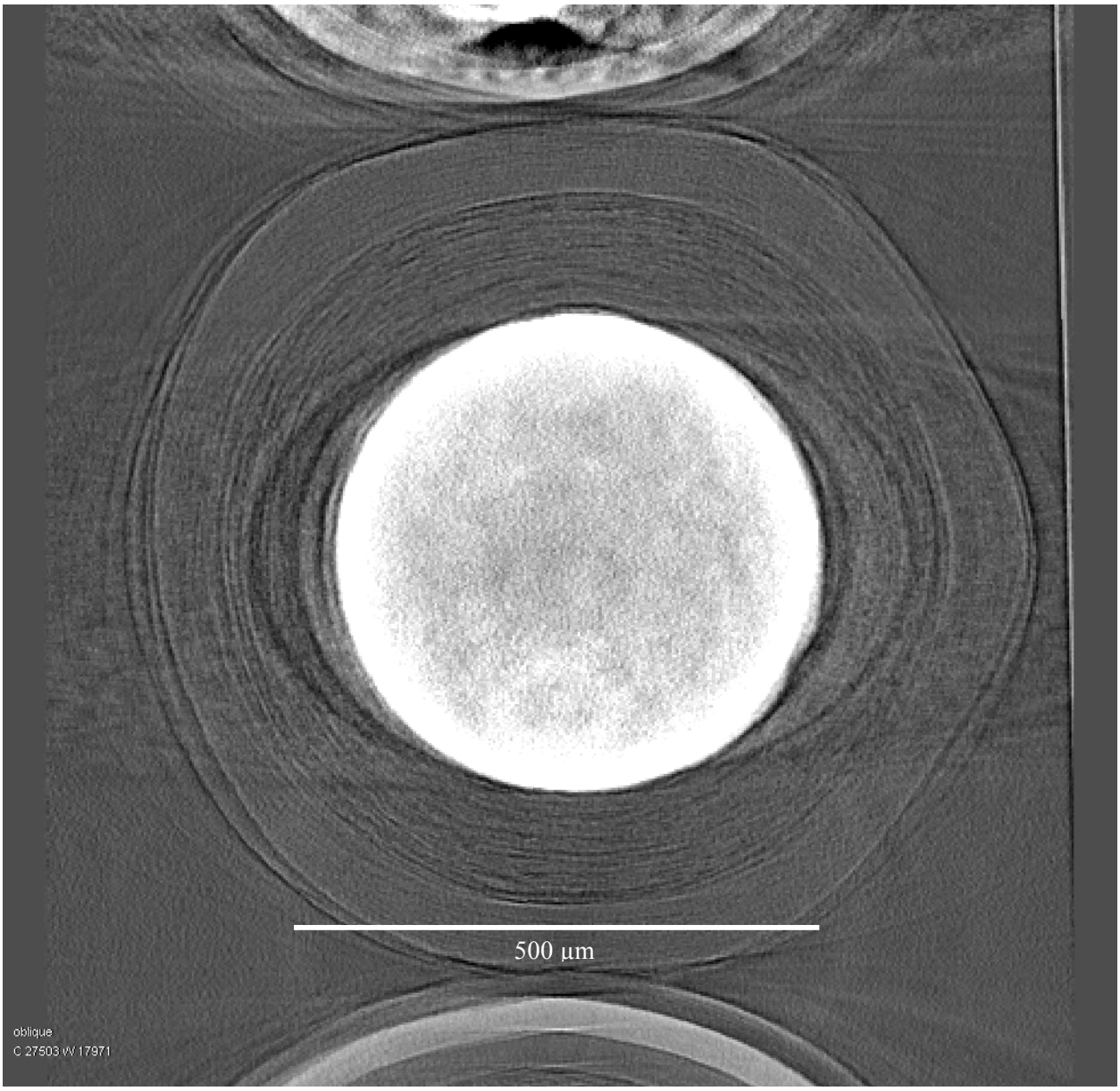

Figure 4-3. Tomographic cross-section of a particle without a SiC layer.

Another coating layer anomaly involving a missing or abnormal layer was particles with thin or missing SiC, as shown in Figure 4-3. The SiC layer is the primary structural layer and a critical diffusion barrier for some of the fission products, such as cesium, that are not well retained by the kernel or the carbon layers; therefore, the absence of this layer is significant. Leach-burn-leach (LBL) analysis will identify particles with missing SiC during the post-burn leaching and they are controlled by the specified limit on the Defective SiC fraction, so their identification here is for information only. A missing SiC layer may be expected to result in particle rejection during sieving; however, this particle had a slightly larger than normal kernel and a thicker than normal buffer layer, resulting in a total particle diameter only slightly smaller than the average.

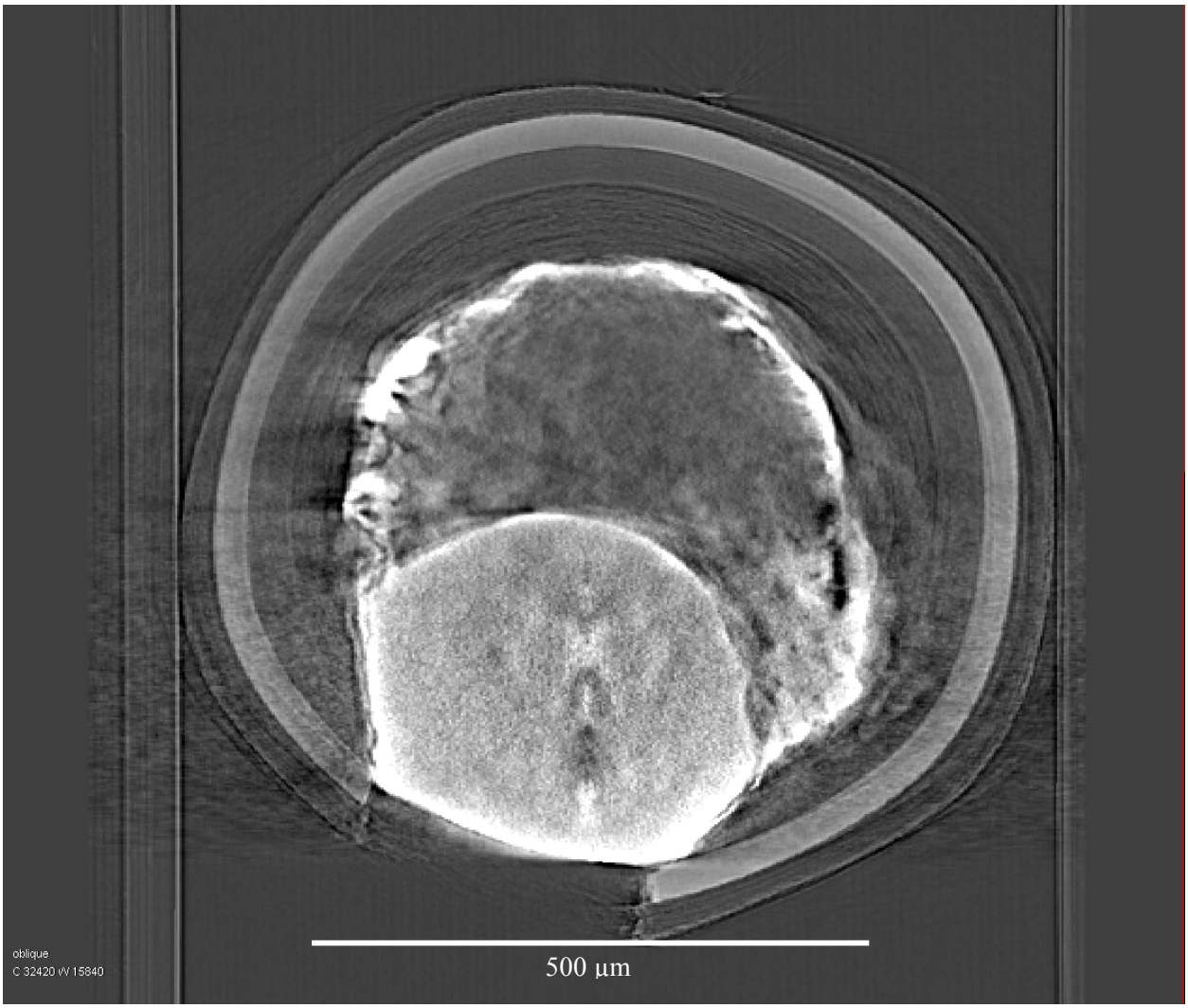

Figure 4-4. Tomographic cross-section of a particle with kernel migration.

Other particle anomalies which would be identified during LBL include those classified as Kernel Migration (Figure 4-4) and Bare Kernels (Figure 4-5), both of which would release uranium during the pre-burn leaching; these are controlled by the specified limit on the exposed kernel fraction. The observed behavior in the particles with kernel migration was directly related to the impact fracture damage to the TRISO coatings that has been identified as the primary cause of the high exposed kernel fraction in the AGR-5/6/7 fuel batches. The broken TRISO coating allows CO gas to escape resulting in an unimpeded reaction between the UO_2 in the kernel and the surrounding carbon layers during the 1800°C heat treatment used to simulate compact heat treatment and produce measurable uranium dispersion in particles with Defective IPyC prior to x-ray radiography. As the kernel consumes carbon, it can migrate through the buffer and IPyC layer.

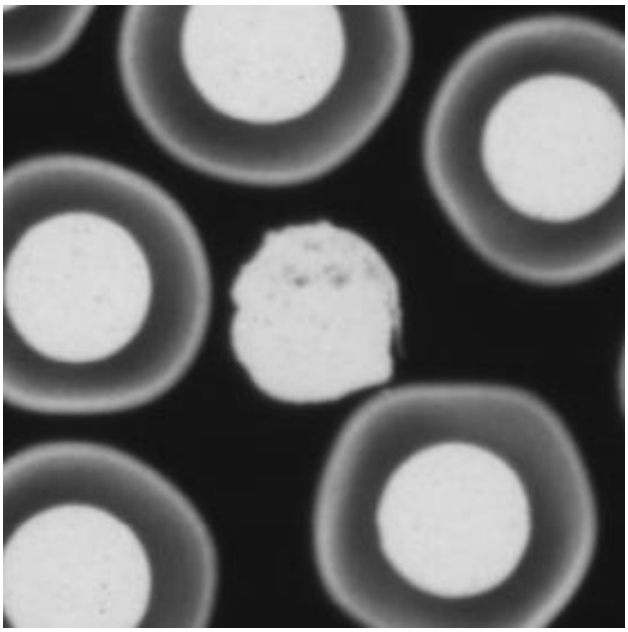

Figure 4-5. Radiograph of a bare kernel.

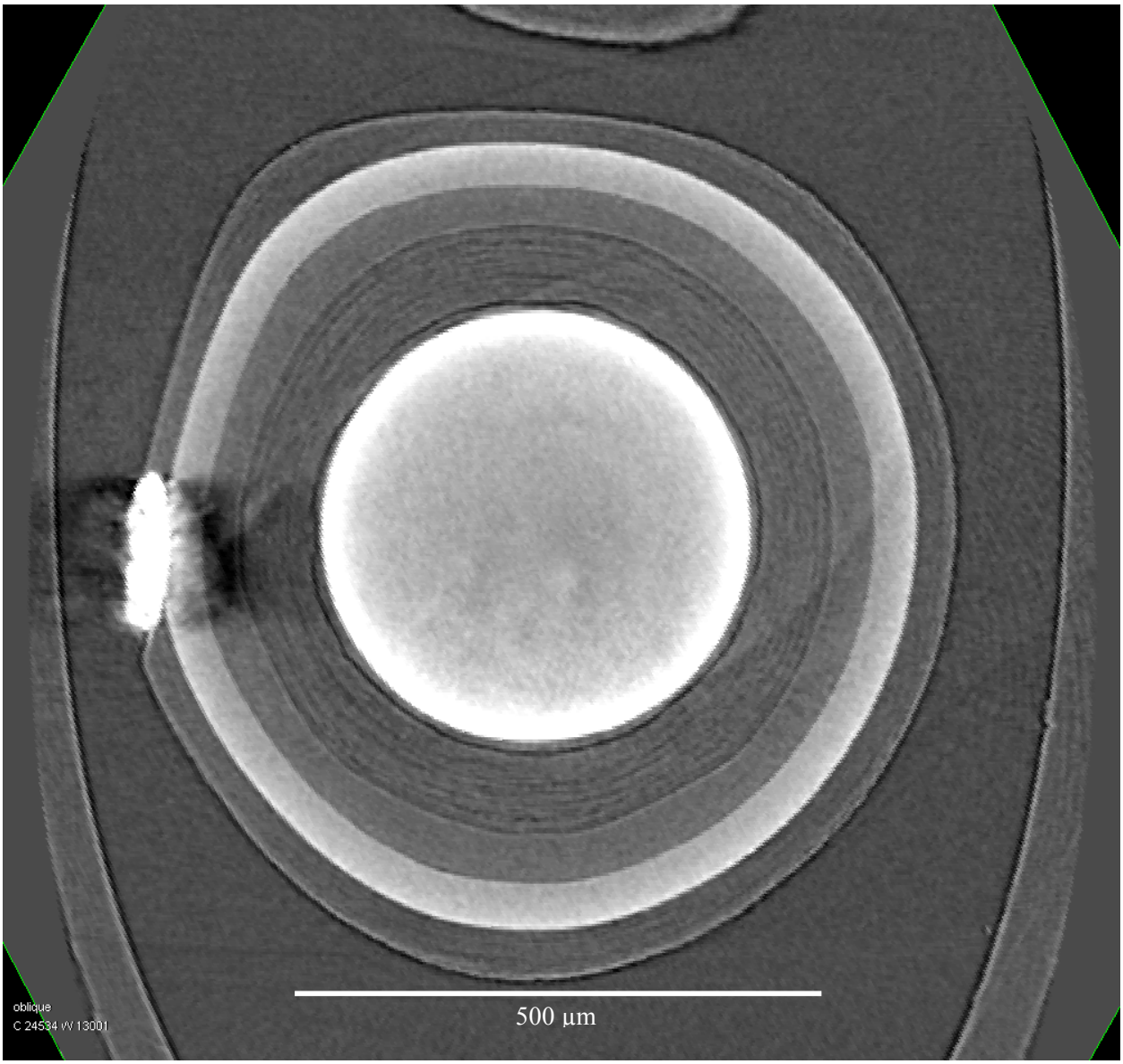

Figure 4-6. Tomographic cross-section of a particle with high-Z material embedded in the OPyC layer.

Whereas most embedded kernel fragments were found in the buffer layer near the primary kernel, as discussed in Section 2, several particles were found which included high-Z material (assumed to be kernel fragments) embedded further away from the kernel in the coating layers. Two particles where identified with apparent kernel fragments embedded in the OPyC (Figure 4-6 and Figure 4-7). These particles would be identified during the preburn leach stage of the LBL analysis and contribute to the dispersed uranium fraction. However, as such they would not be counted as an attribute property or recognized as individual defective particles. In addition, one particle was found with multiple kernel fragments embedded in the buffer/IPyC interface (Figure 4-8). While these particles were not included in Table 4-1, they indicate that kernel fragments were present during coating well past initial buffer deposition.

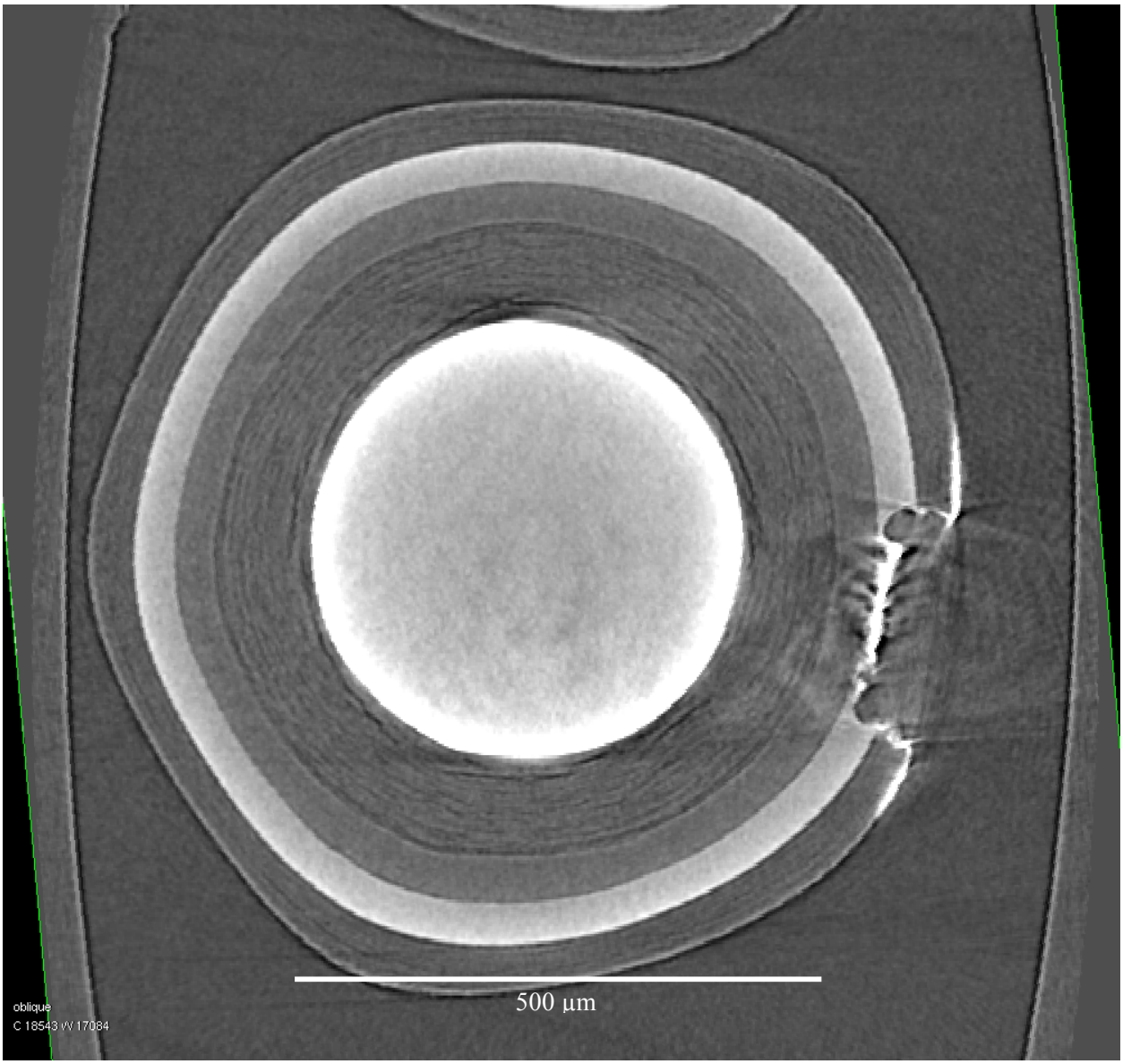

Figure 4-7. Tomographic cross-section of a particle in which high-Z material has consumed a portion of the OPyC and SiC layers.

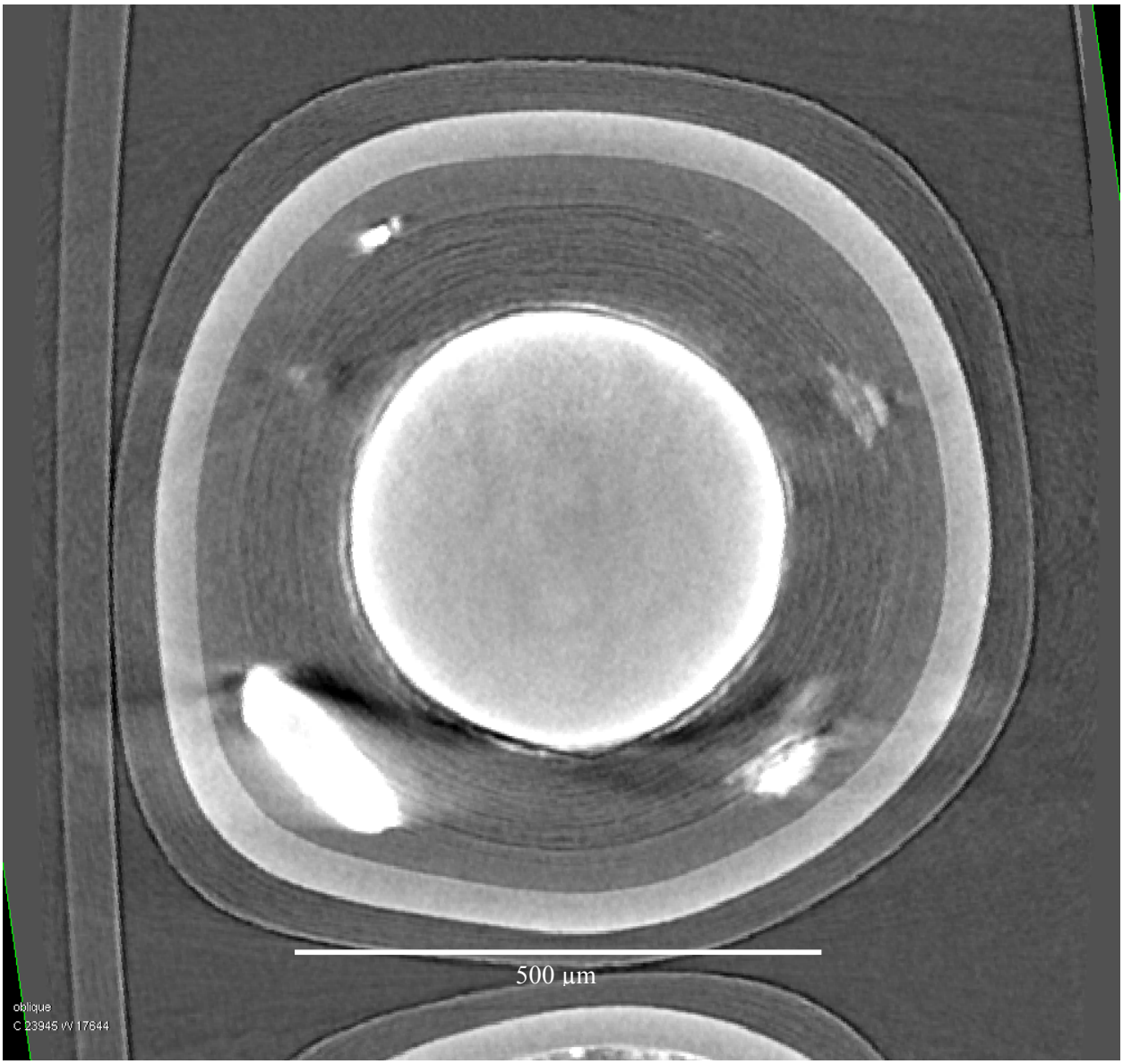

Figure 4-8. Tomographic cross-section of a particle with high-Z material embedded in the buffer/IPyC interface.

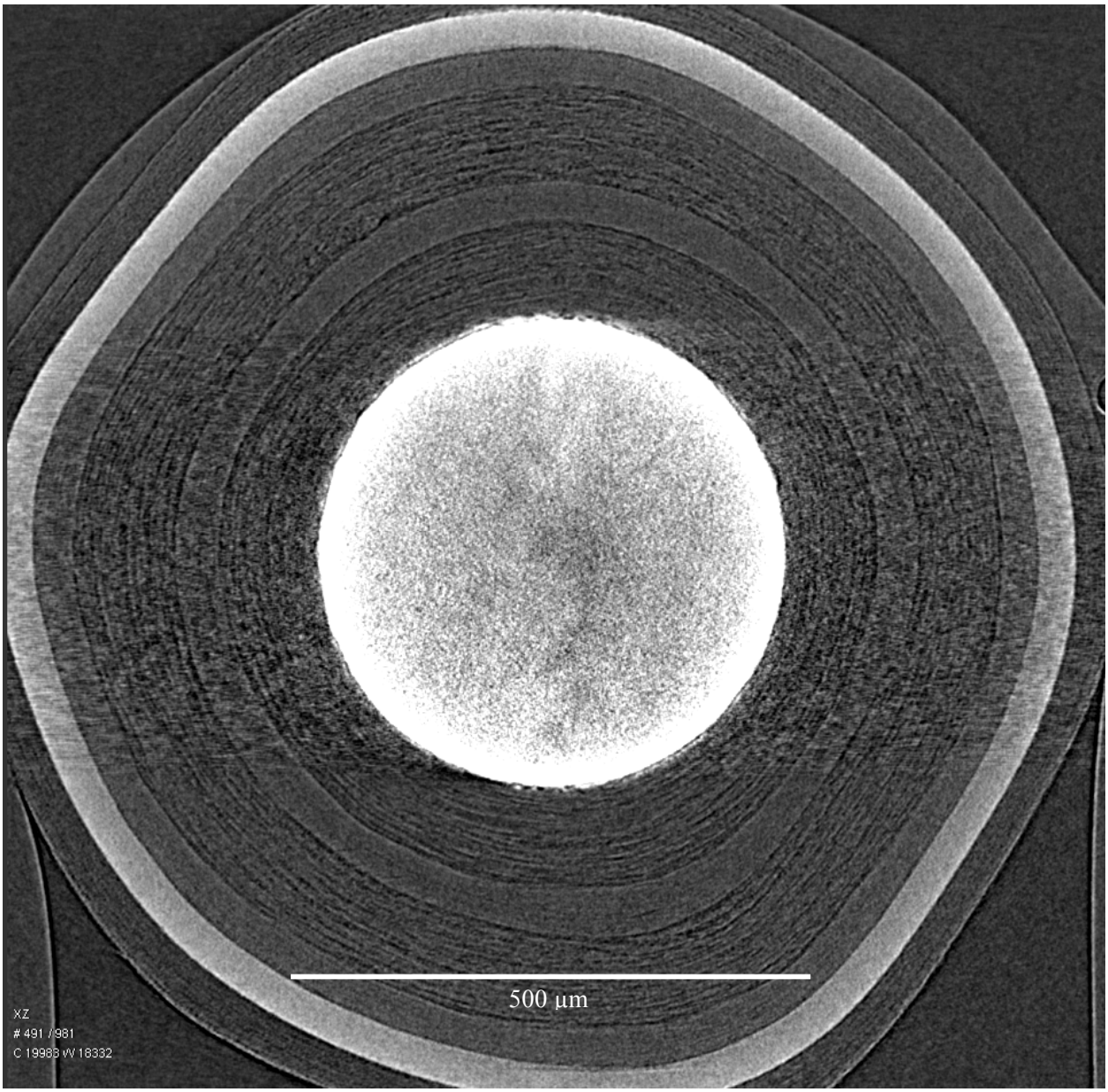

Figure 4-9. Tomographic cross-section of a particle with extra buffer and IPyC layers.

While some anomalous particles were missing layers, a small number were coated with additional layers, including extra buffer and IPyC layers (Figure 4-9) or extra outer layers (Figure 4-10 and Figure 4-11). Several of these particles were identified throughout the coated particle batches analyzed, but it is possible that more were present which were not identified. Particles with extra buffer and SiC layers were identifiable in low-resolution radiographs due to either a significant increase in particle diameter (extra buffer), or a significant increase in x-ray attenuation (extra SiC). In contrast, particles with extra IPyC or OPyC layers would not necessarily be identifiable in low-resolution radiographs as the increase in particle diameter would be within the range of normal variation, and the increase in attenuation would be negligible. It is known whether these anomalous particles would have a negative impact on fuel performance, and structural analysis to determine their impact is beyond the current scope of work. Related anomalous particles which consisted of TRISO coatings on soot or other non-kernel material

(Figure 4-12) would not impact fuel performance because of the lack of any fission product generating material.

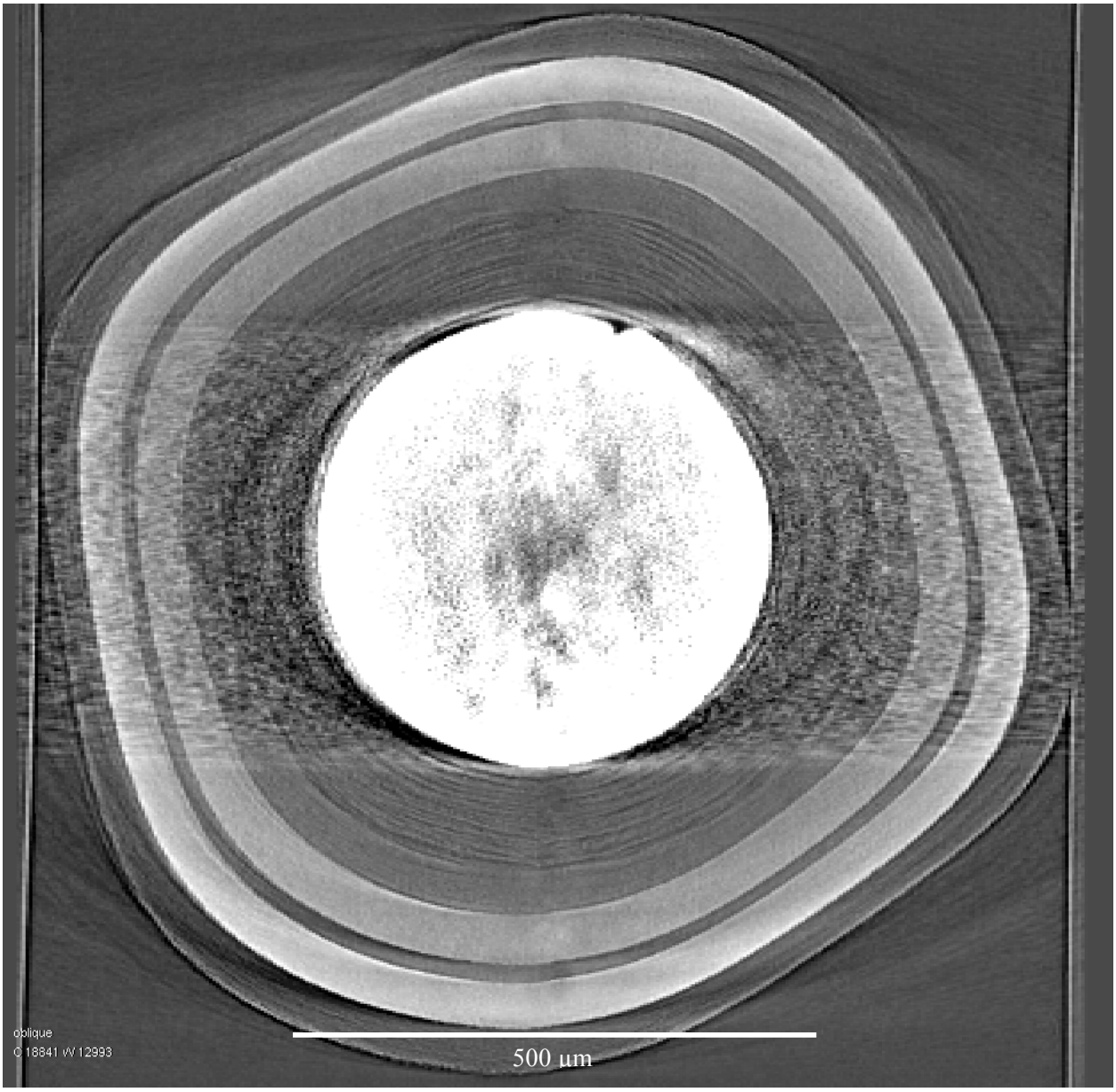

Figure 4-10. Tomographic cross-section of a particle with extra outer layers.

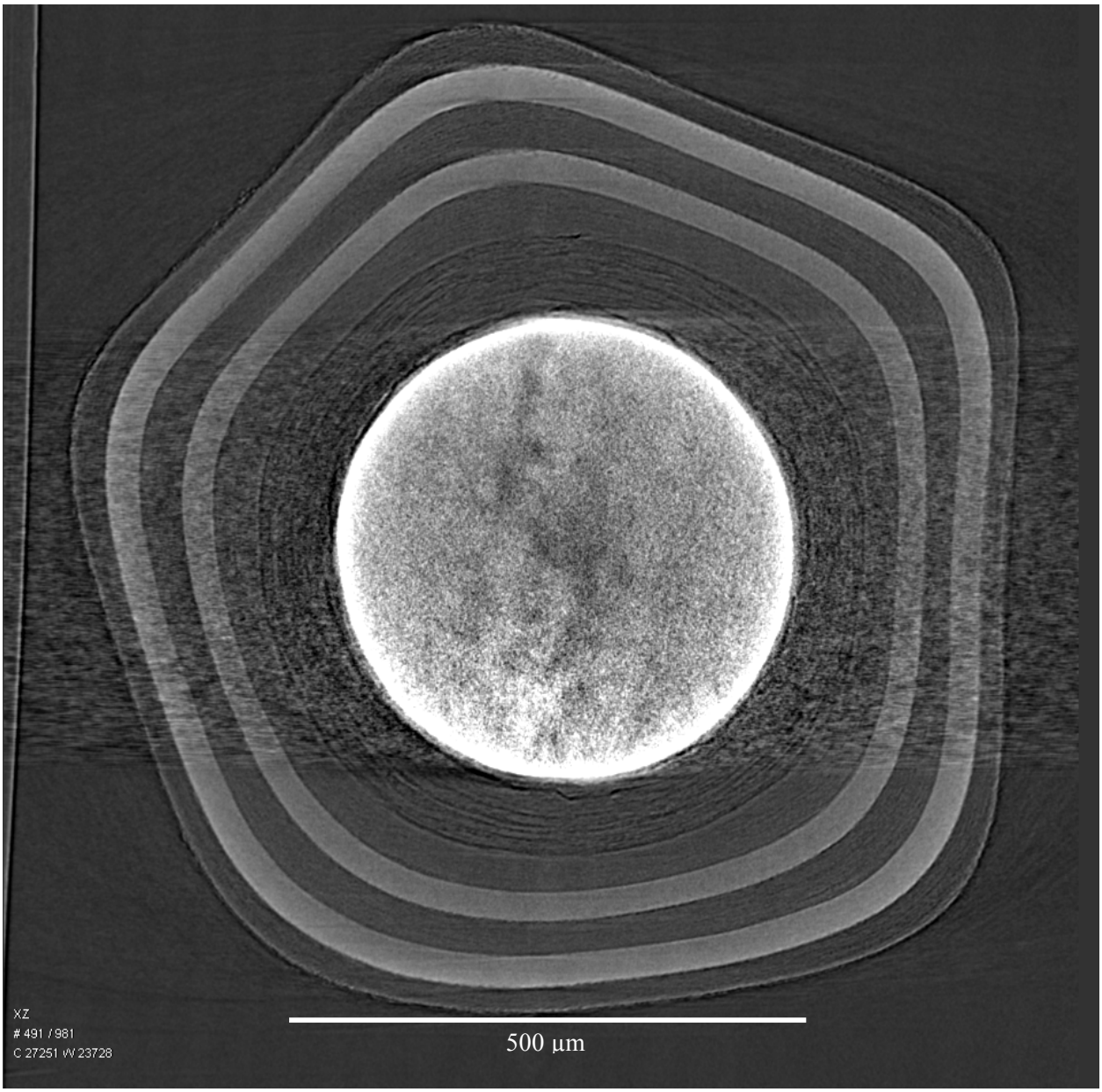

Figure 4-11. Tomographic cross-section of a particle with extra SiC and OPyC layers.

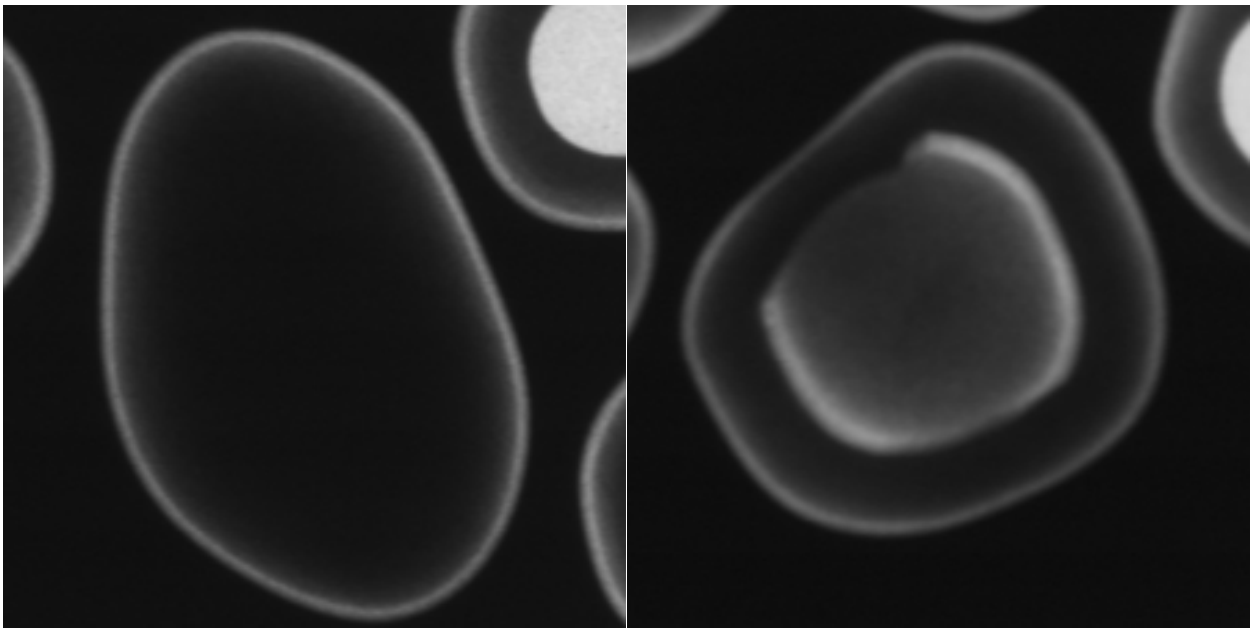

Figure 4-12. Radiographs of particles without kernels.

5. CONCLUSION

The analyses called out in the ORNL Product Inspection Plan for AGR-5/6/7 Coated Particles, PIP-28, was completed as part of the acceptance testing of BWXT TRISO-coated particle Batches 93164A, 93165A, 93166RA, 93168A, 93169A, 93170A, 93172A and BWXT TRISO-coated composite 98005. During this analysis, particles with uranium dispersion that is a marker for Defective IPyC layers were identified along with several other particle anomalies based on low-resolution radiography. Further analysis was performed on these particles using high-resolution x-ray tomography to provide additional information regarding the nature of these defects and anomalies.

Particles with uranium dispersion were classified into three categories: relatively symmetric dispersion out to the buffer/IPyC interface that was assumed to be related to abnormally-permeable IPyC, dispersion due to particles with a missing or structurally-defective IPyC layer, and localized dispersion due to embedded kernel fragments. The variation in the observed fraction of particles with uranium dispersion in each batch was found to be primarily due to kernel-fragment related dispersion, indicating the importance of minimizing the presence of kernel fragments during the coating process. Particles with localized uranium dispersion were not counted as having Defective IPyC when determining whether the AGR-5/6/7 fuel composite (J52R-16-98005) satisfied the specified limit on the Defective IPyC fraction. This was based on the understanding that the source of this dispersion was distinct from HCl infiltration of abnormally-permeable IPyC layers which the Defective IPyC specification seeks to control. However, the presence and population of particles with embedded kernel fragments was recorded as it may impact understanding of the performance of the fuel during the irradiation test and subsequent safety testing.

A wide range of particle anomalies were identified and inspected as an added-value analysis during the x-ray radiography primarily performed for determination of the Defective IPyC fraction. Several of the observed anomalies are of importance for fuel performance. Particles were identified with missing buffer layers, missing IPyC layers, and missing SiC layers. Particles with a missing buffer layer are likely to fail during irradiation due to kernel swelling. Secondary upgrading on batches selected for the composite used for the AGR-5/6/7 fuel compact fabrication was effective in removing these defects. Particles with missing IPyC layers were found to result in significant uranium dispersion. Particles with missing SiC layers are a source of defects identified by leach-burn-leach analysis. These particles with missing layers, as well as particles with extra layers or embedded fragments of TRISO layers from other particles, indicate that particles are exiting and entering the active coating region of the fluidized-bed chemical vapor deposition furnace in an unpredictable manner during the deposition of TRISO coating layers.

Several anomalies were identified which were related to fragmented or fissured kernels. These irregular kernels sometimes led to severe dimpling of the coating layers, creating stress-concentration points which may lead to fuel failure. In addition, loose kernel fragments during coating were found to be embedded in the buffer layer, sometimes leading to uranium dispersion, or in the other coating layers, which would result in partial kernel inventories of leached uranium in the LBL analysis. Other anomalies which were identified are useful as a feedback to particle fabrication, but are not expected to affect fuel performance.

6. REFERENCES

Hanson, D. 2009. *Technical Basis for NGNP Fuel Performance and Quality Requirements.* GA-911168. San Diego, California: General Atomics.

Helmreich, G.W., J.D. Hunn, D.J. Skitt, J.A. Dyer, A.T. Schumacher. 2017. *Acceptance Test Data for the AGR-5/6/7 Irradiation Test Fuel Composite—Defective IPyC Fraction and Pyrocarbon Anisotropy.* ORNL/TM-2017-037. Oak Ridge, Tennessee: Oak Ridge National Laboratory.

Helmreich, G.W. and J.D. Hunn. 2016. *Standard Operating Guideline: Xradia MicroXCT*. AGR-CHAR-SOG-22, Revision 0. Oak Ridge, Tennessee: Oak Ridge National Laboratory.

Hunn, J.D. 2013. *Data Acquisition Method for Counting of TRISO Particles with Excessive Uranium Dispersion Inside SiC*. AGR-CHAR-DAM-47, Revision 0. Oak Ridge, Tennessee: Oak Ridge National Laboratory.

Hunn, J.D. 2016. *Product Inspection Plan for AGR-5/6/7 Coated Particles.* AGR-CHAR-PIP-28, Revision 1. Oak Ridge, Tennessee: Oak Ridge National Laboratory.

Hunn, J.D., G.W. Helmreich, D.J. Skitt, J.A. Dyer, A.T. Schumacher. 2017. *Acceptance Test Data for Candidate AGR-5/6/7 TRISO Particle Batches.* ORNL/TM-2017-036. Oak Ridge, Tennessee: Oak Ridge National Laboratory.

Hunn, J.D., G.W. Helmreich, D.J. Skitt, J.A. Dyer. 2017. *Acceptance Test Data for BWXT Coated Particle Batch 93164A—Defective IPyC Fraction and Pyrocarbon Anisotropy*. ORNL/TM-2017-035. Oak Ridge, Tennessee: Oak Ridge National Laboratory.

Marshal, D.W. 2016. *AGR-5/6/7 Fuel Specification.* SPC-1352, Revision 7. Idaho Falls, Idaho: Idaho National Laboratory.

Petti, D.A., J.T. Maki, M.A. Ebner, G.K. Miller. 2004. *Preliminary AGR Fuel Specification.* EDF-4198, Revision 1. Idaho Falls, Idaho: Idaho National Laboratory.

Scheffel, W. and J. Saurwein. 2003. *Preliminary Fuel Product Specification for the Baseline Advanced Gas Reactor Fuel Design.* GA-911034. San Diego, California: General Atomics.

APPENDIX A. Images of Particles with Uranium Dispersion

Note: Low-resolution radiographs sharing a page with high-resolution tomographic projections are of the same particle.

A1. Particles from sample NP-C1349 of BWXT coating batch J52O-16-93164A

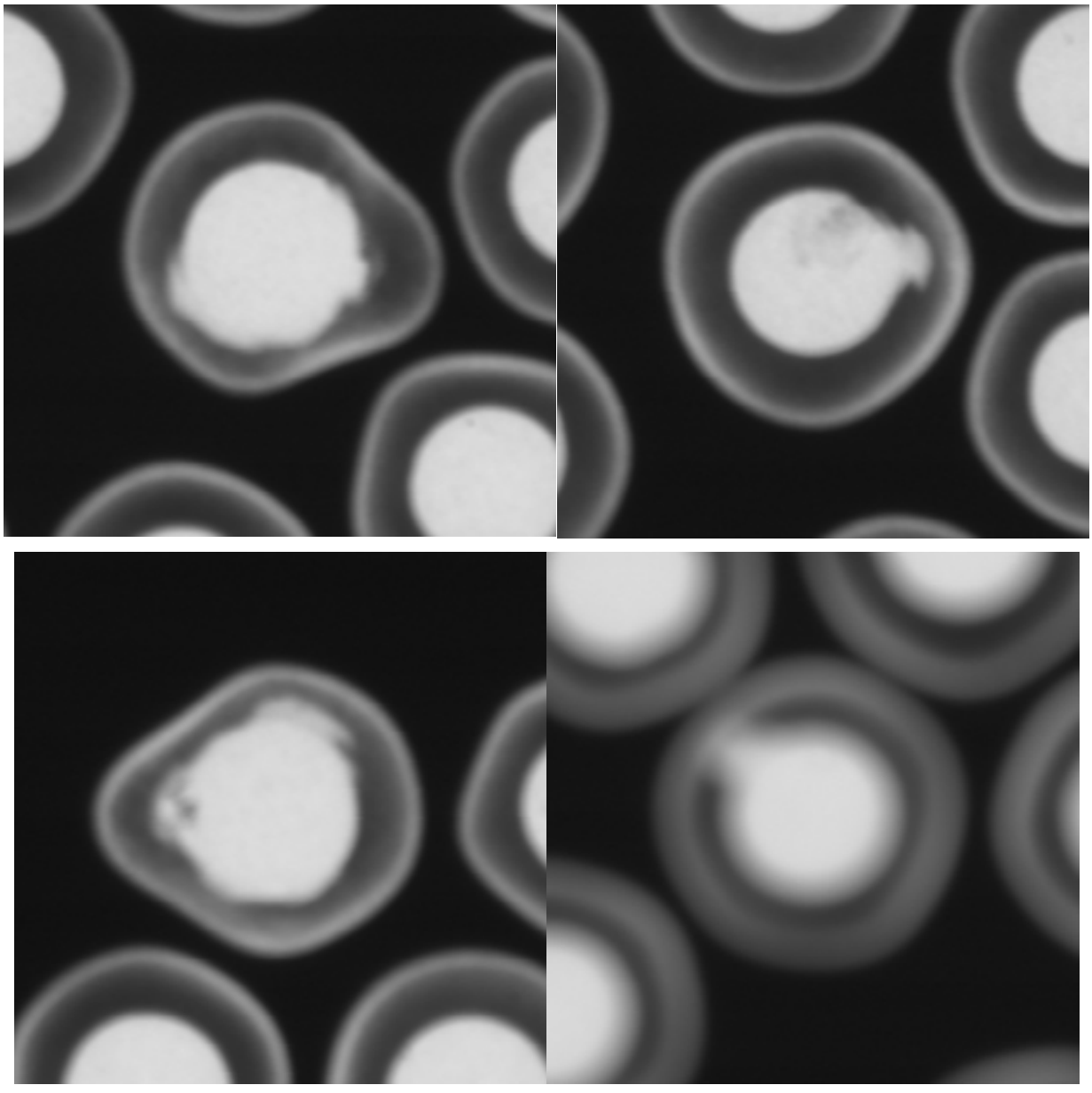

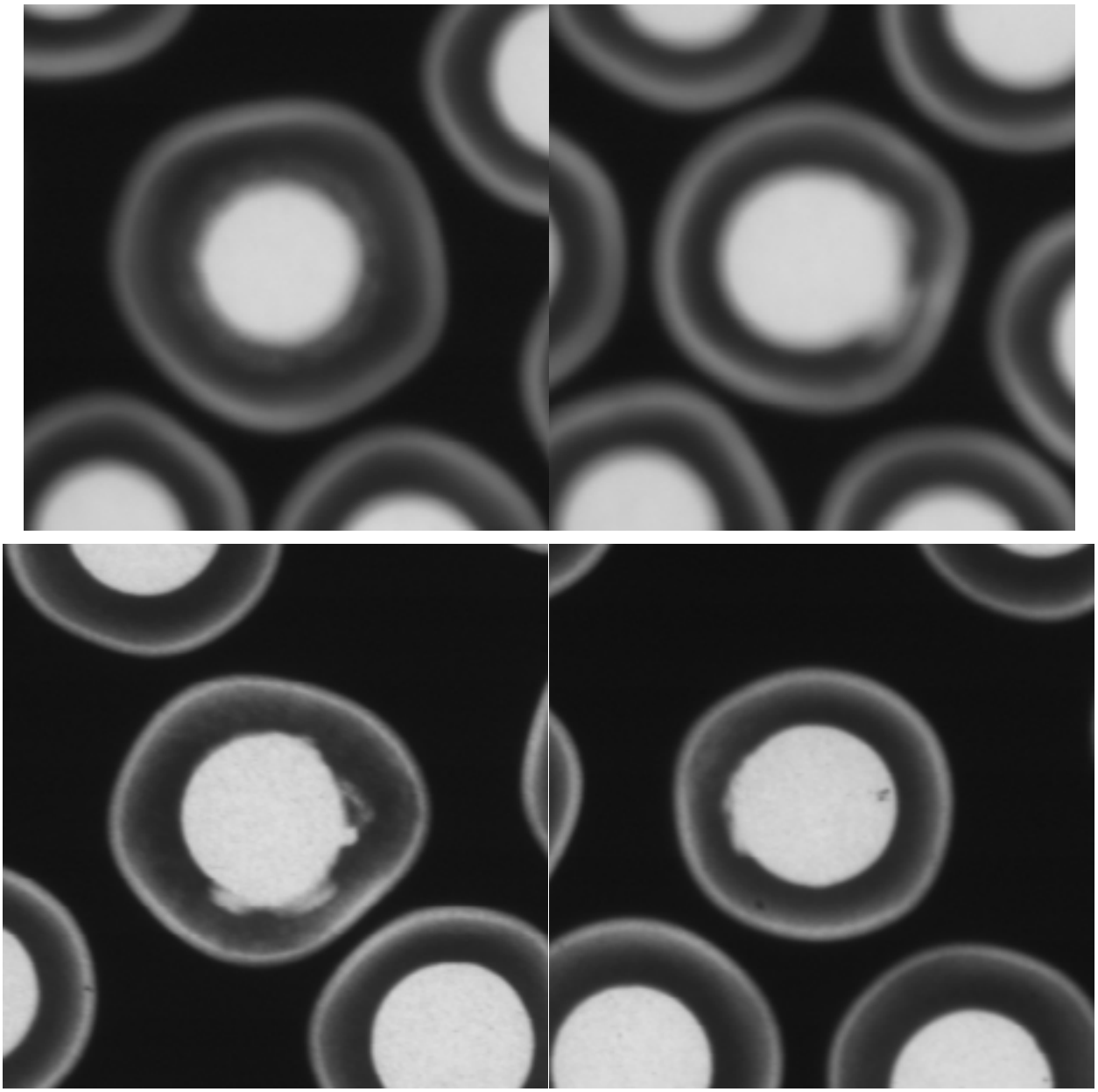

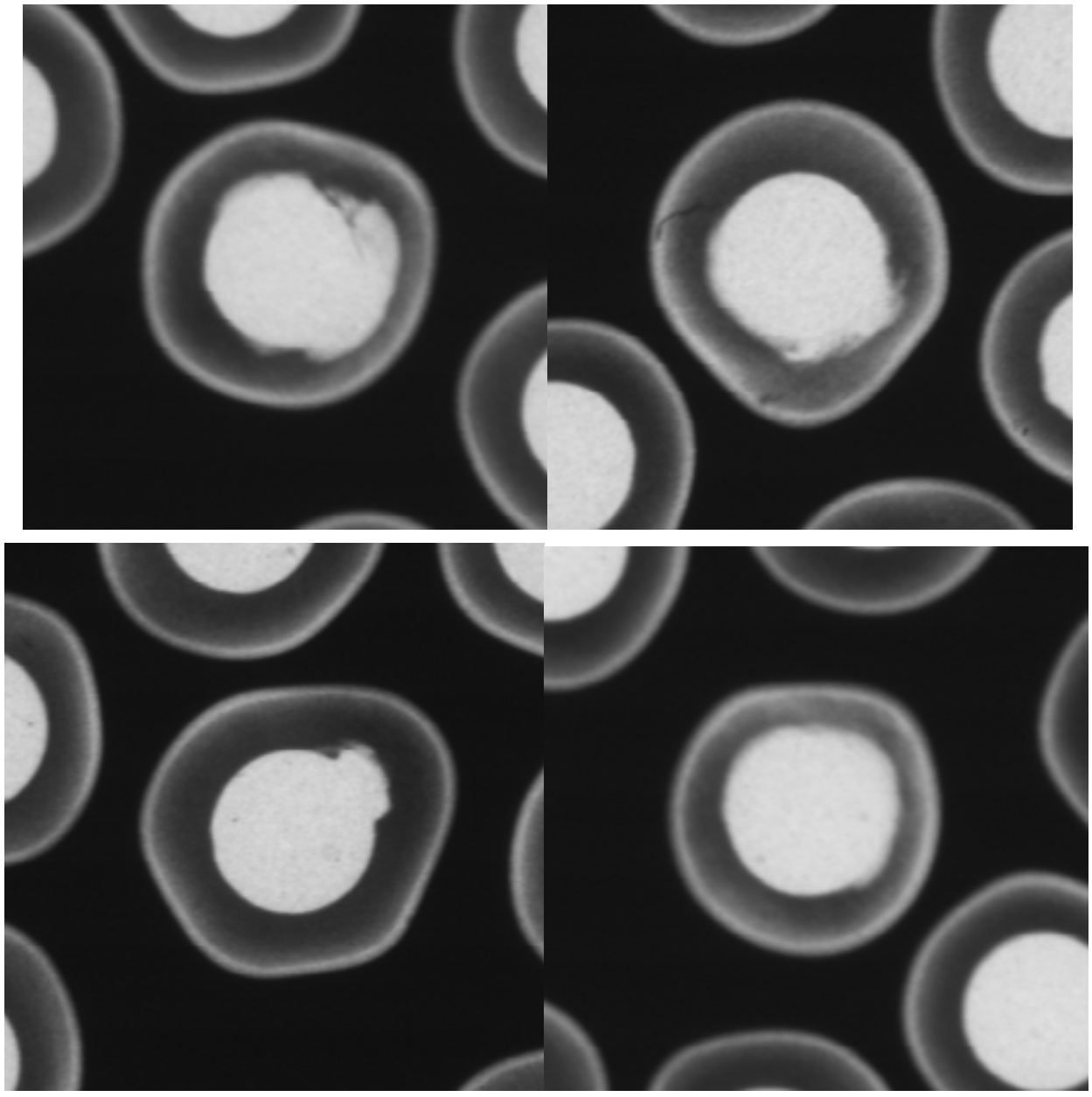

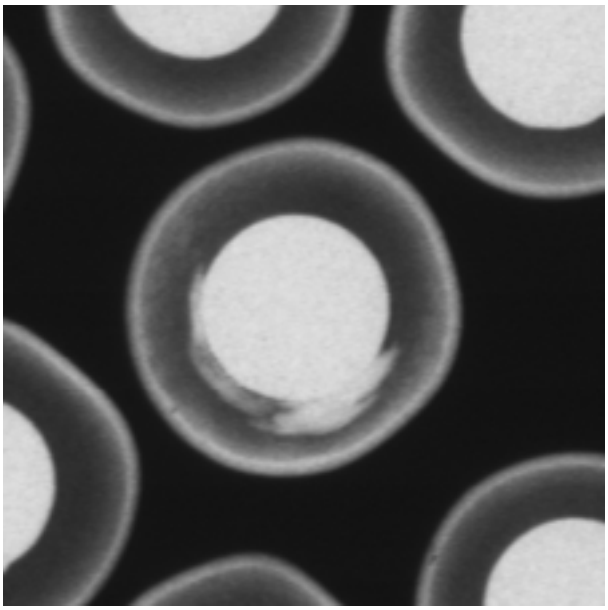

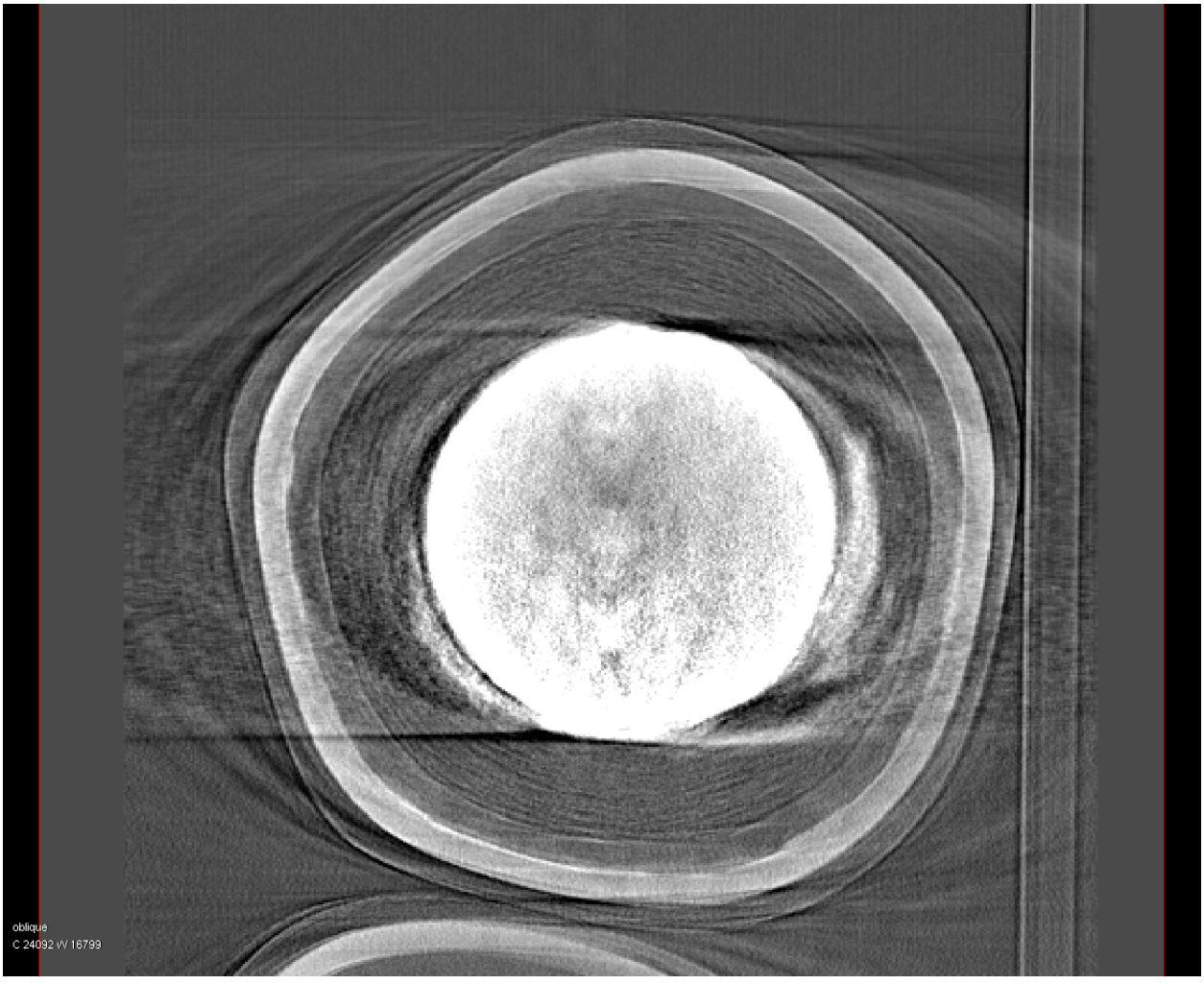
oblique
C 24092 W 16799

A2. Particles from sample NP-C1350 of BWXT coating batch J52O-16-93165A

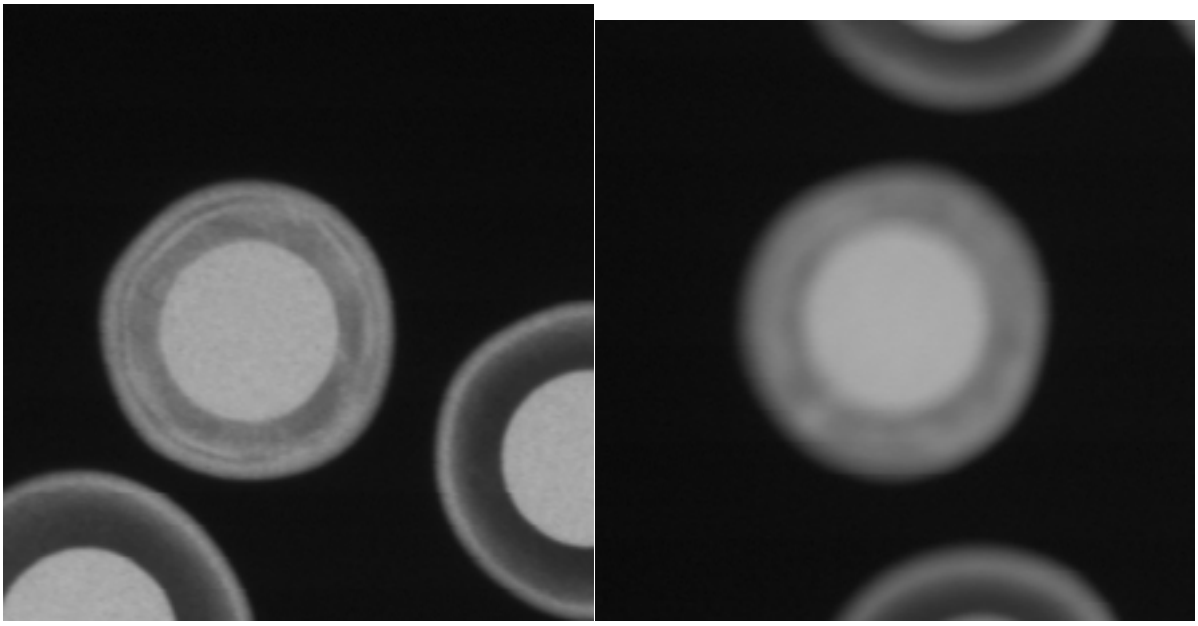

A3. Particles from sample NP-C1364 of BWXT coating batch J52O-16-93164A

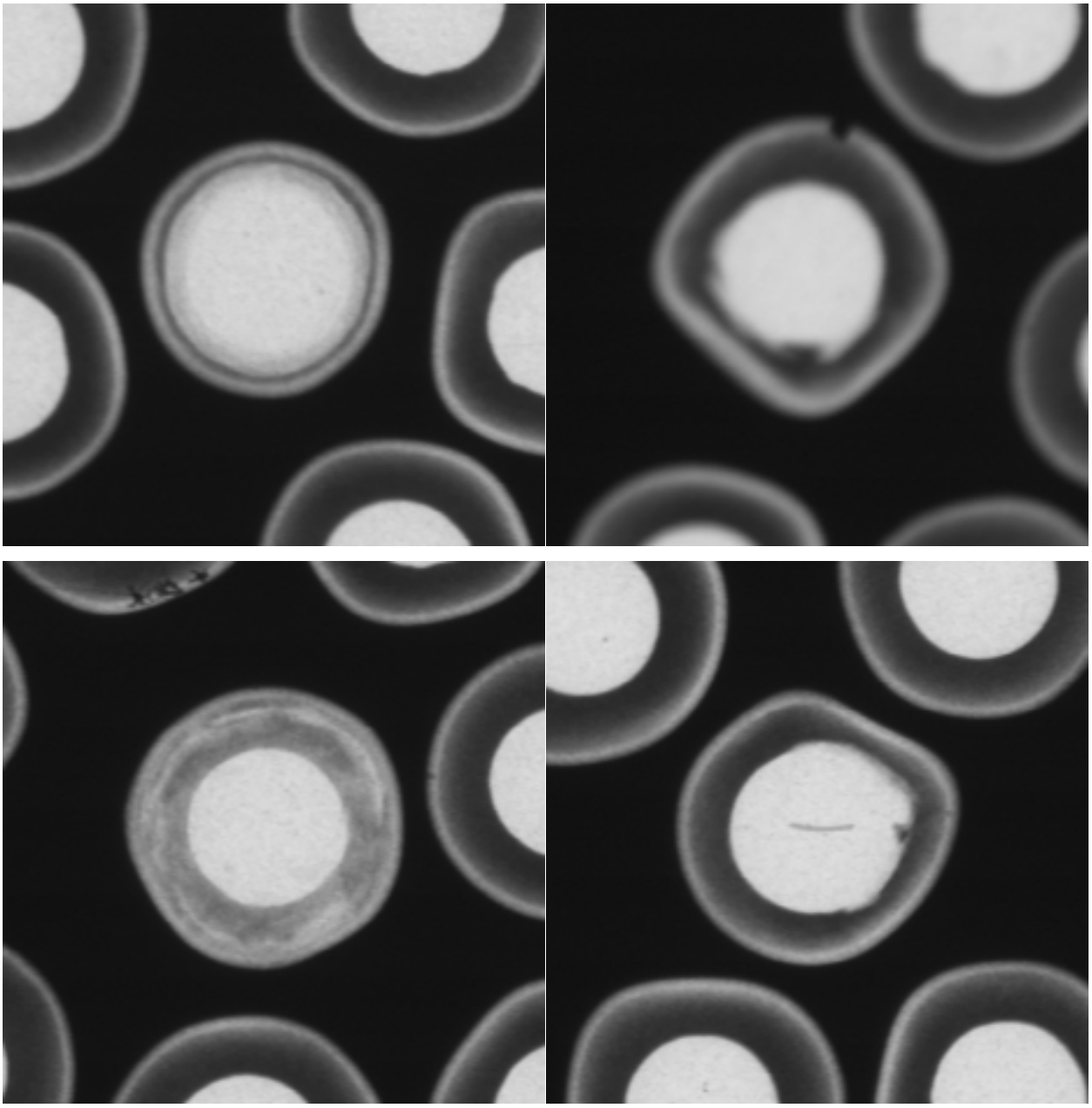

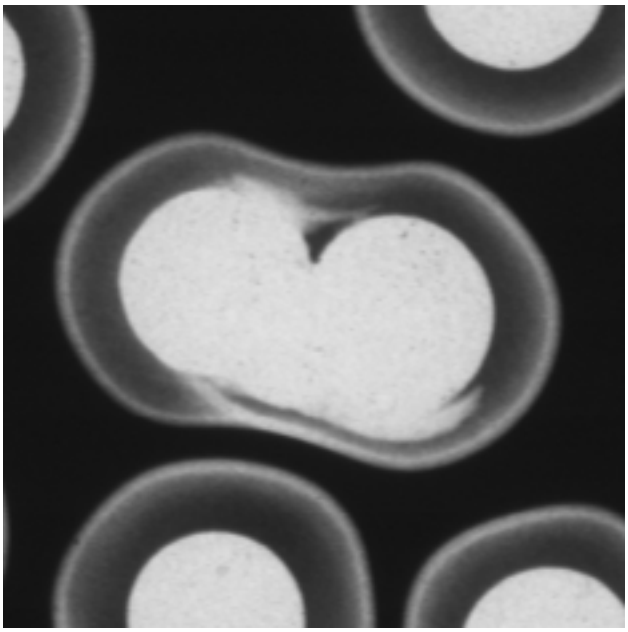


oblique
C 27418 vV 15495

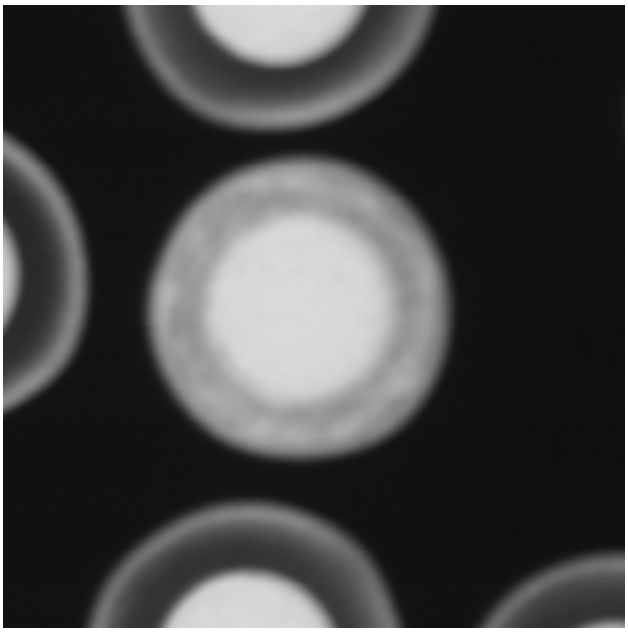

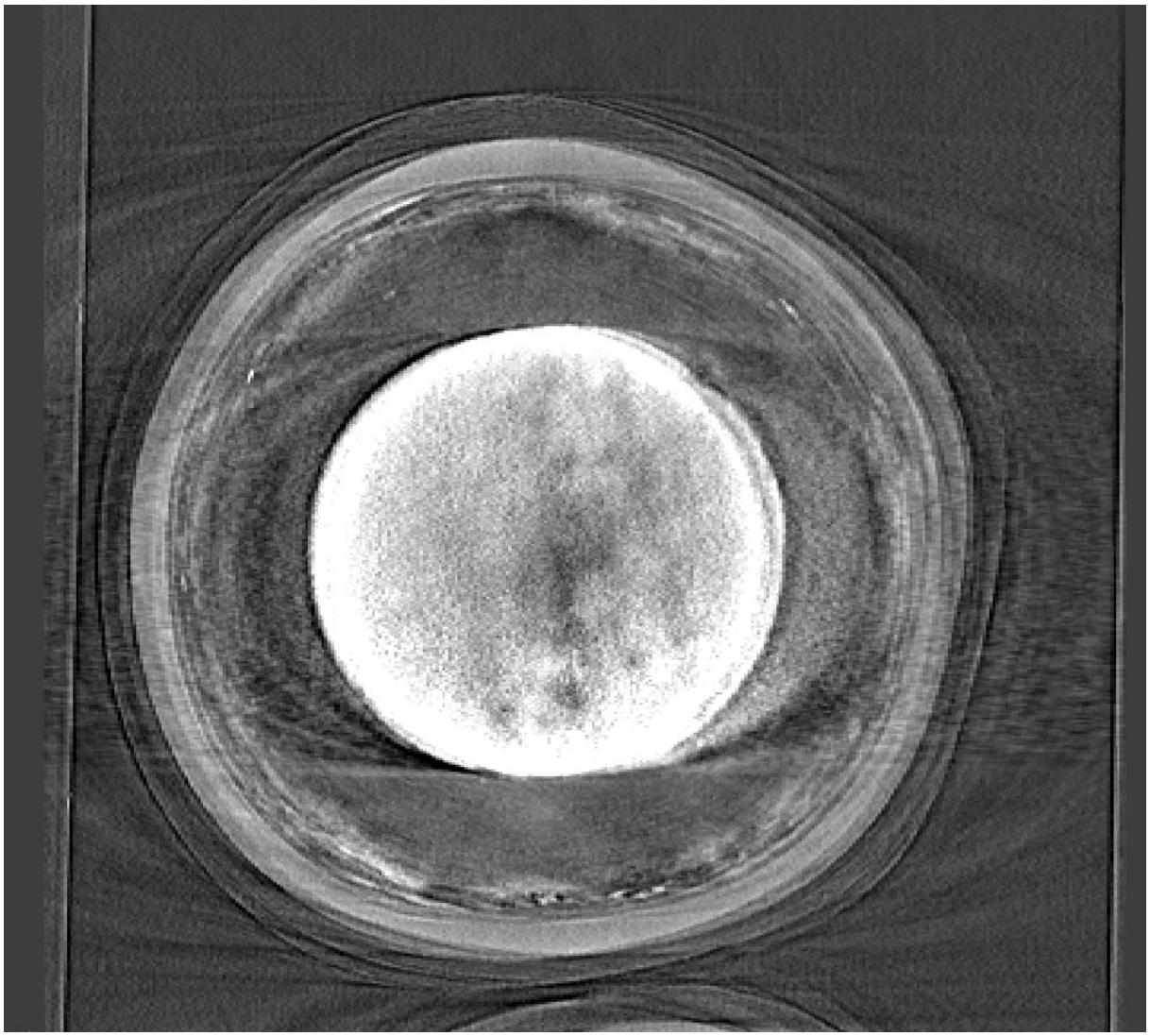

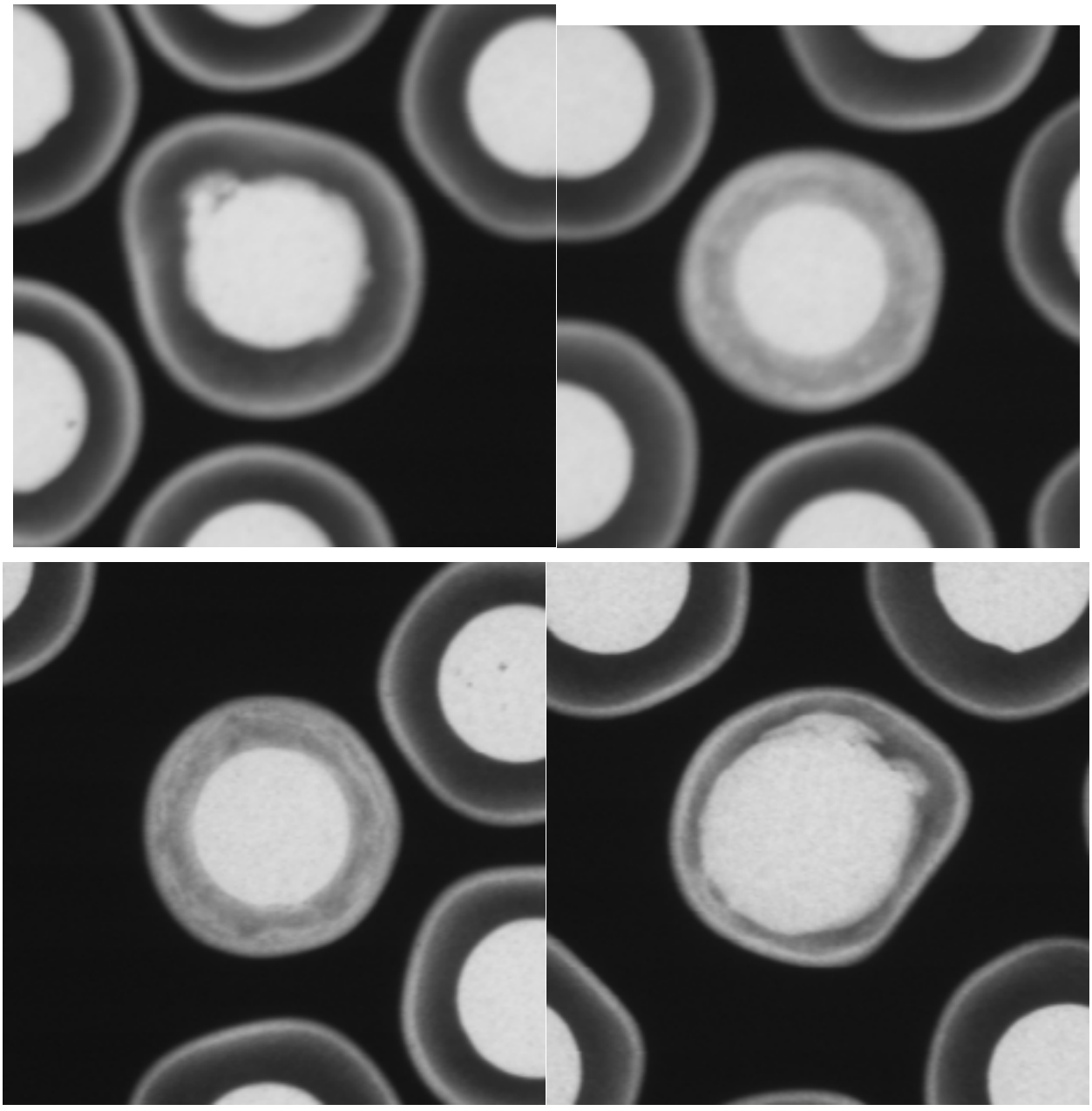

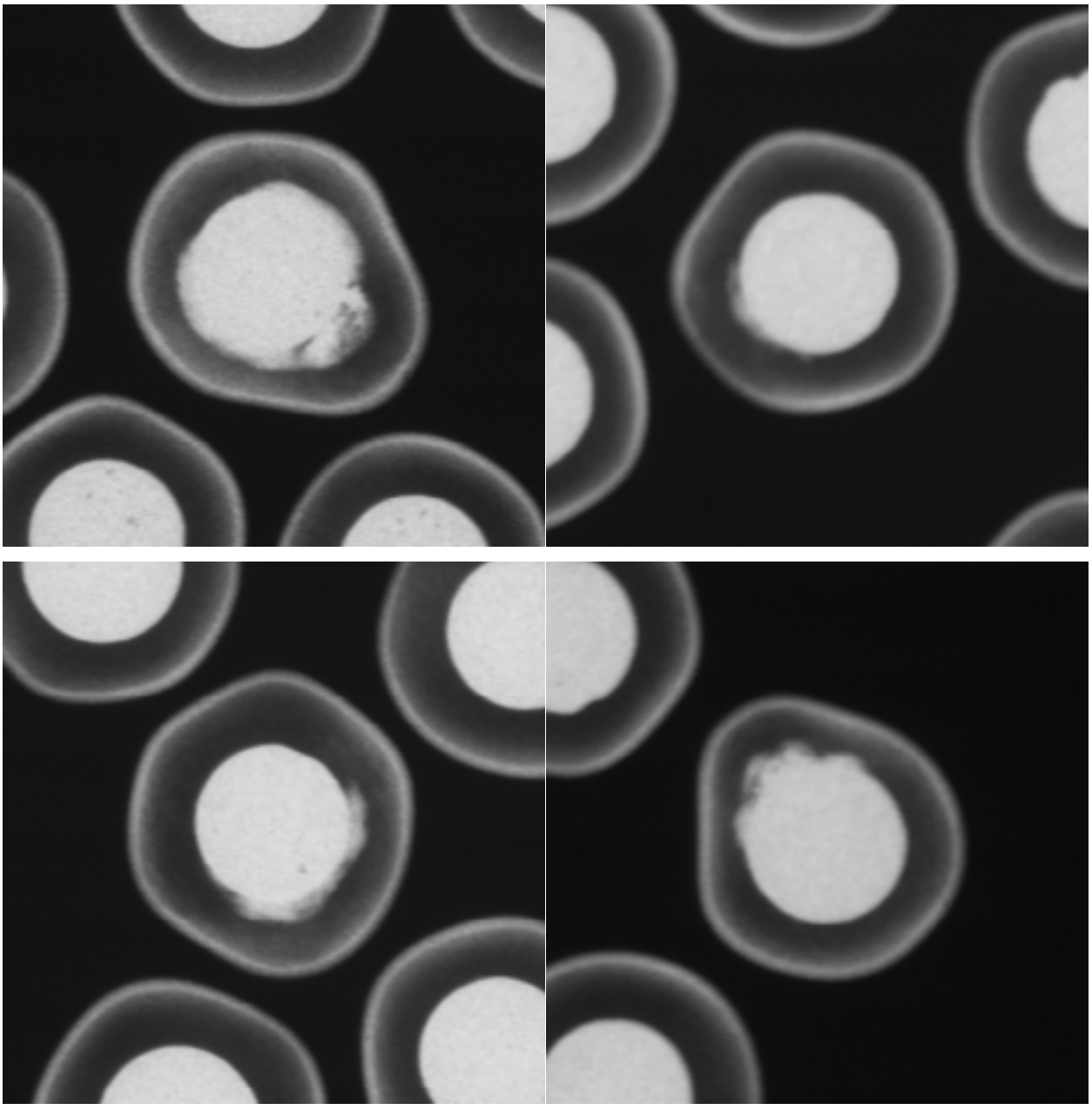

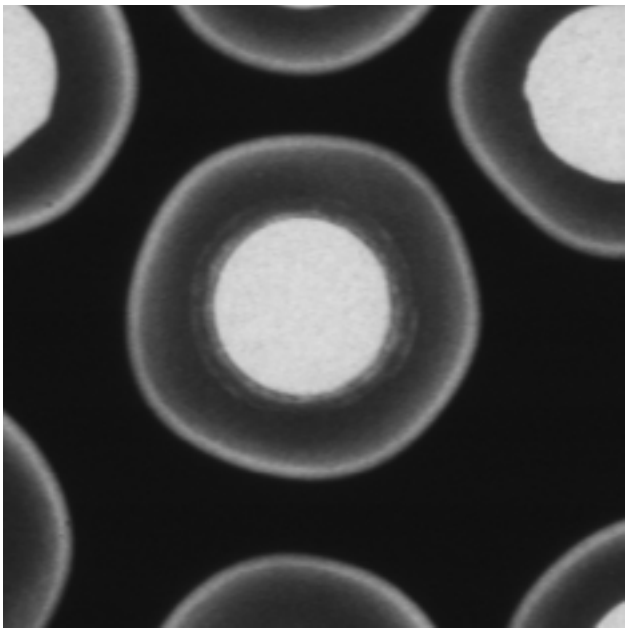

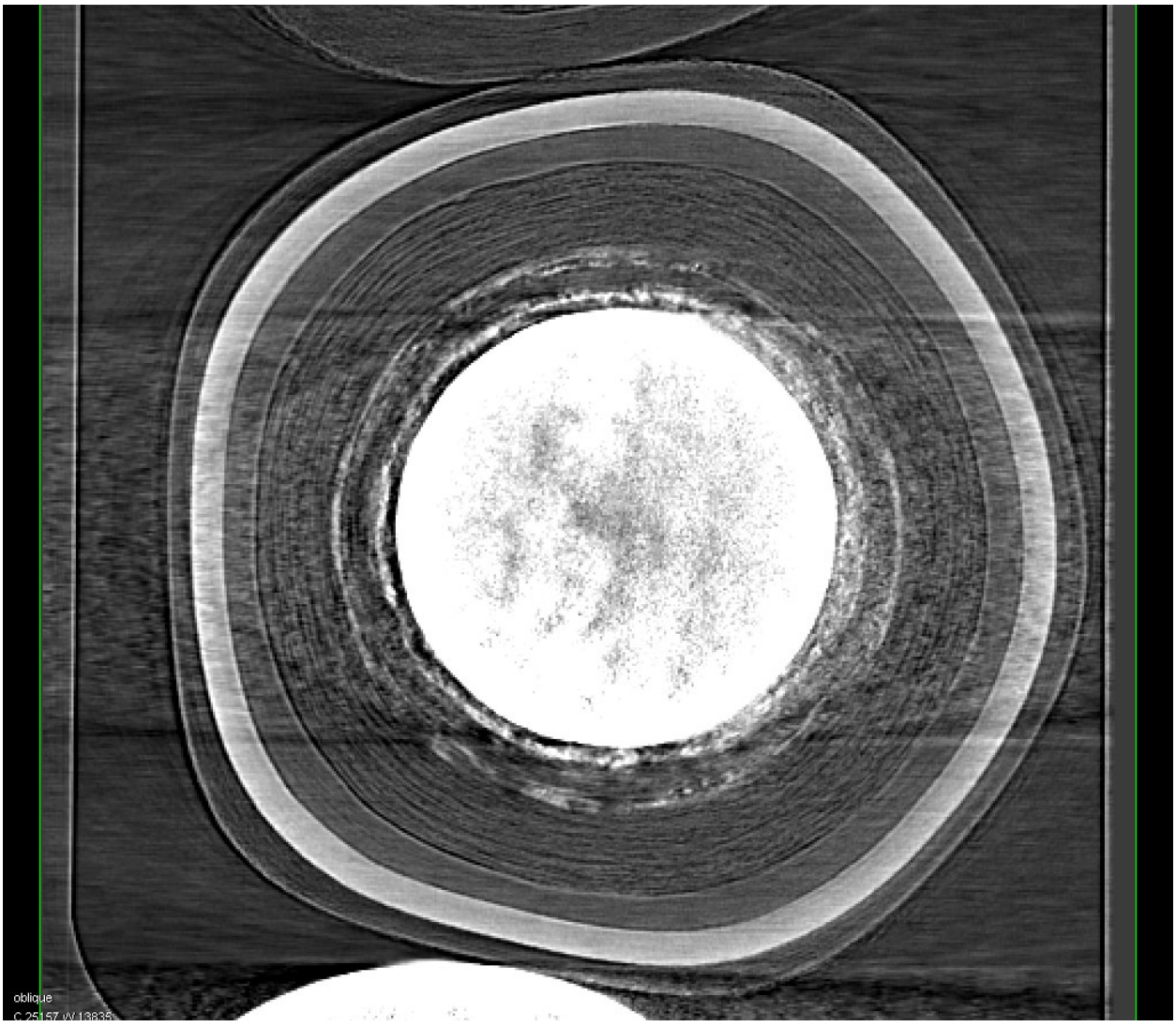
oblique

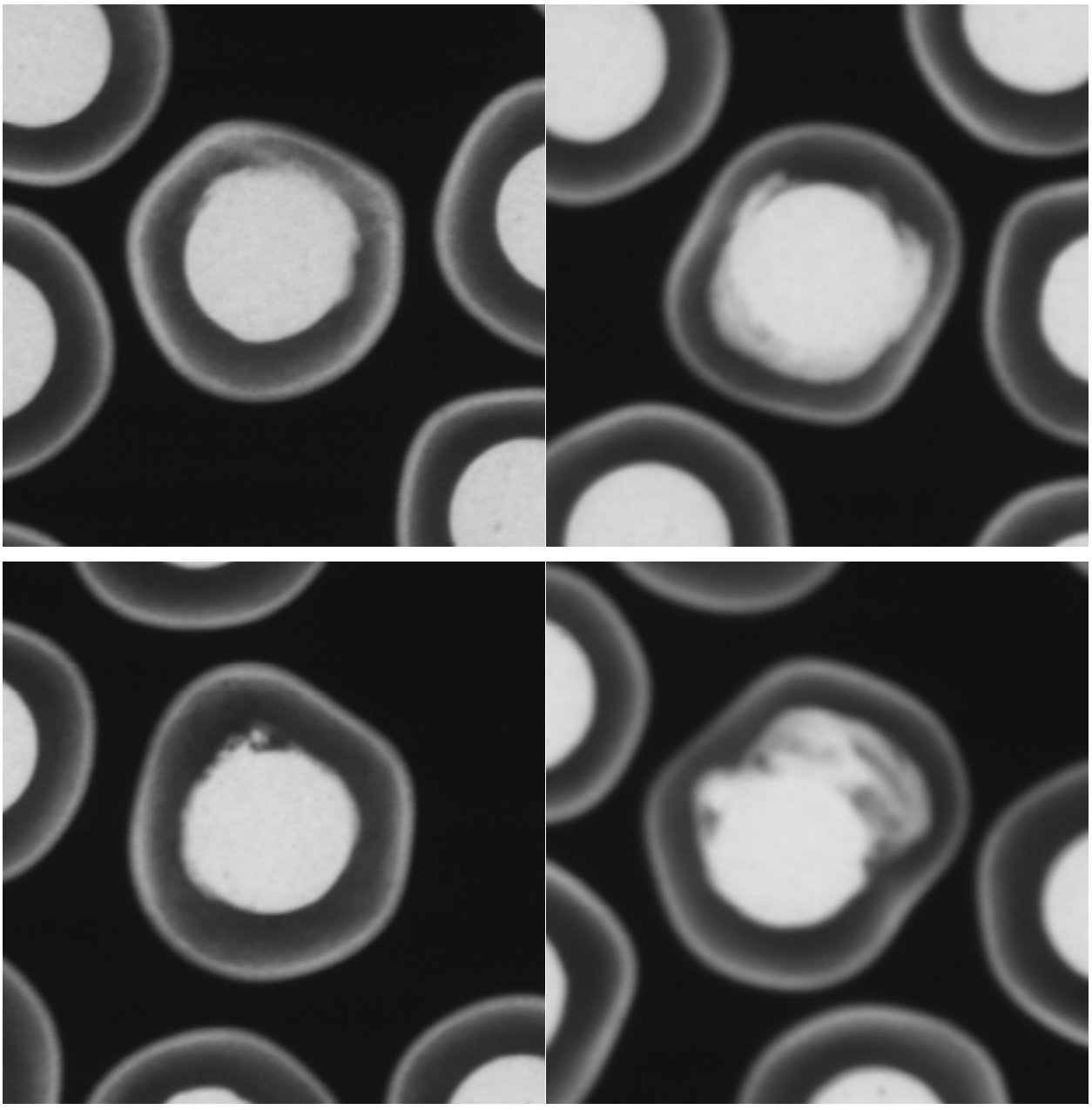

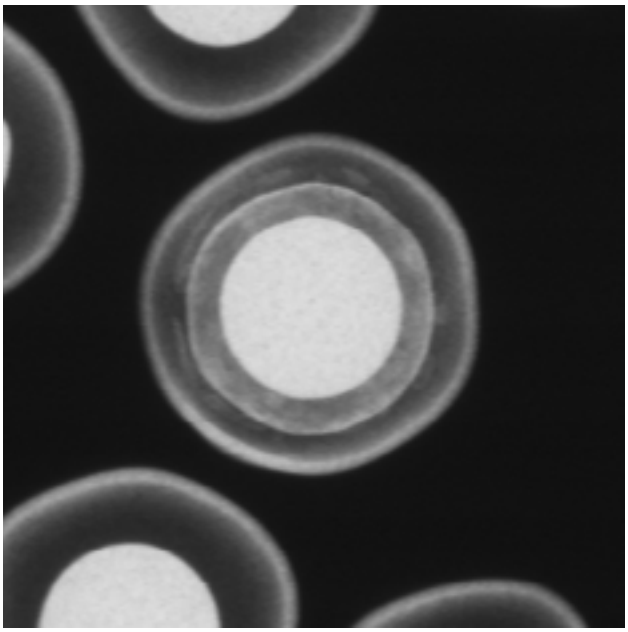

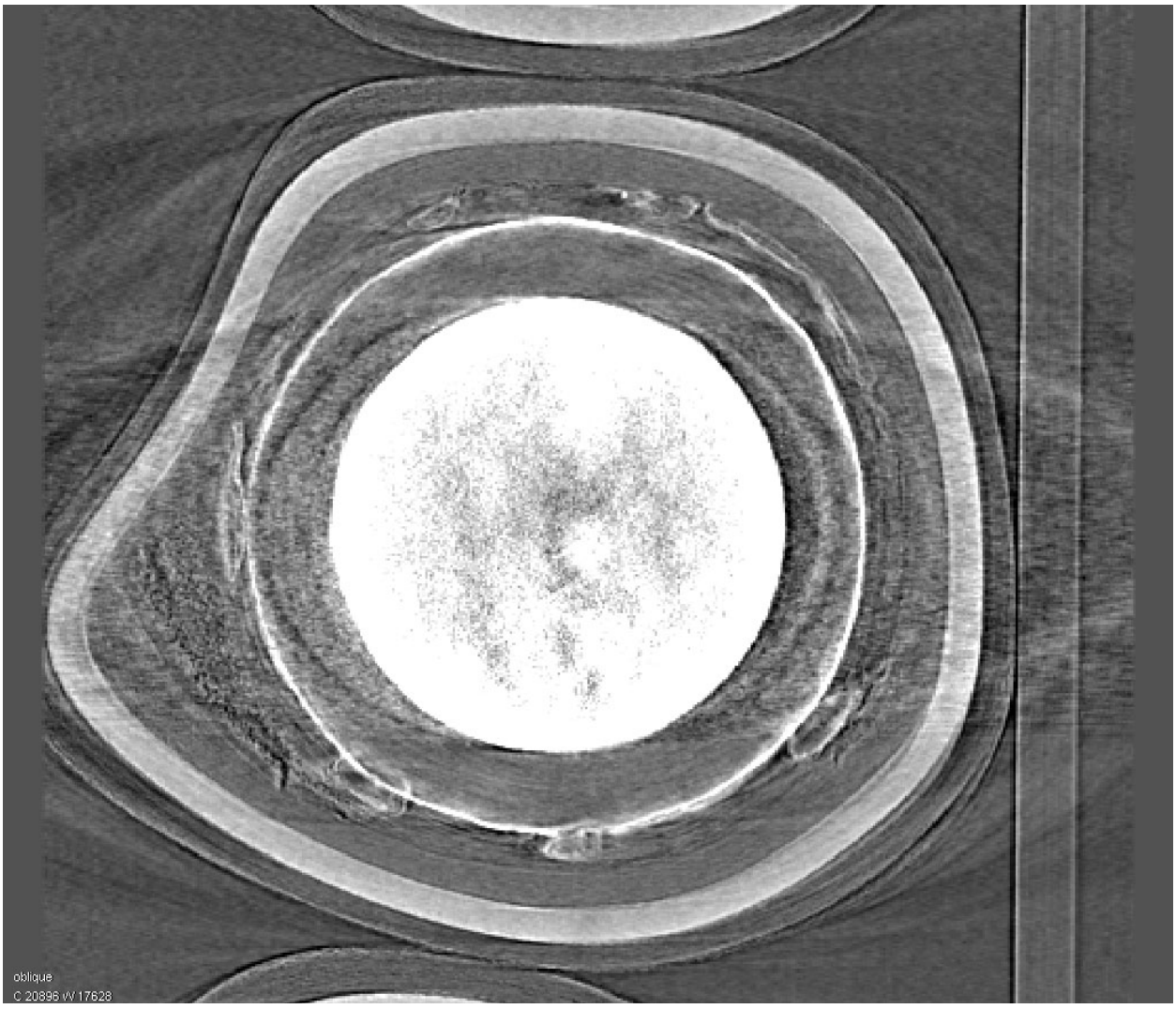
oblique
C 20895 W 17628

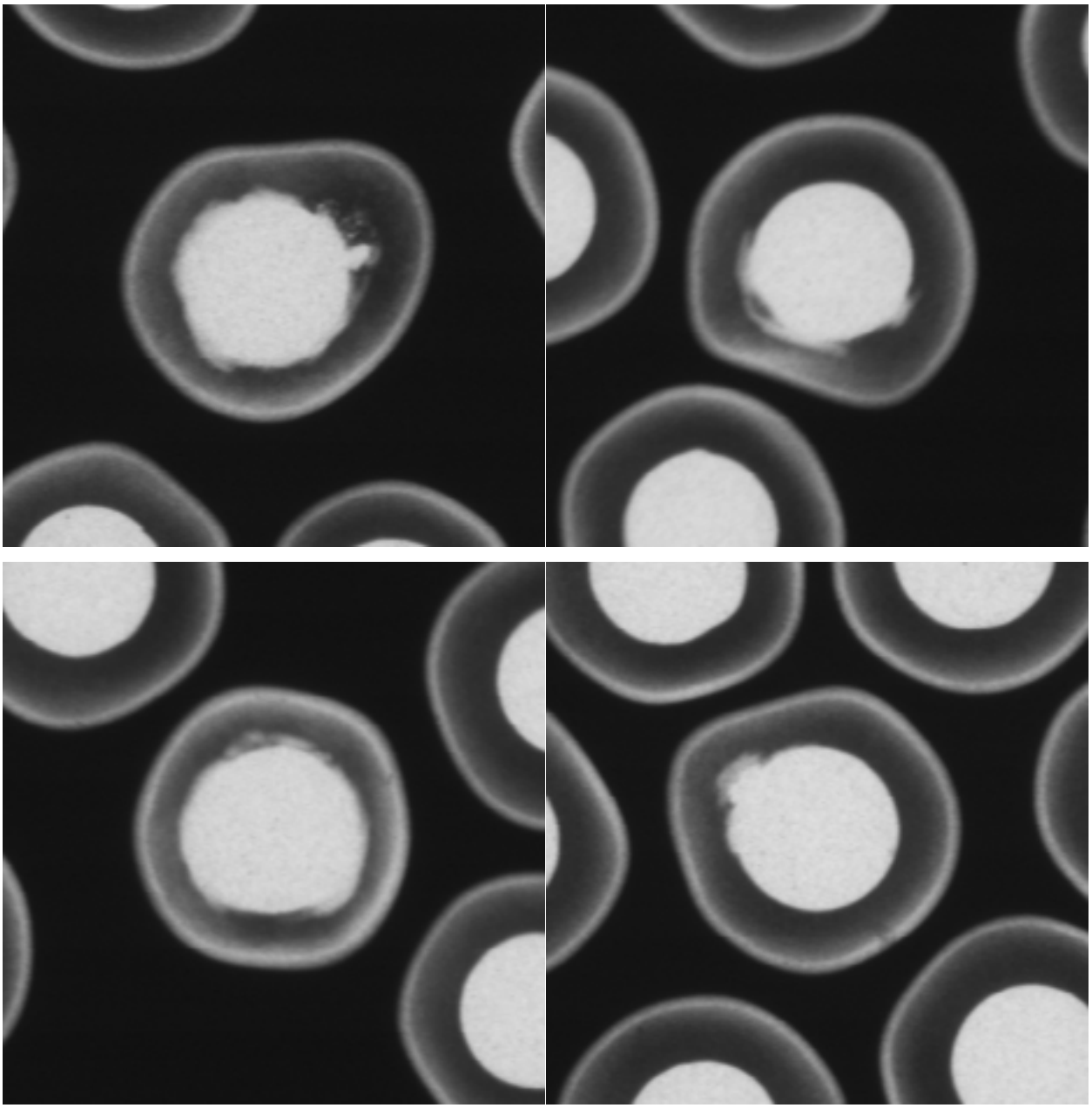

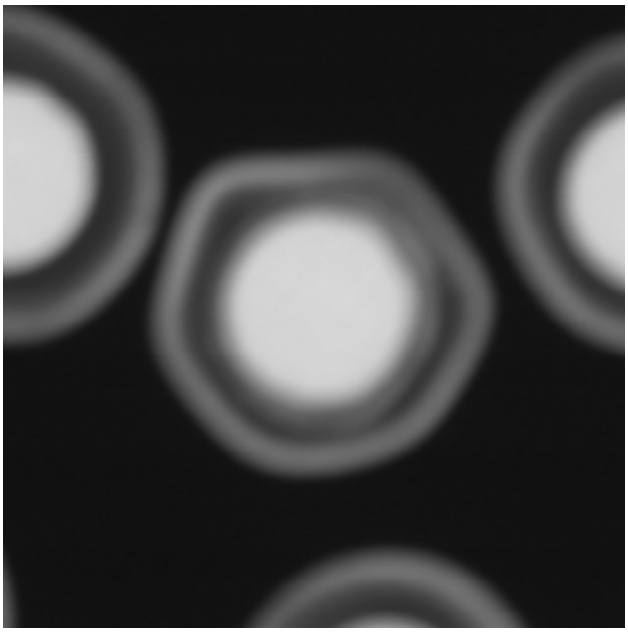

A4. Particles from sample NP-C1358 of BWXT coating batch J52O-16-93166RA

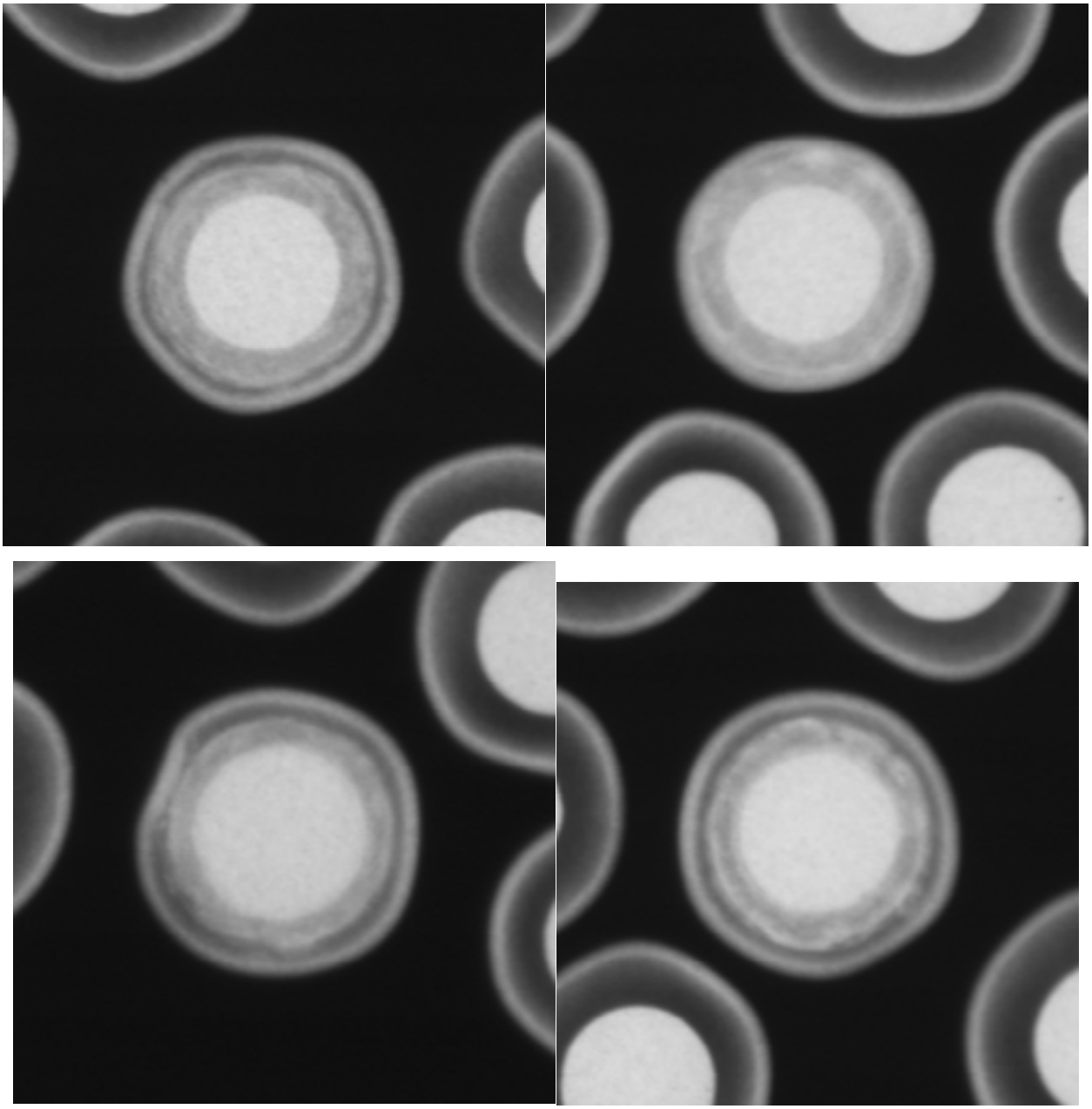

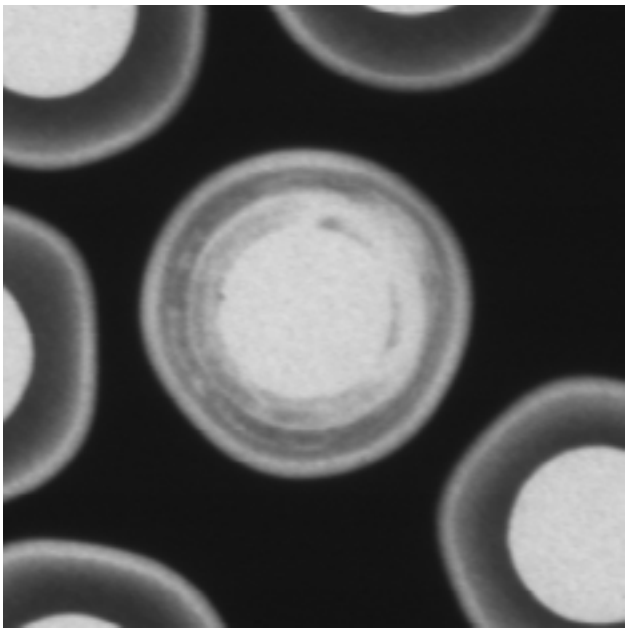

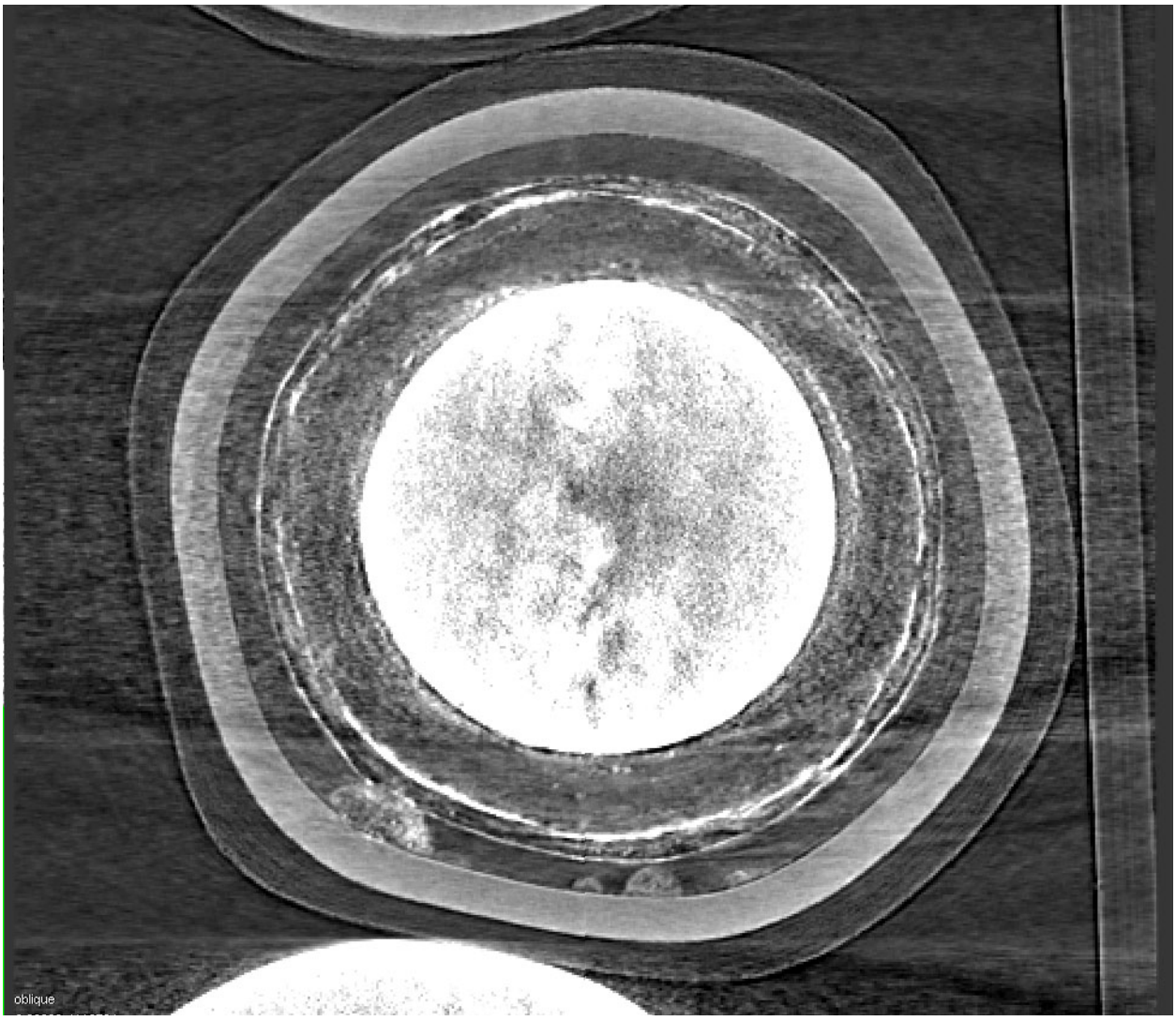
oblique

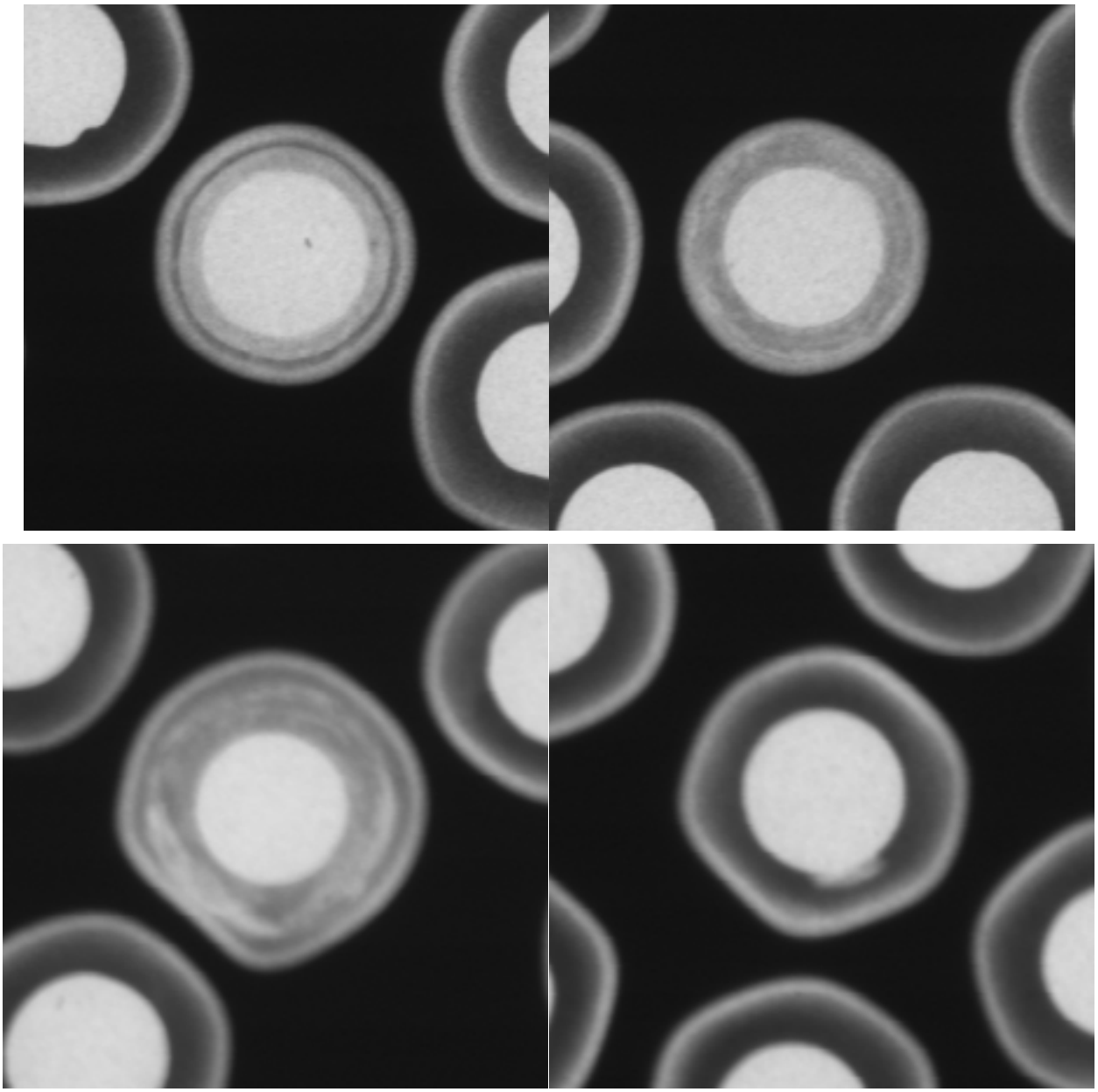

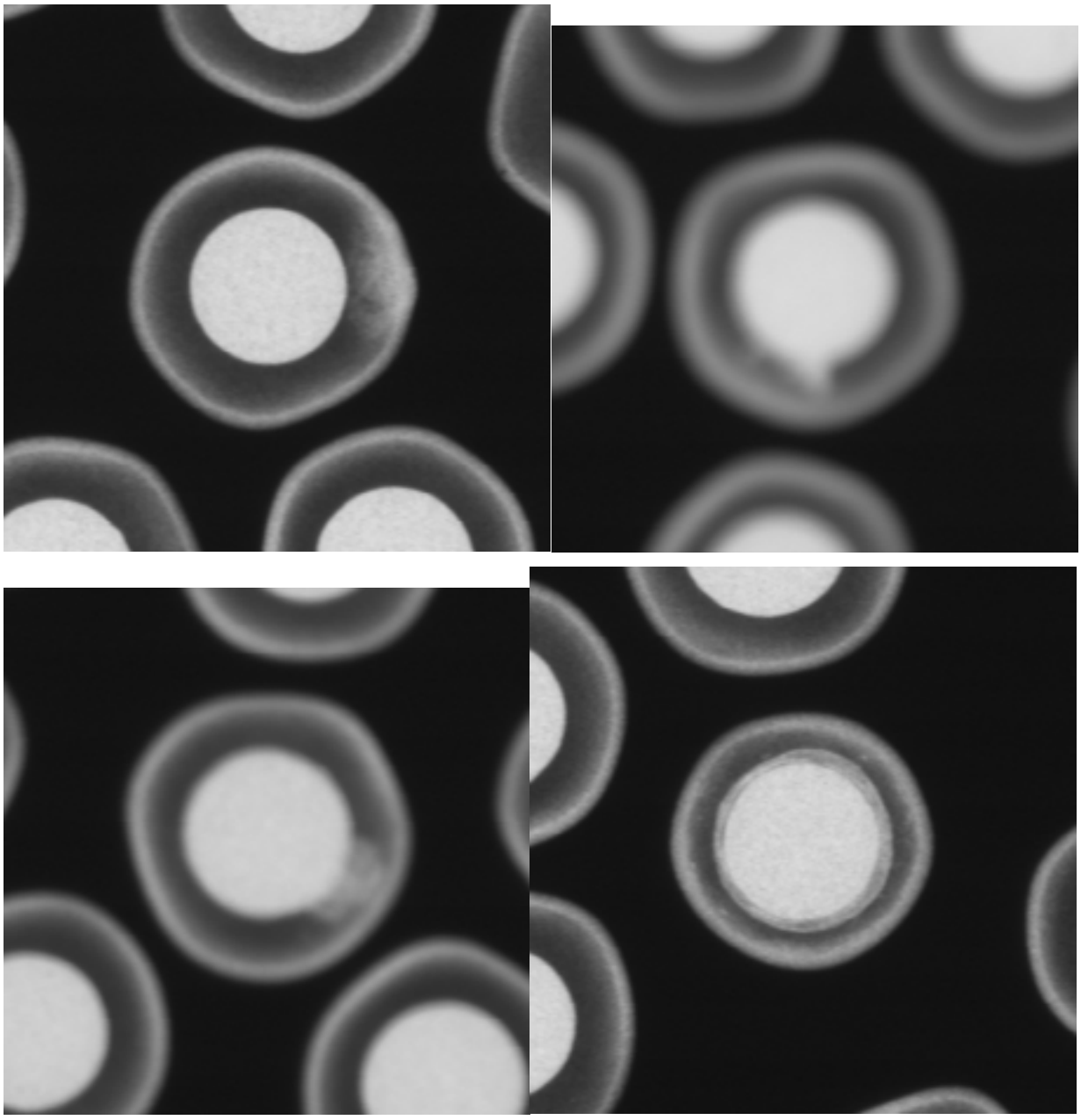

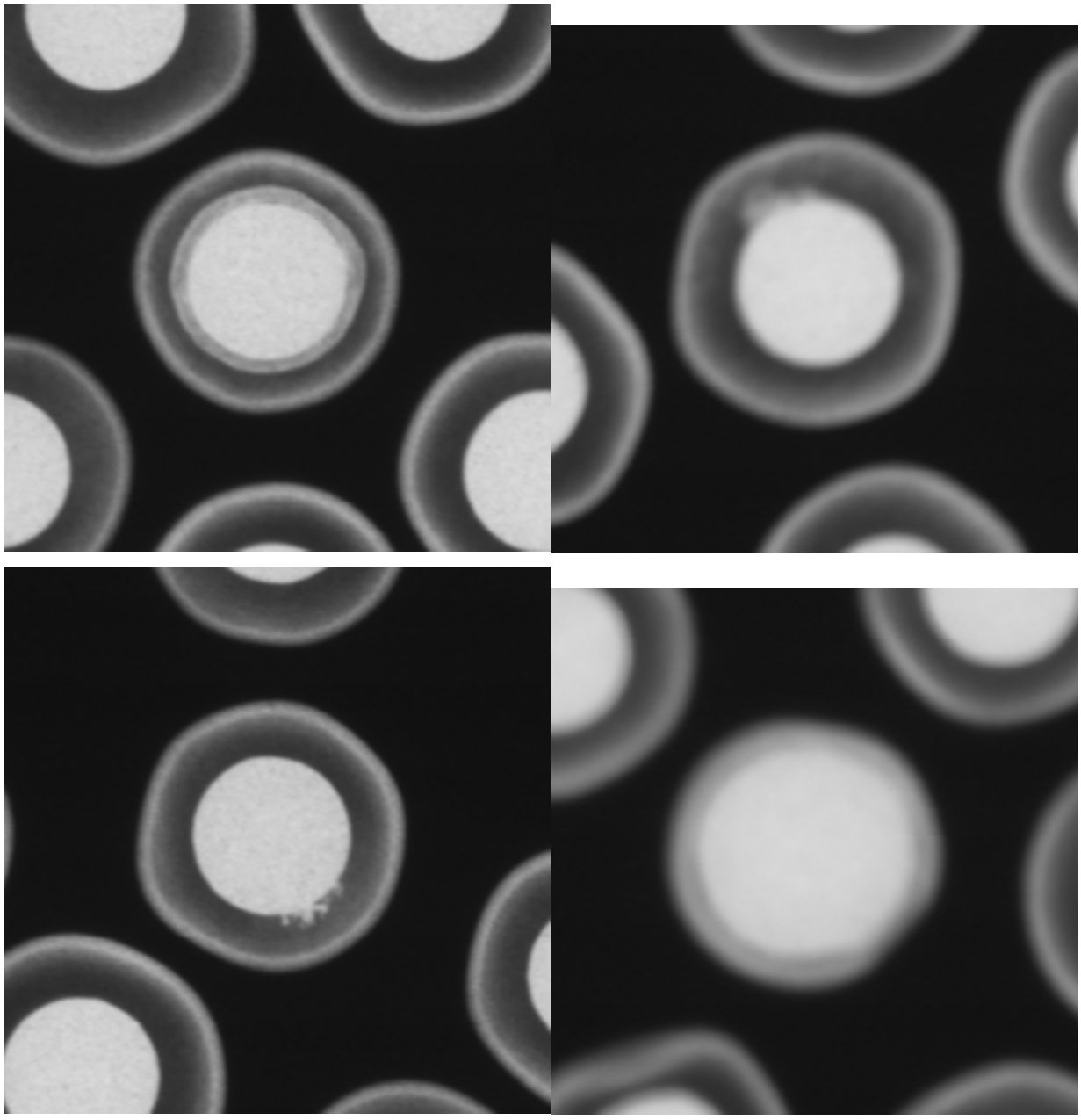

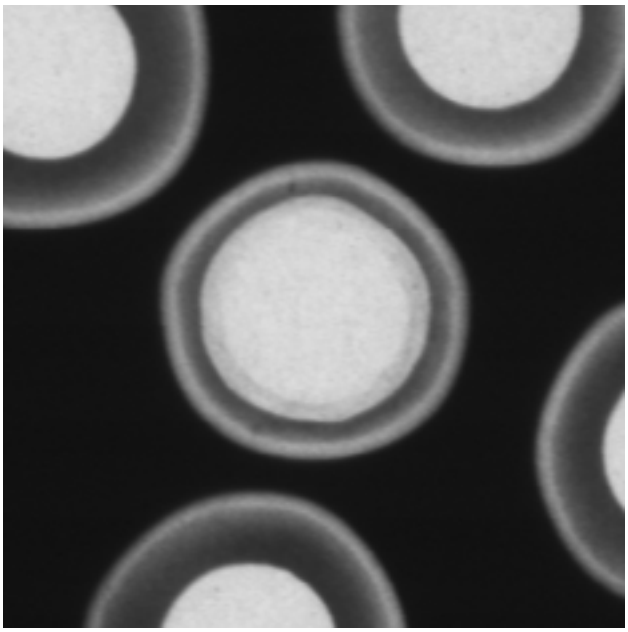

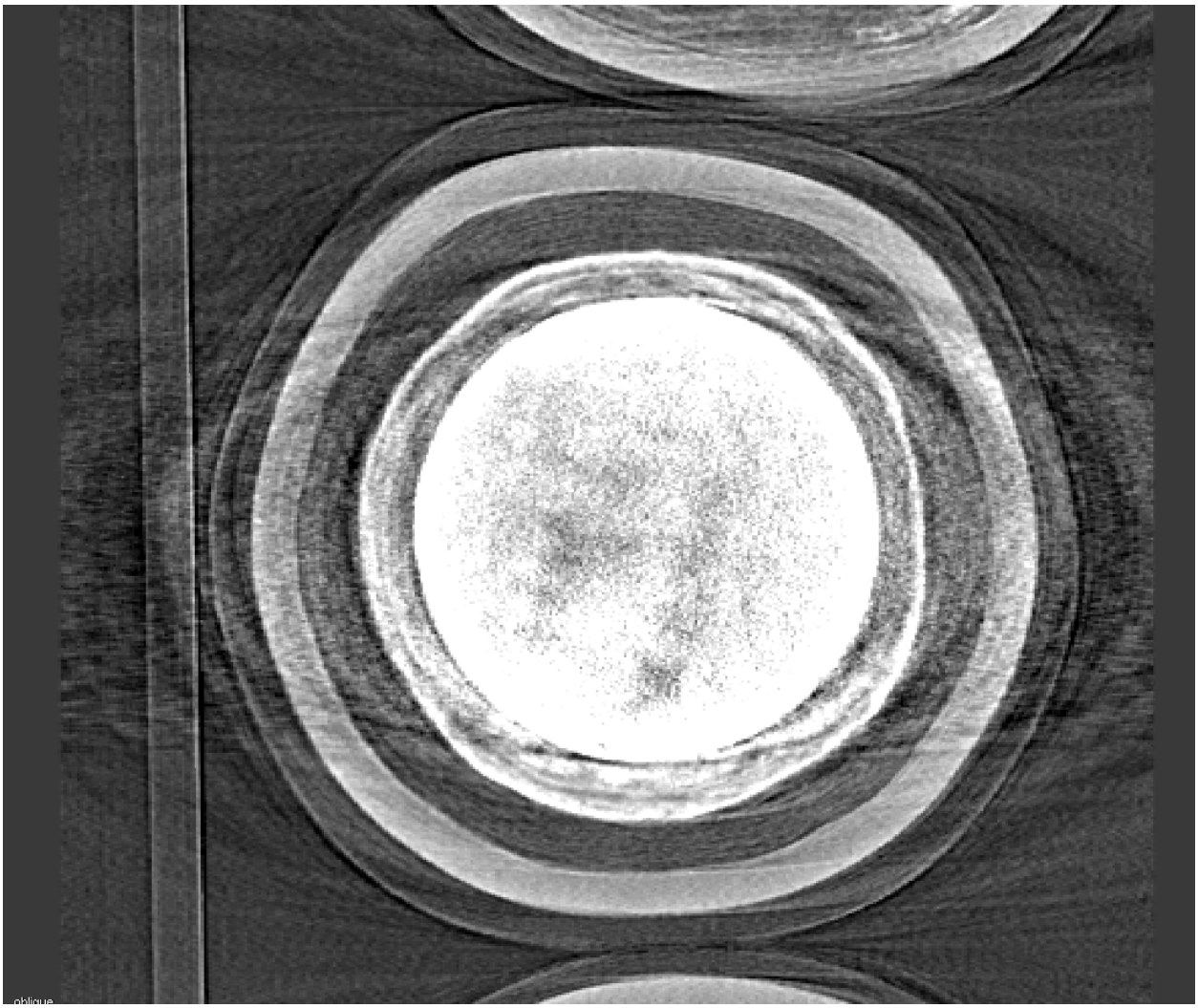
oblique

A5. Particles from sample NP-C1369 of BWXT coating batch J52O-16-93168A

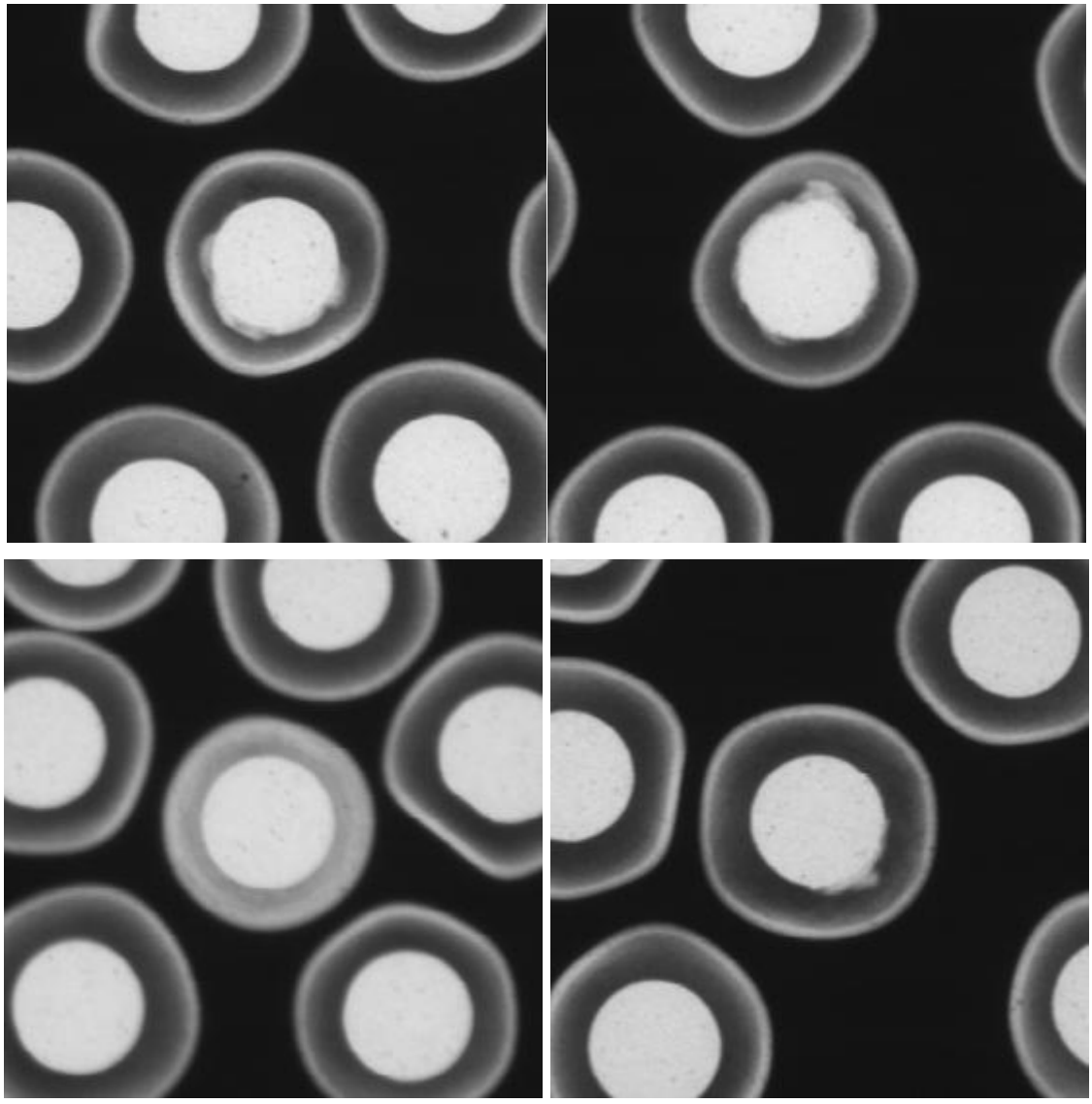

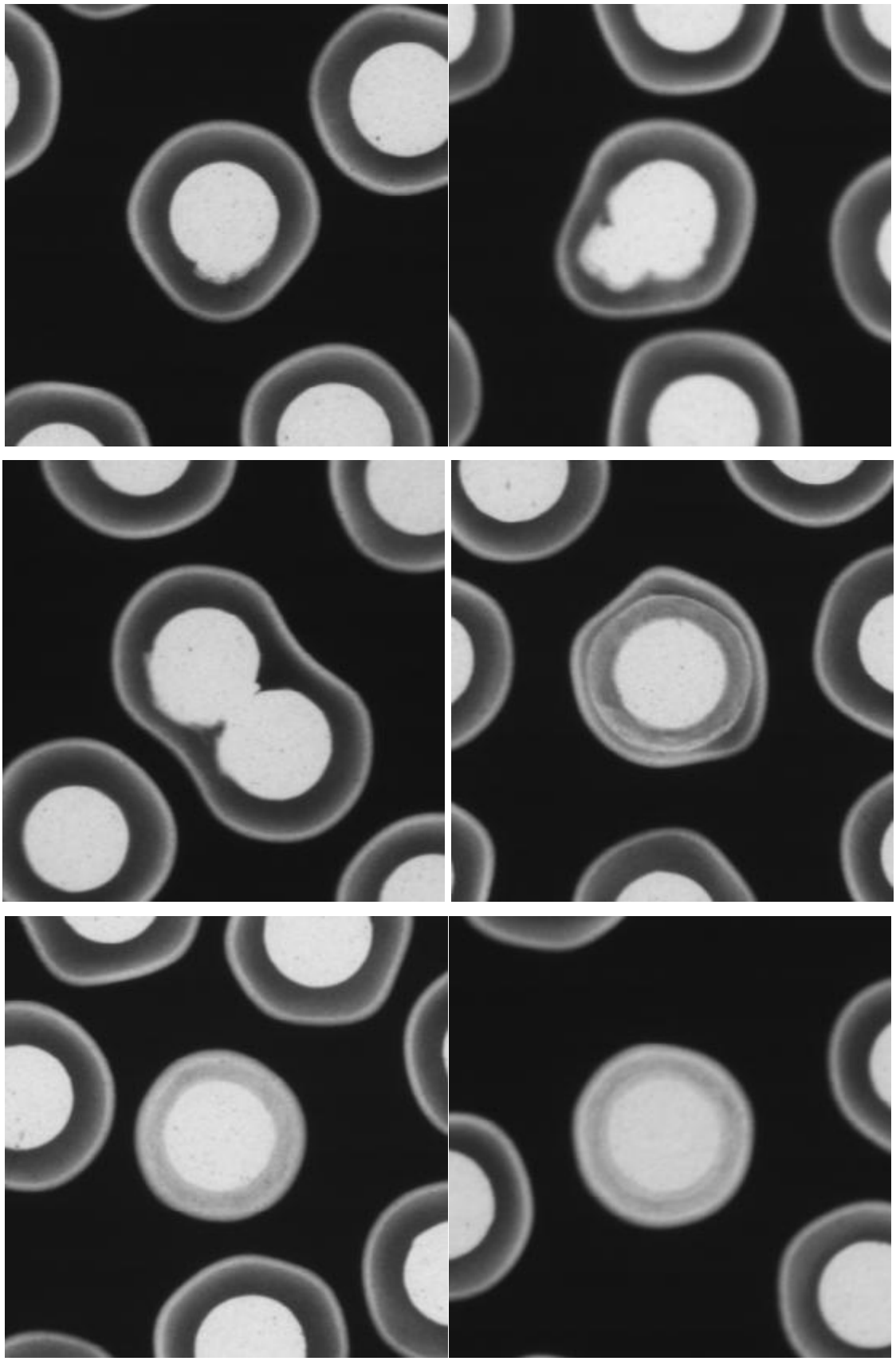

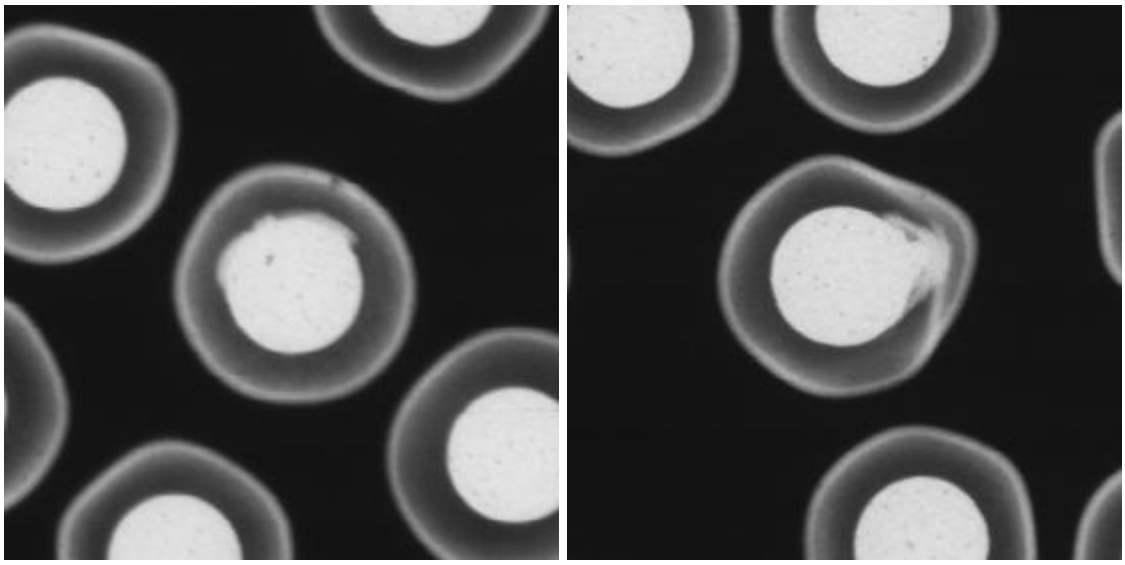

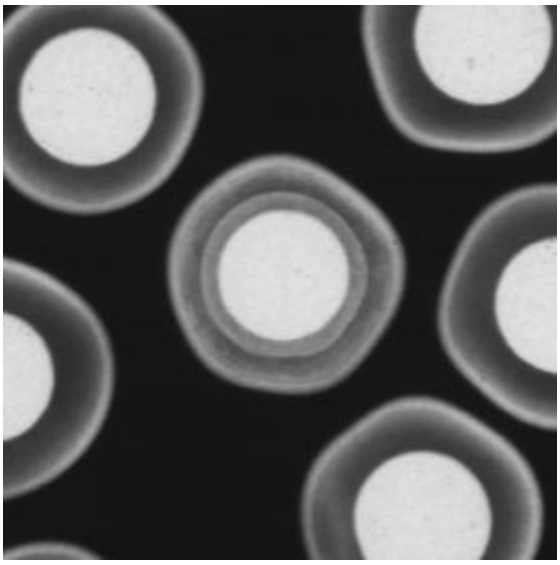

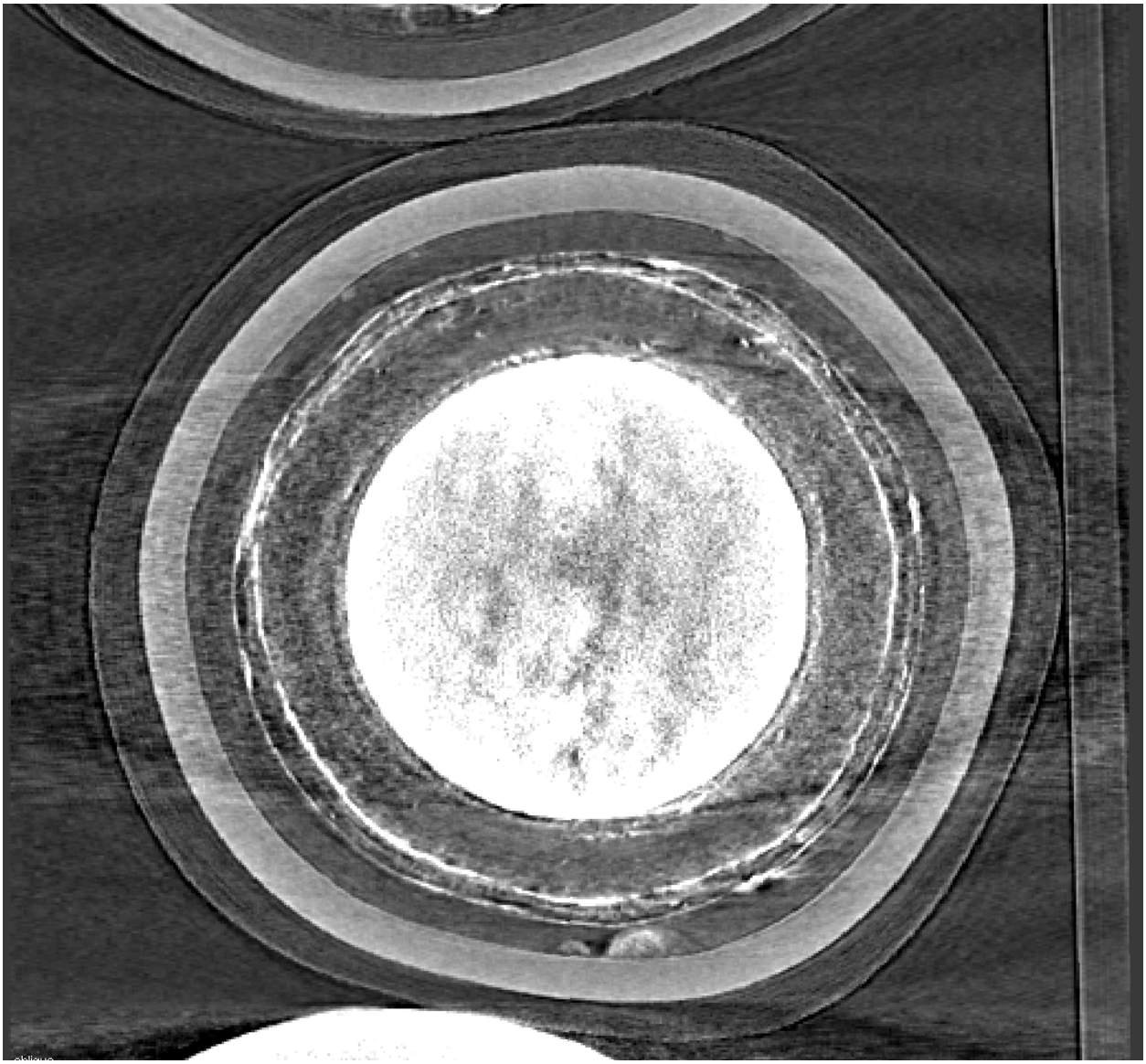

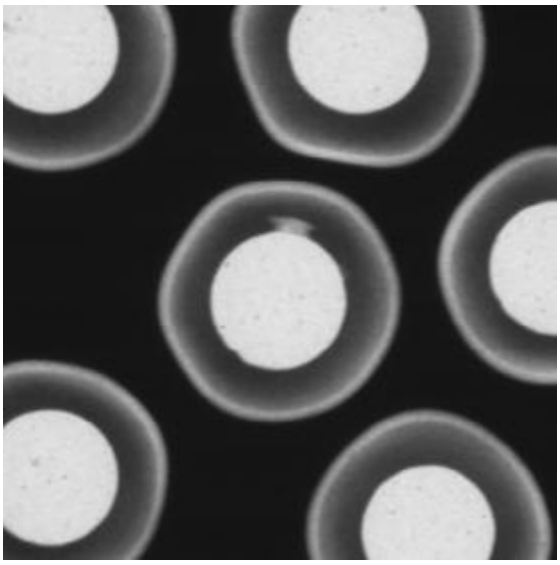

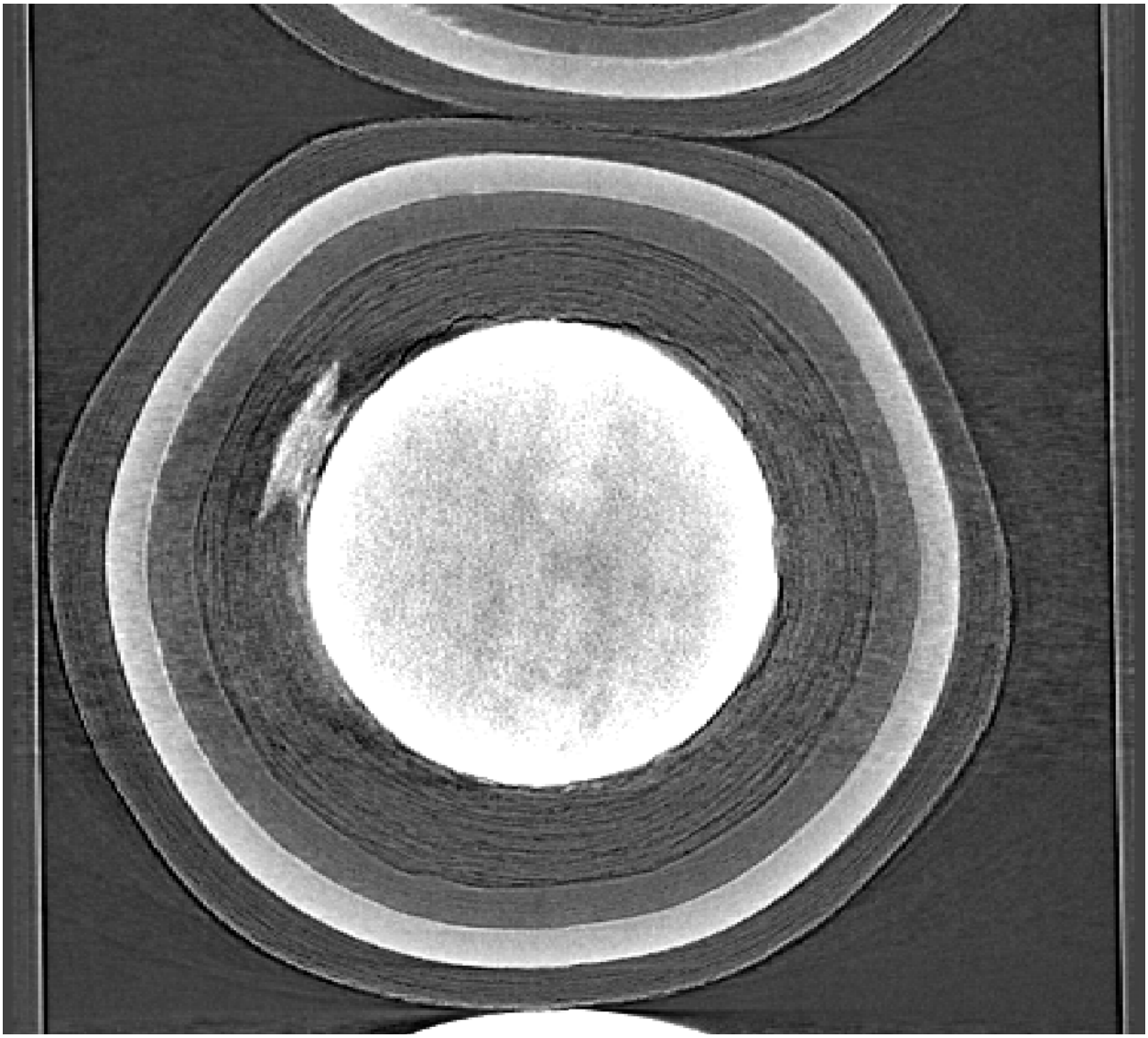

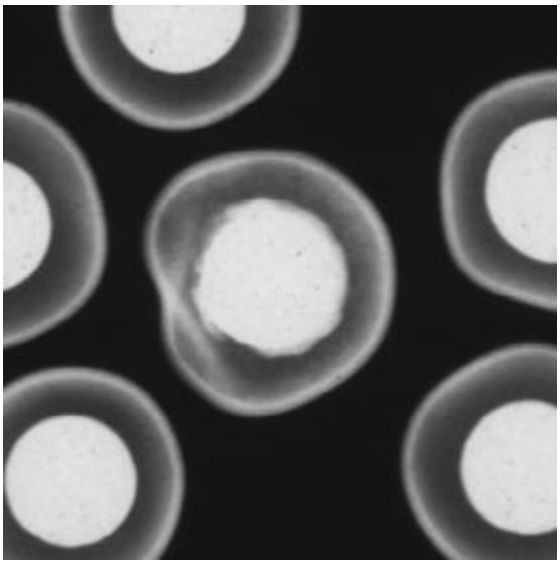

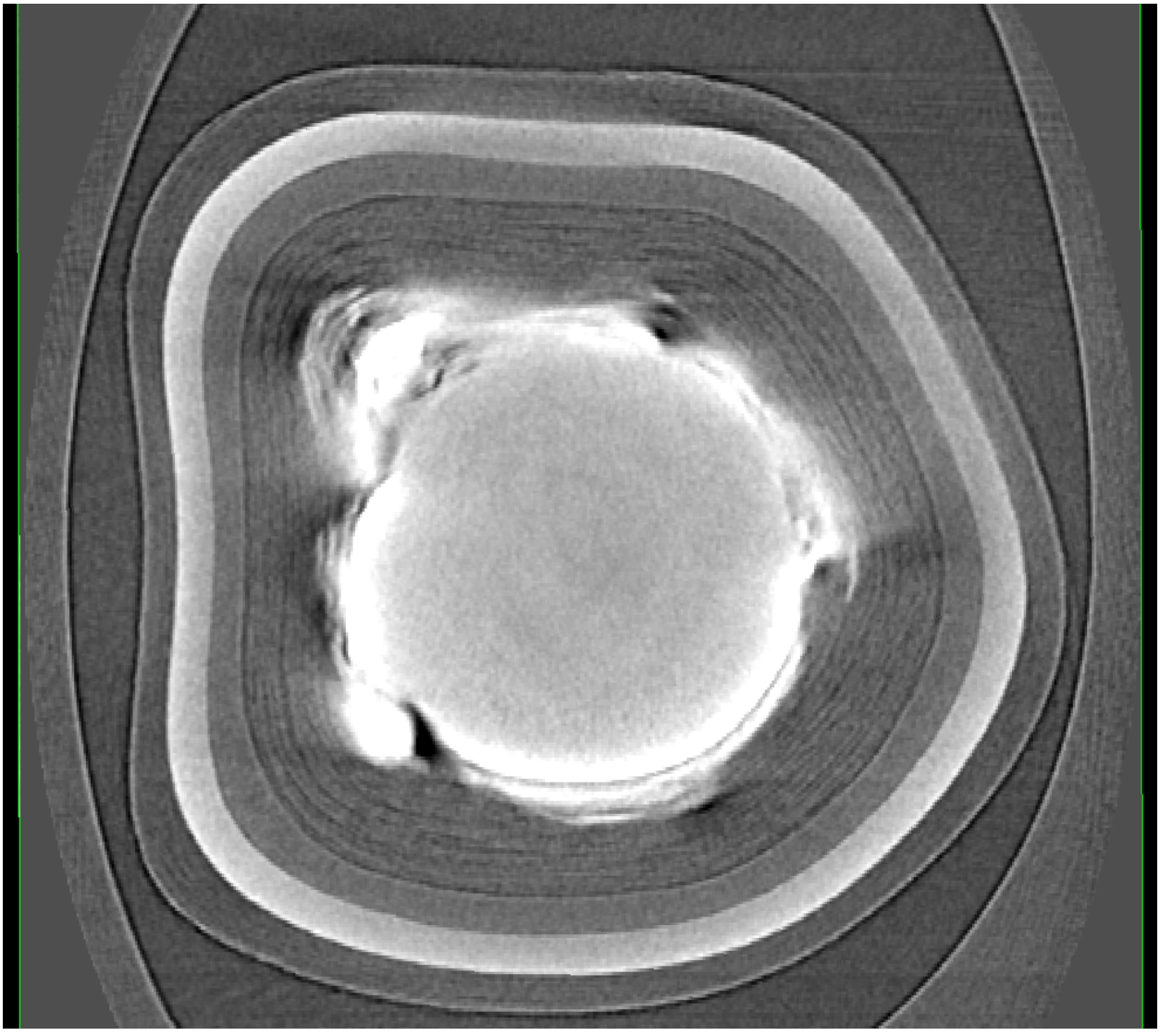

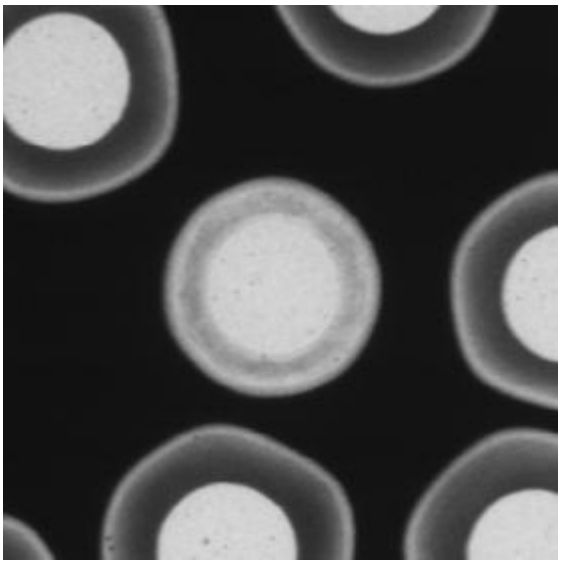

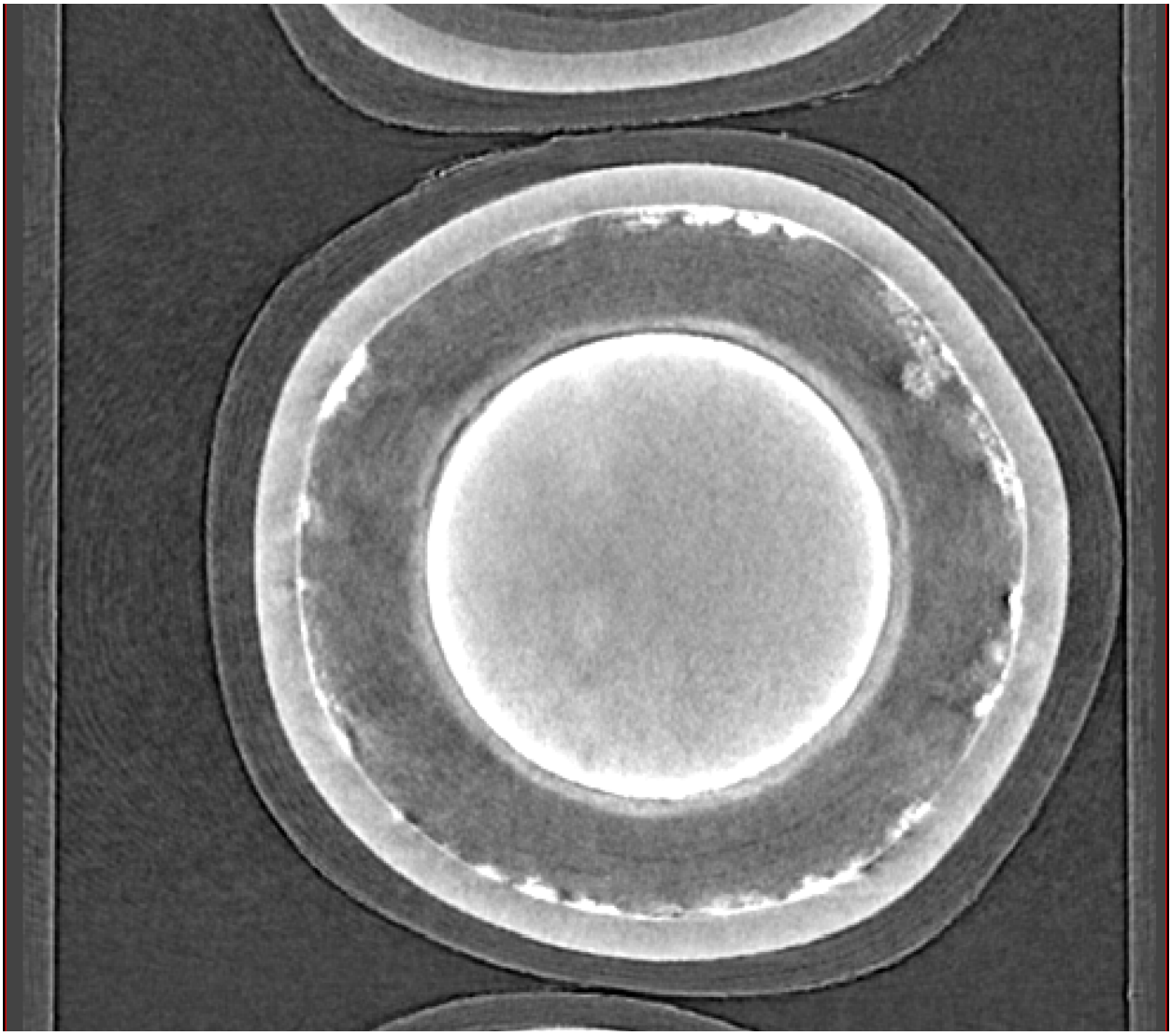

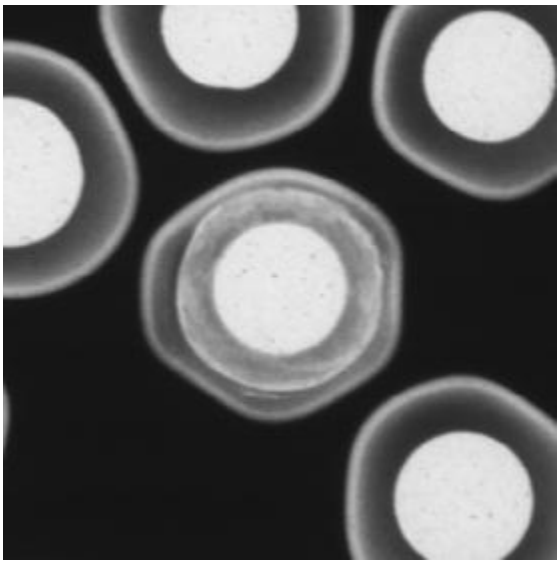

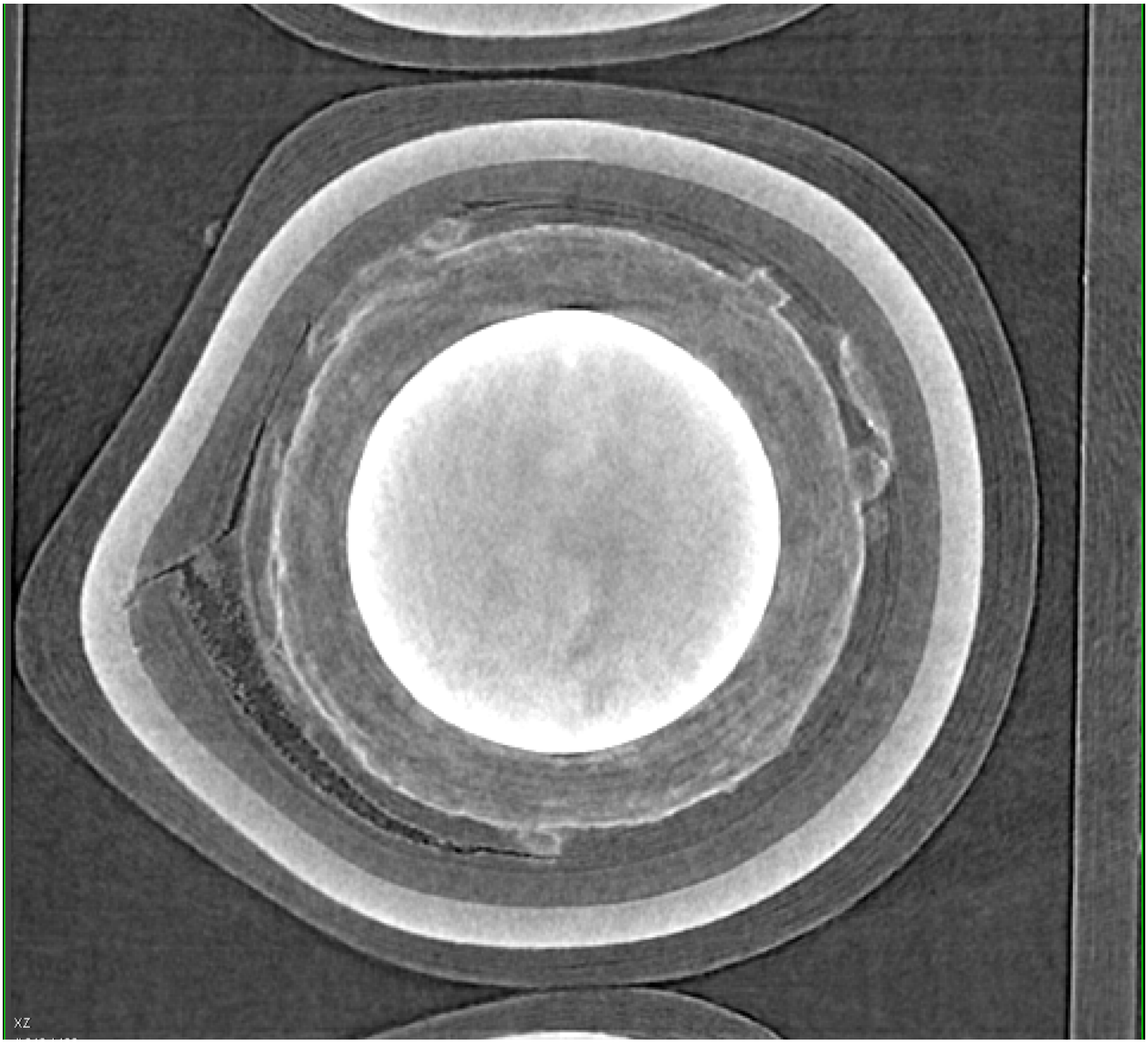
XZ

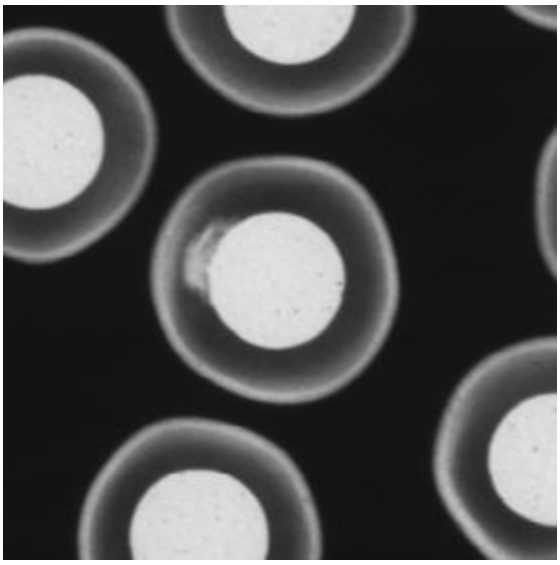

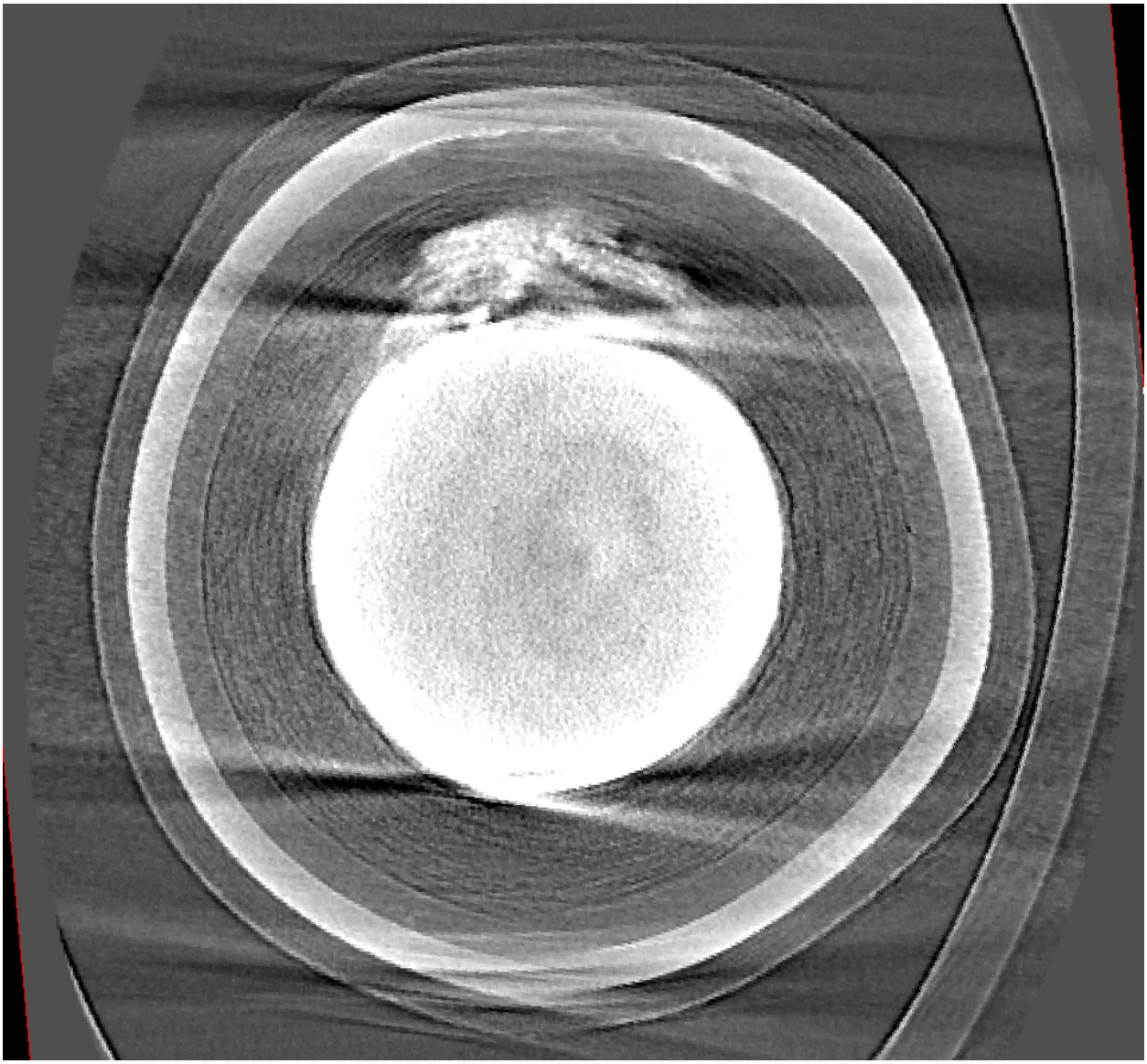

A6. Particles from sample NP-C1391 of BWXT coating batch J52O-16-93169A

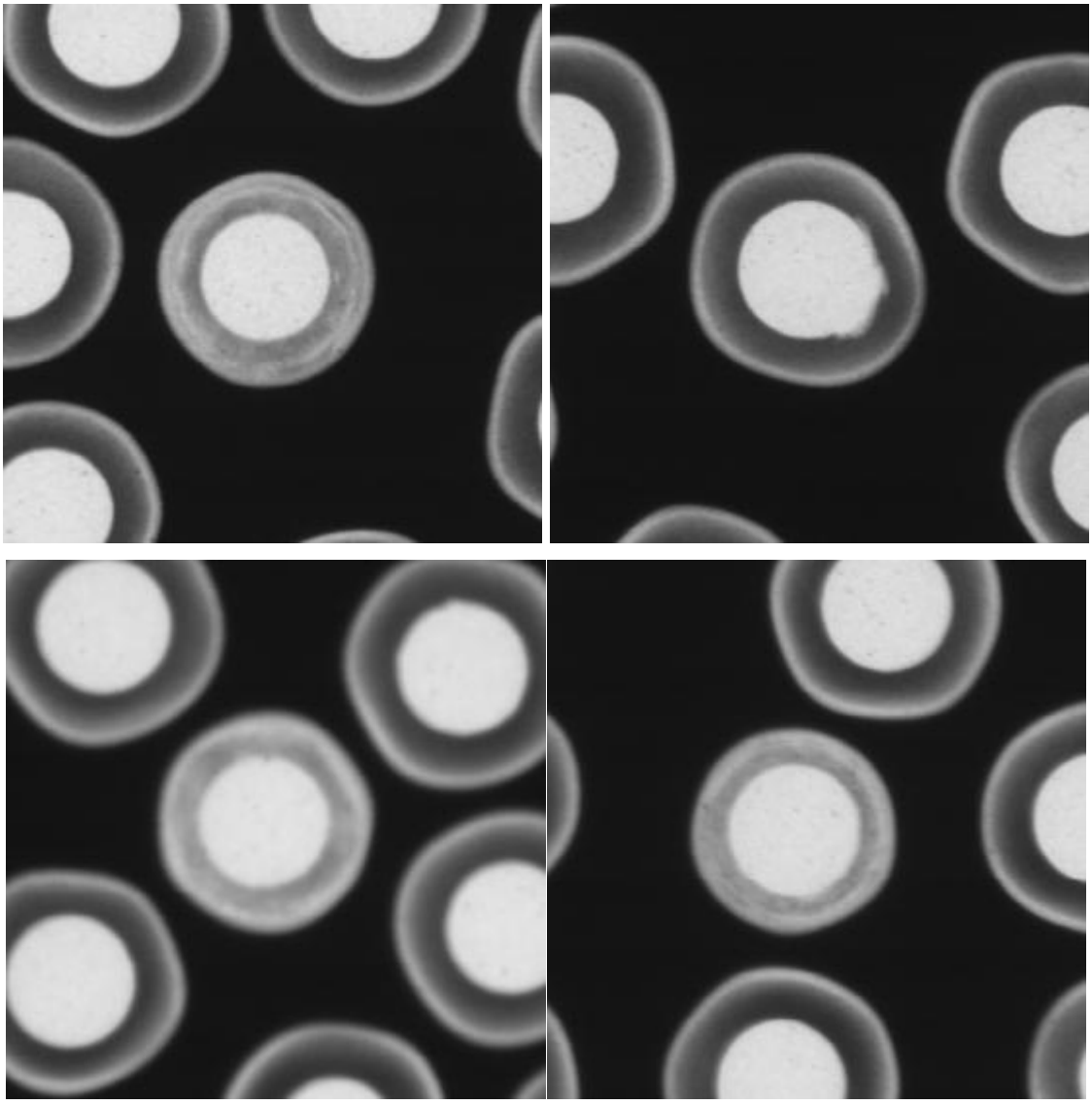

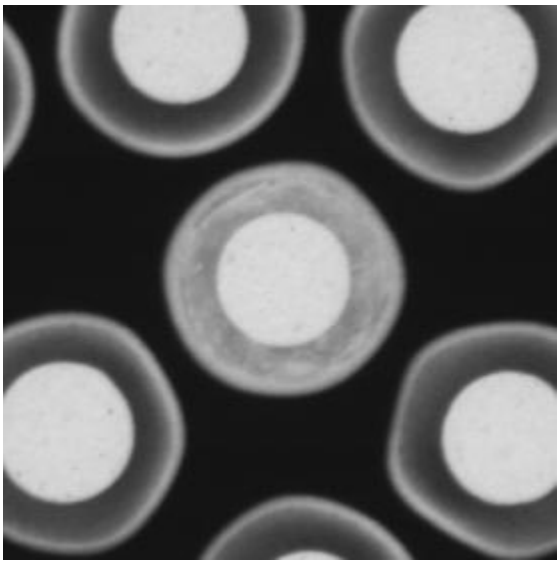

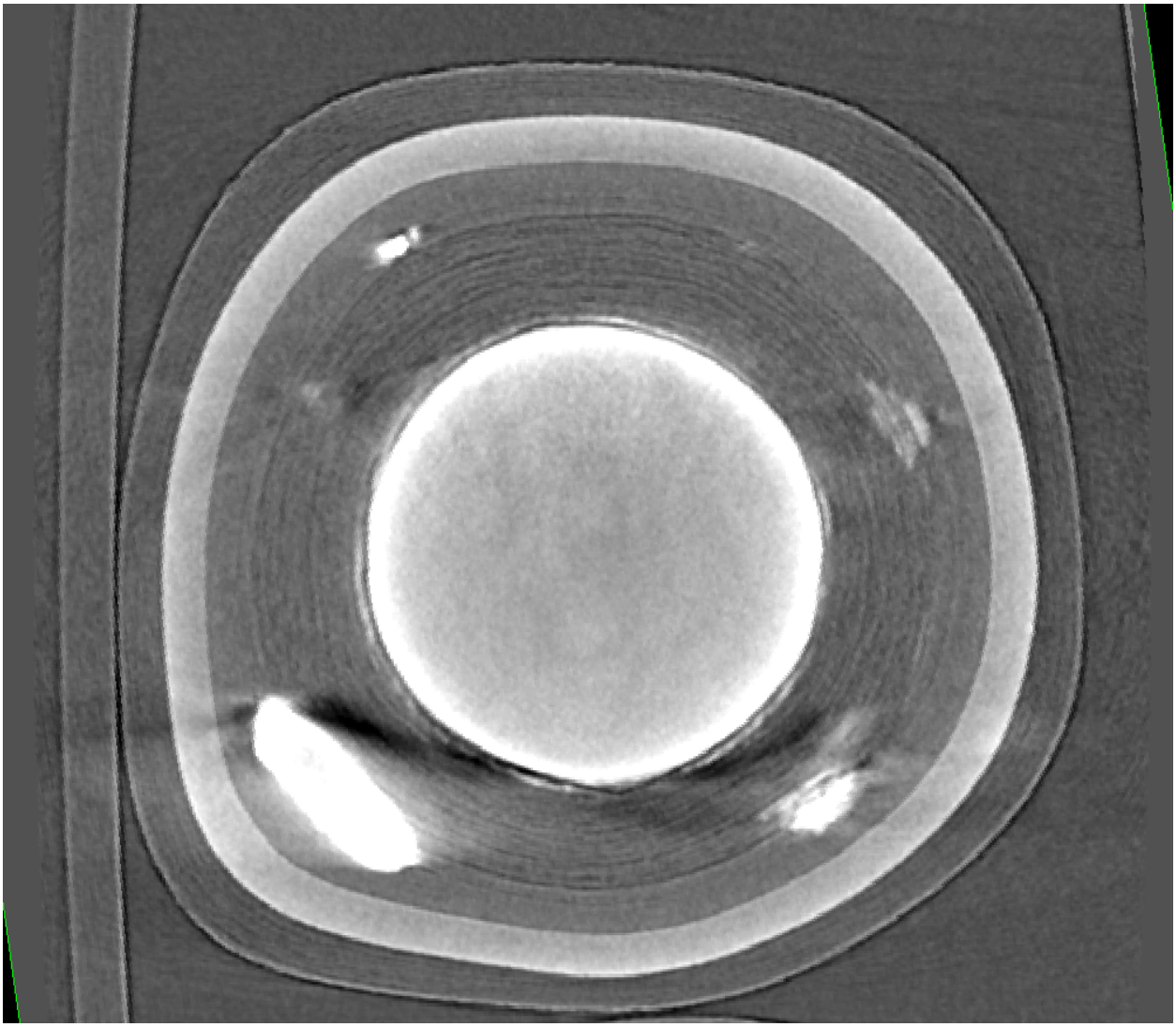

A7. Particles from sample NP-C1402 of BWXT coating batch J52O-16-93170A

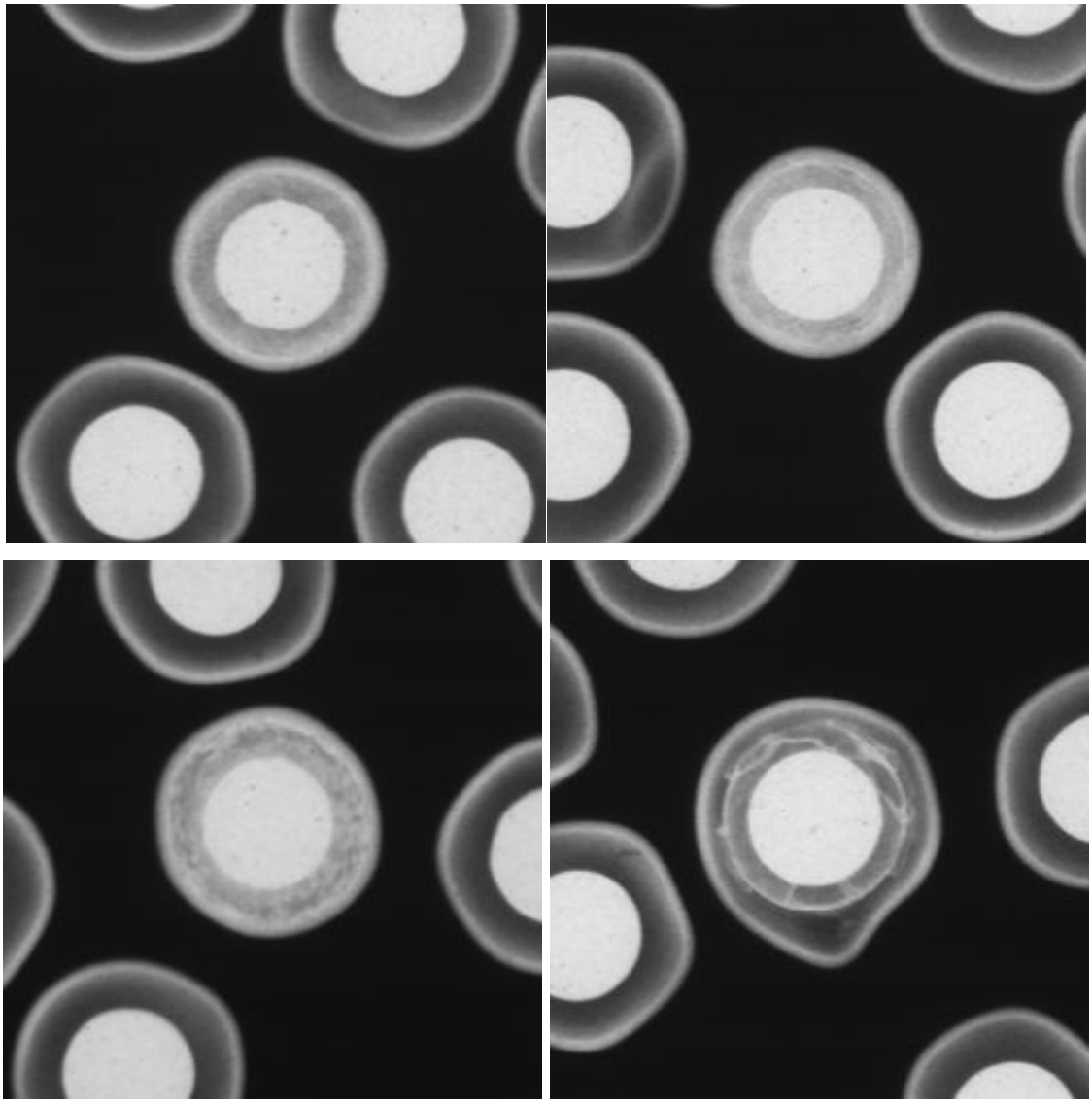

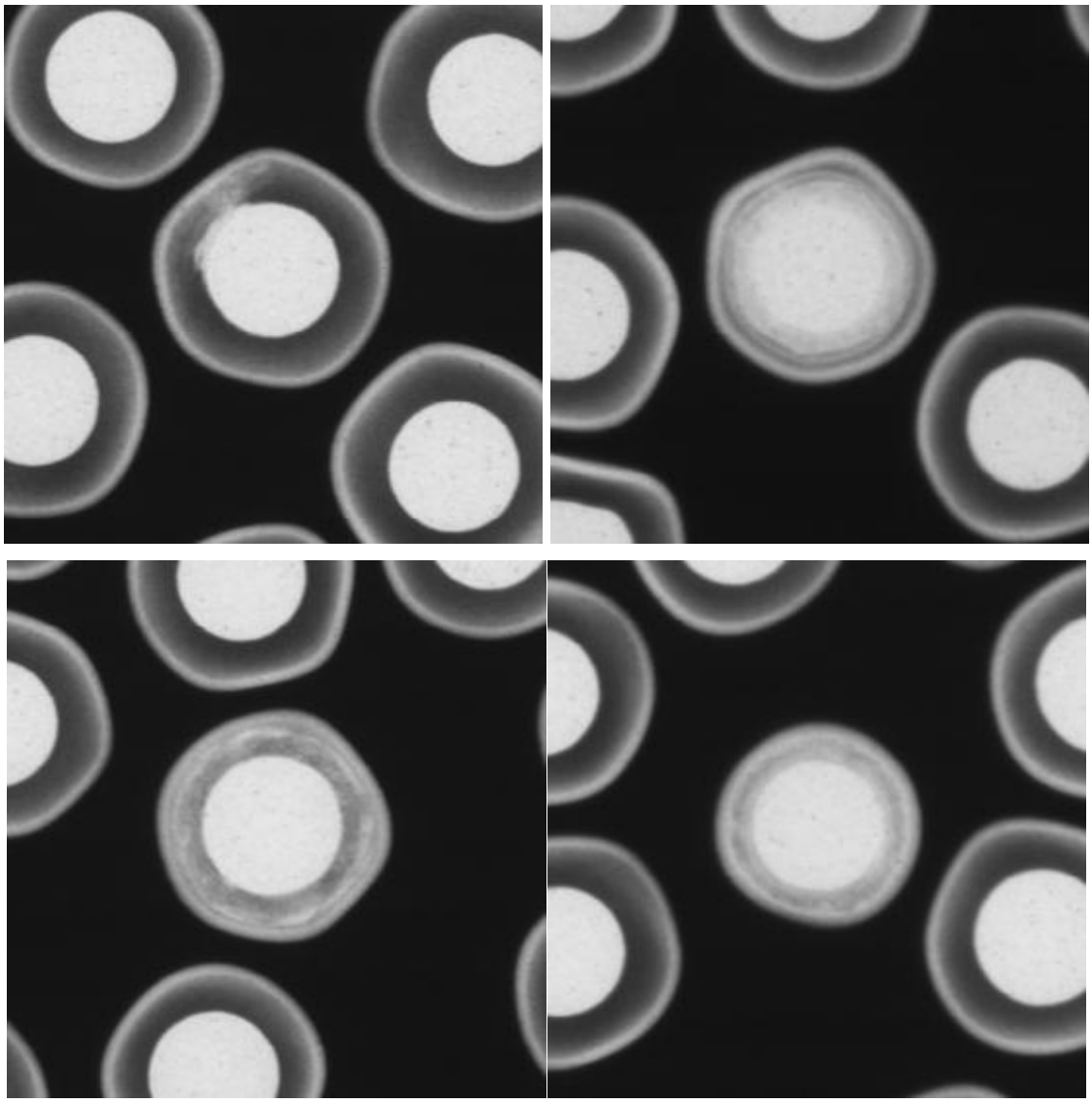

A8. Particles from sample NP-C1421 of BWXT coating batch J52O-16-93172A

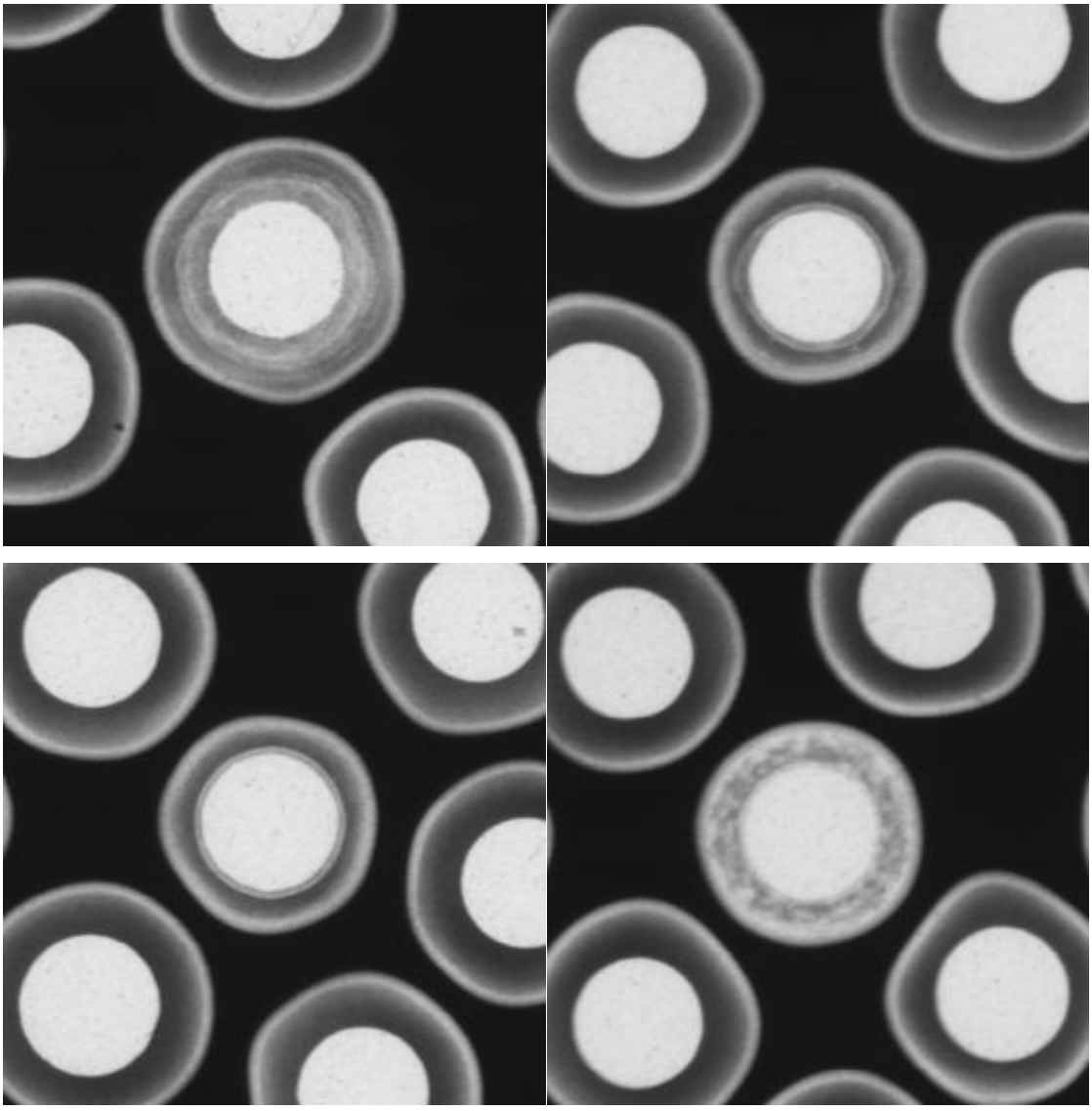

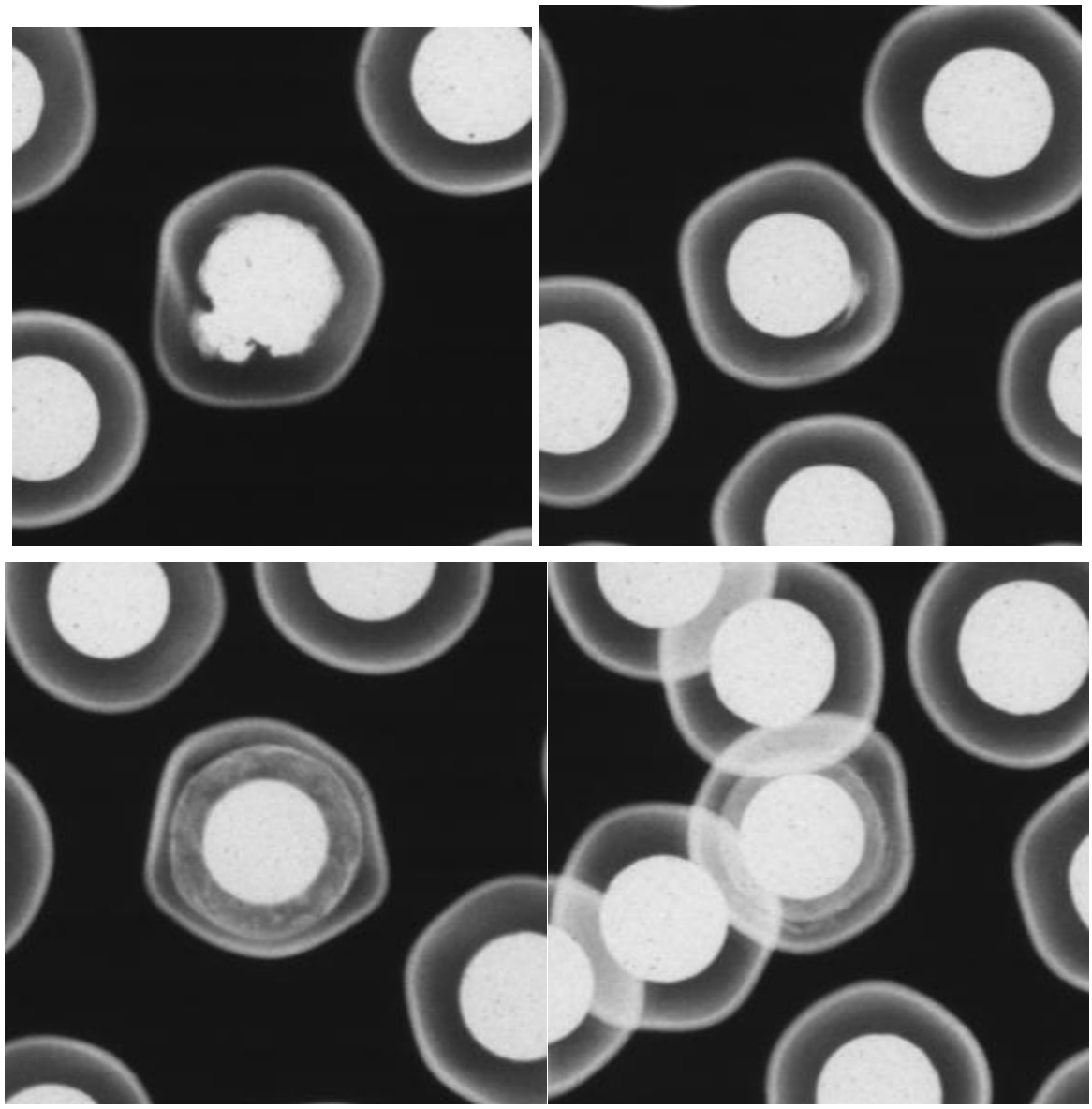

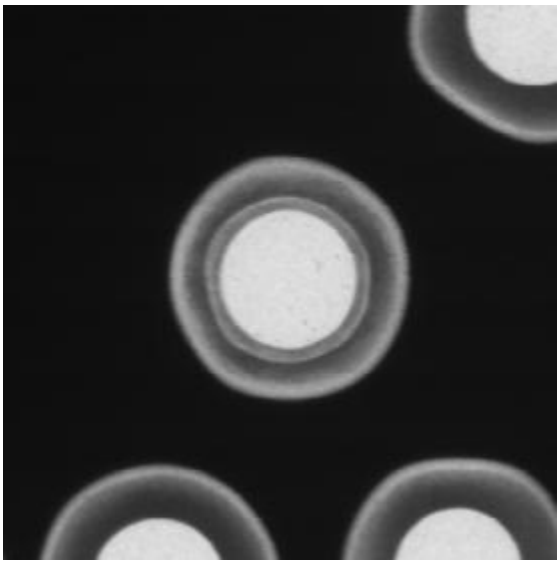

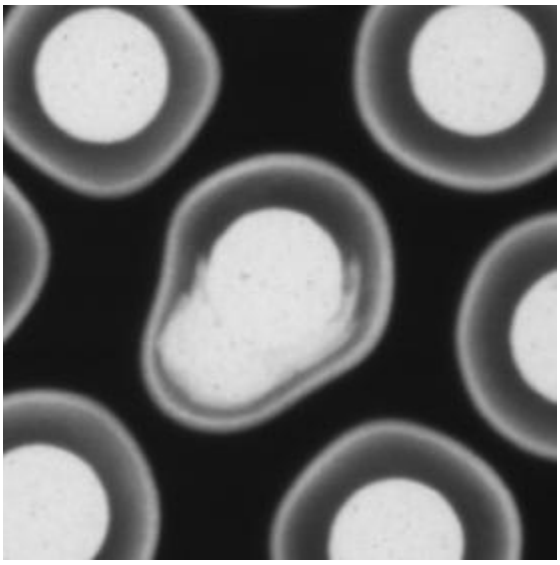

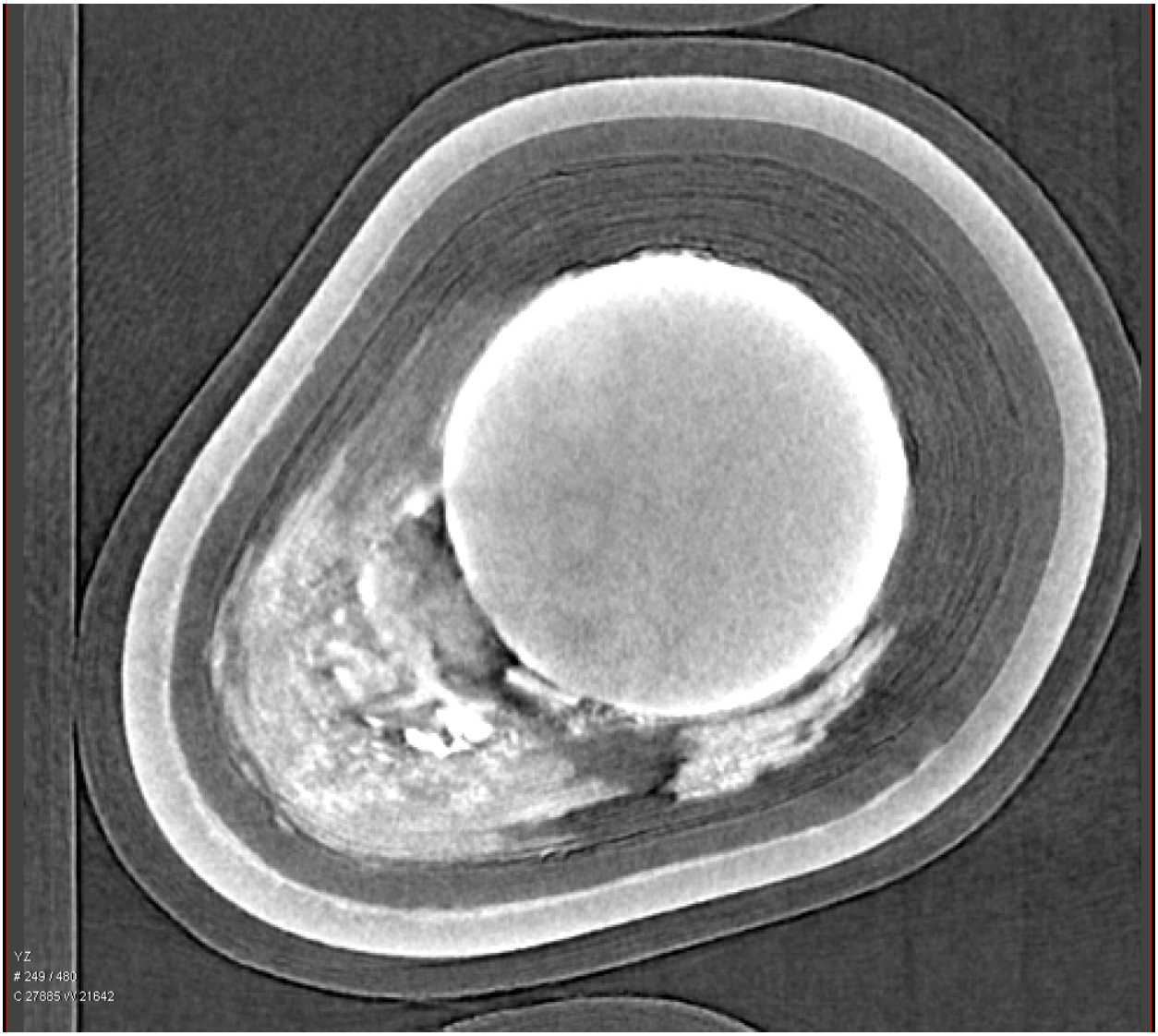
YZ
249 / 480
C 27885 W 21642

A9. Particles from sample NP-C1498 of BWXT coating batch J52R-16-98005

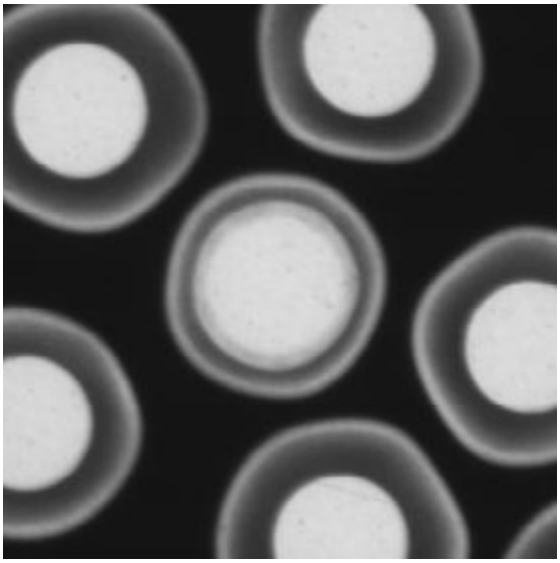

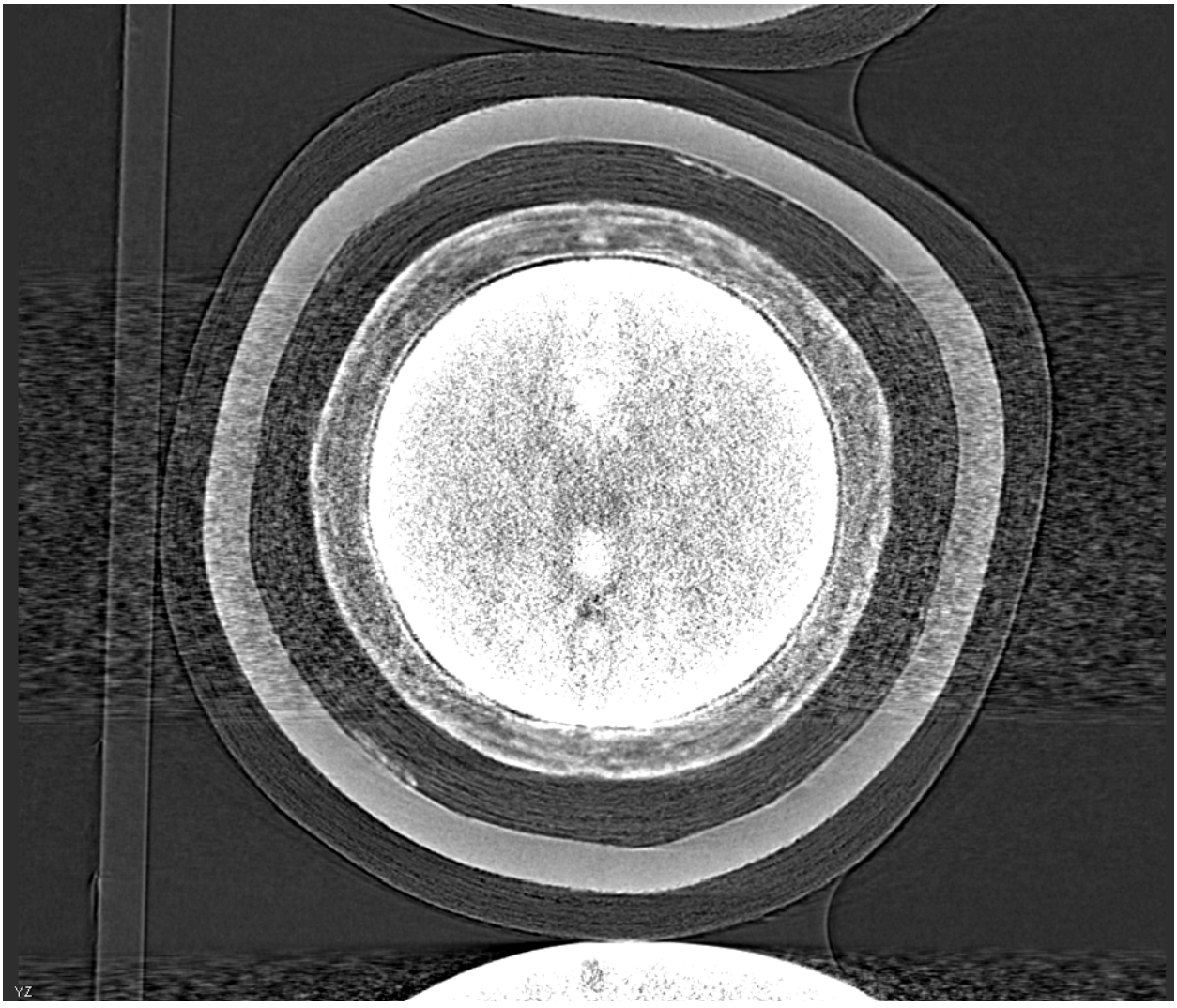

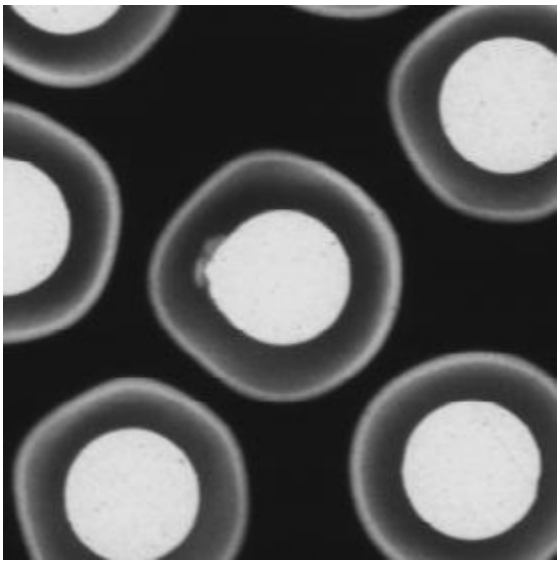

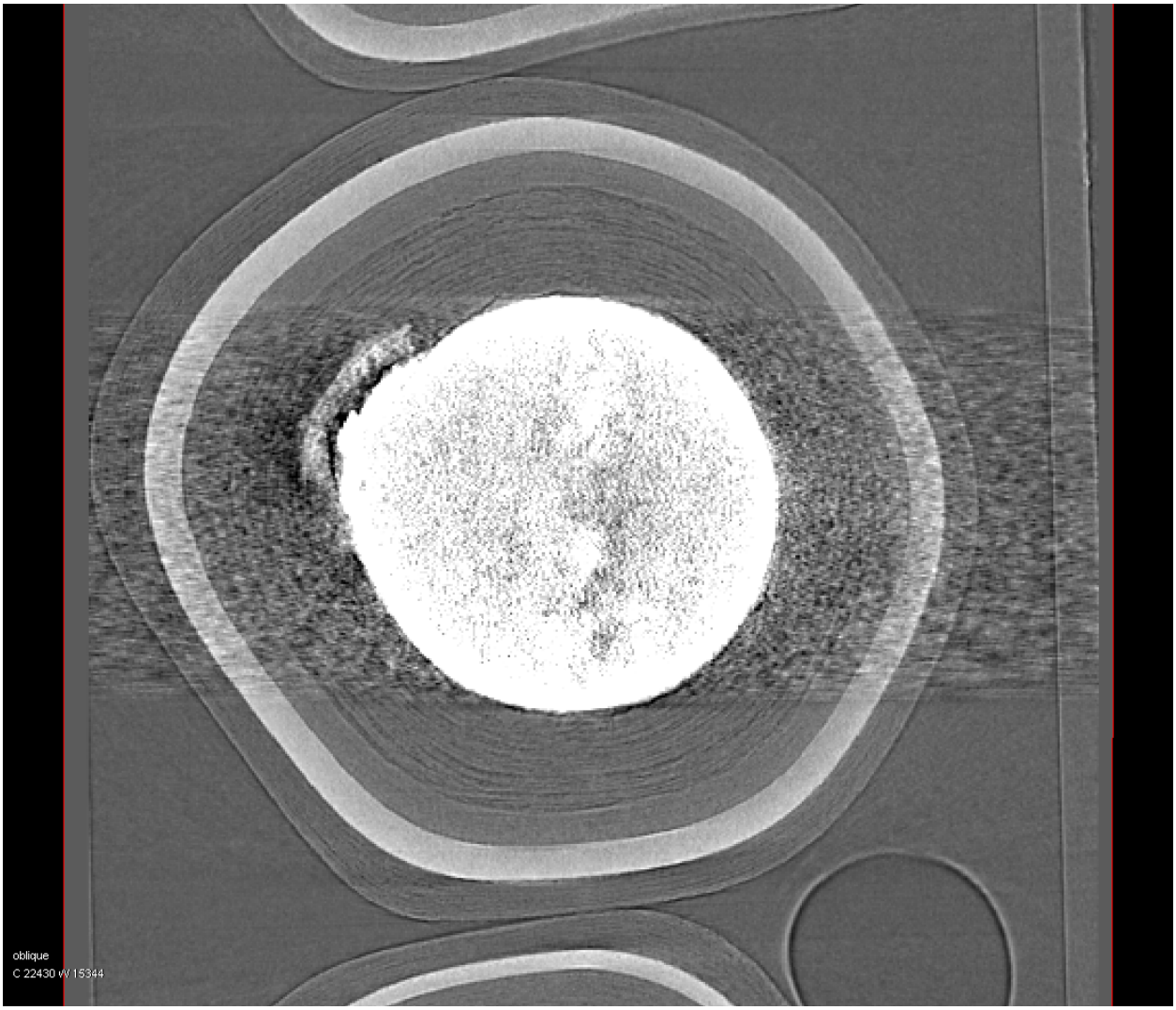
oblique
C 22430 W 15344

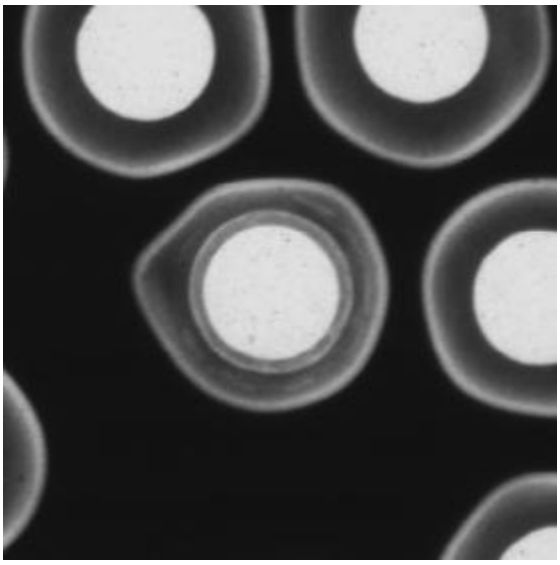

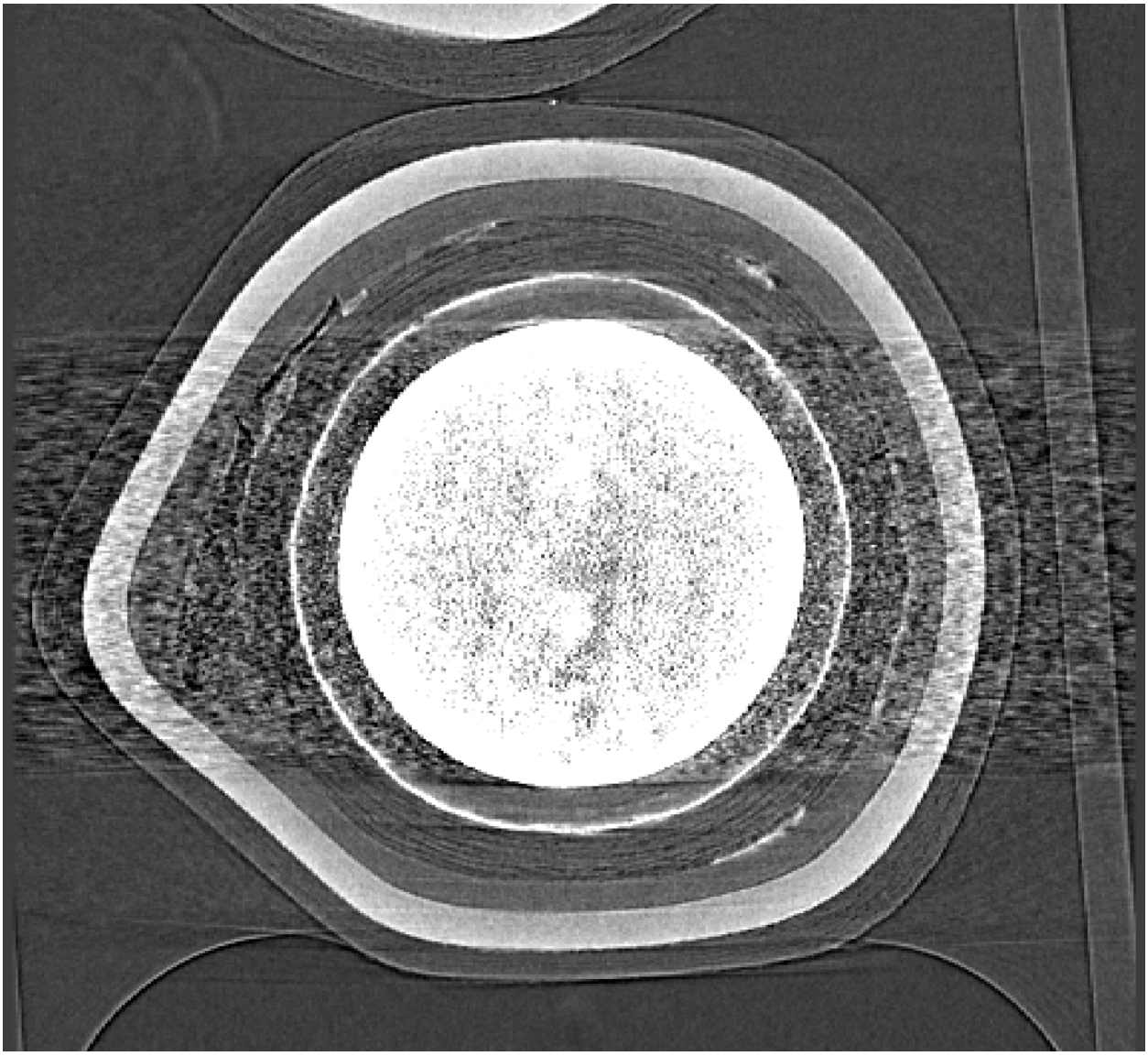

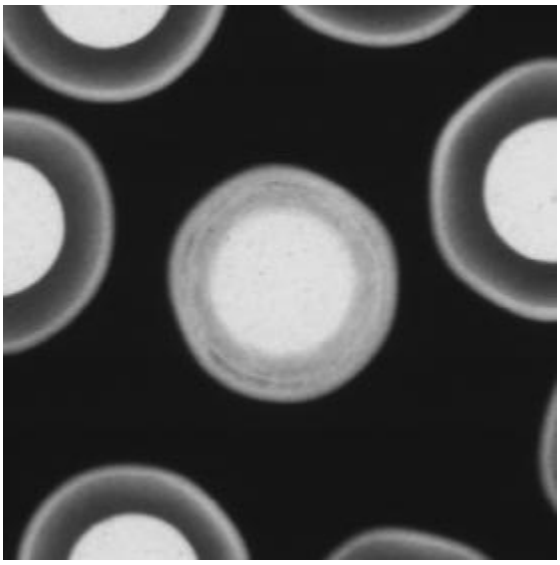

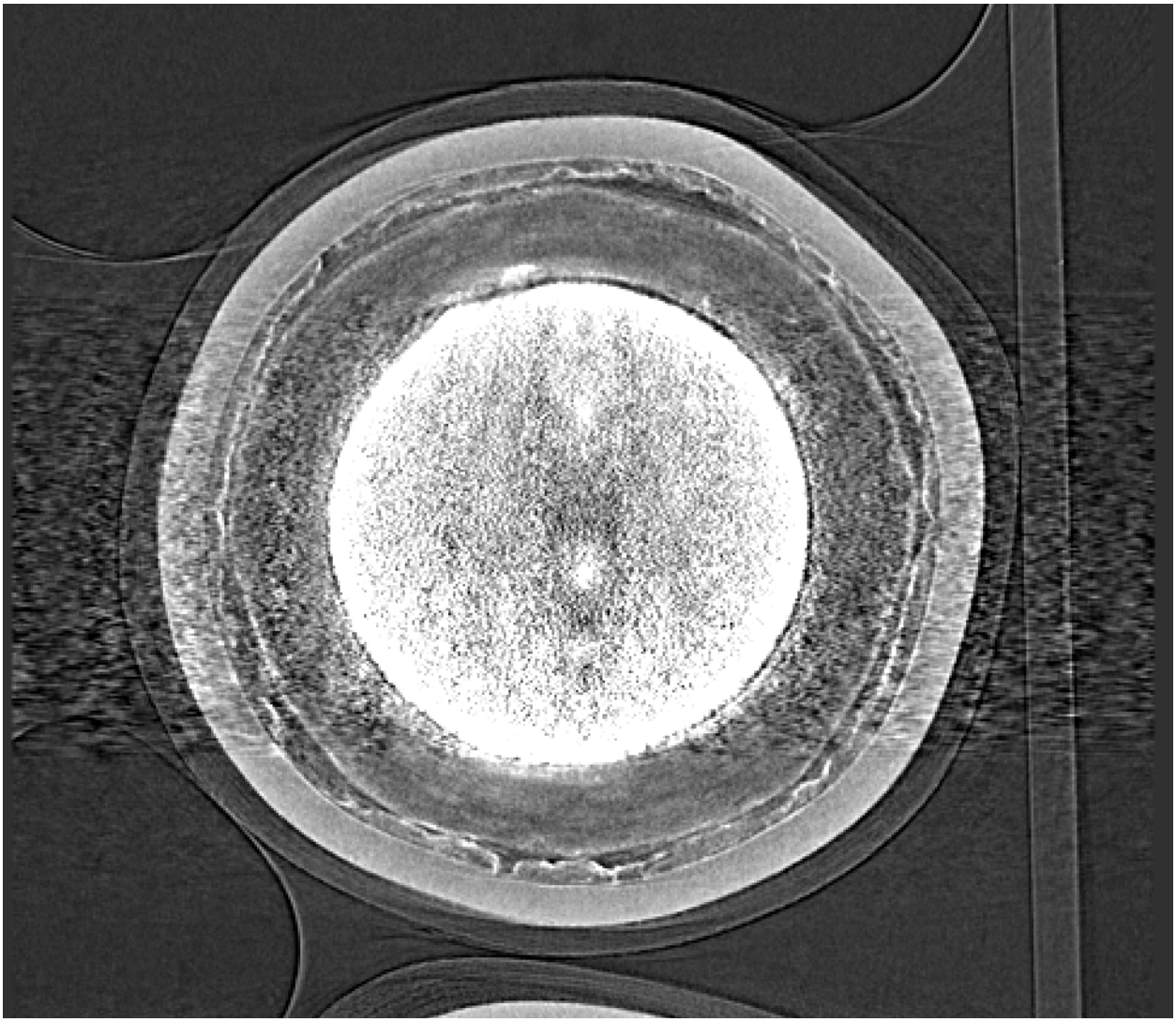

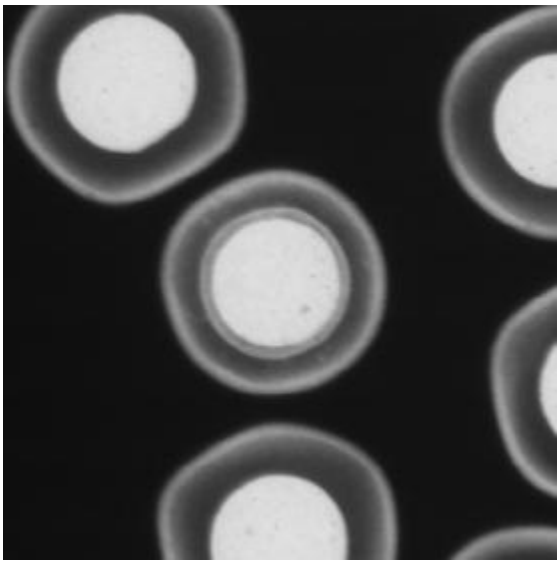

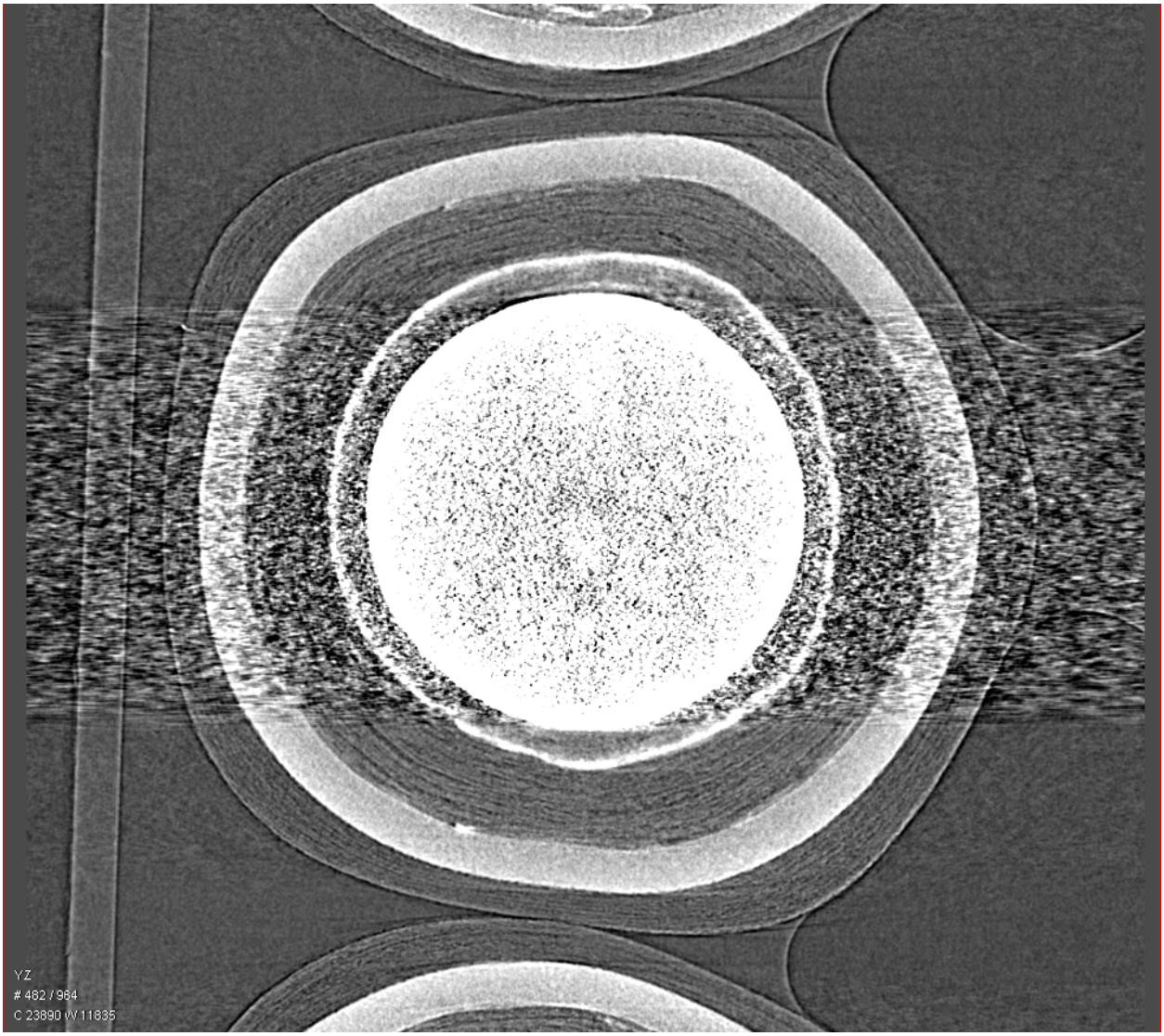
YZ
482 / 964
C 23890 W 11835

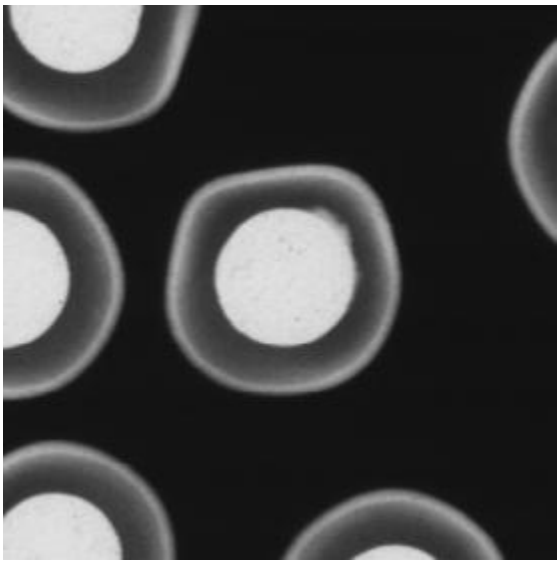

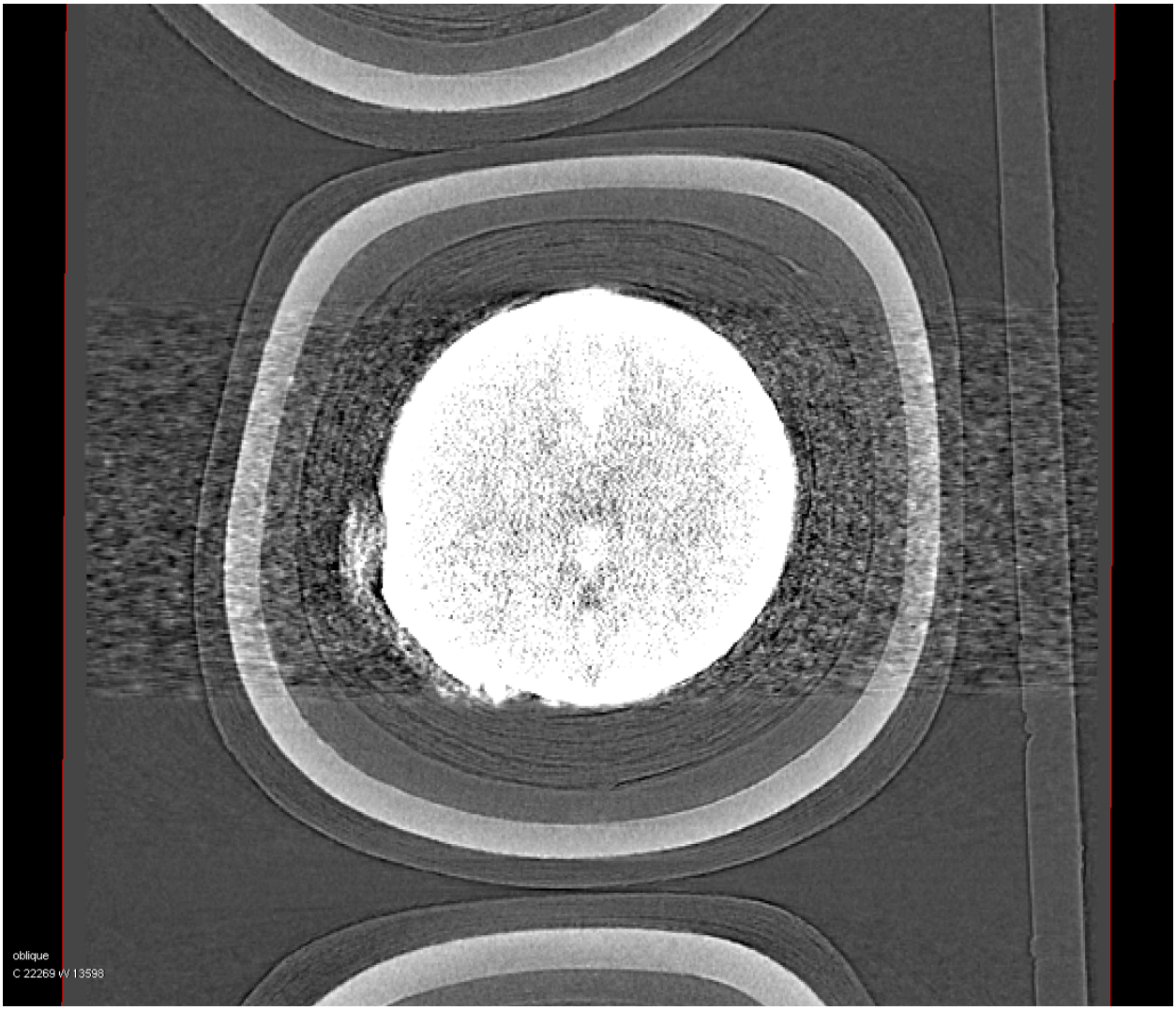
oblique
C 22269 W 13598

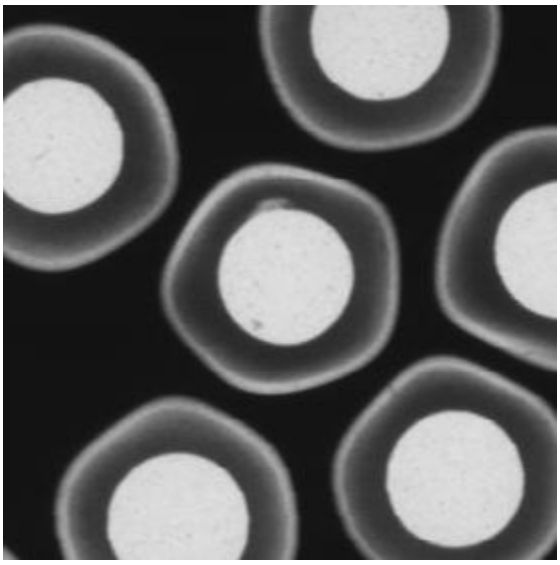

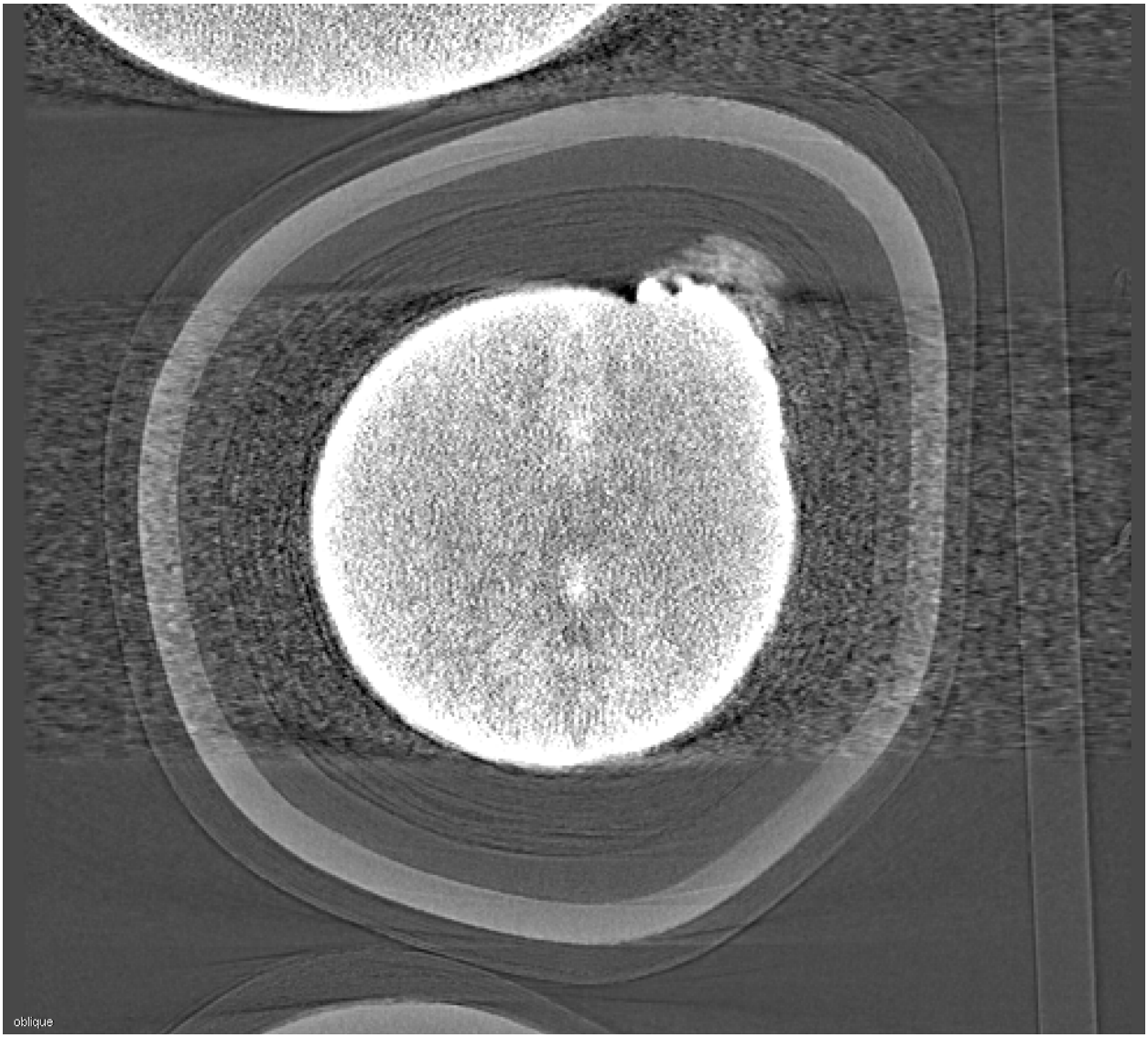
oblique

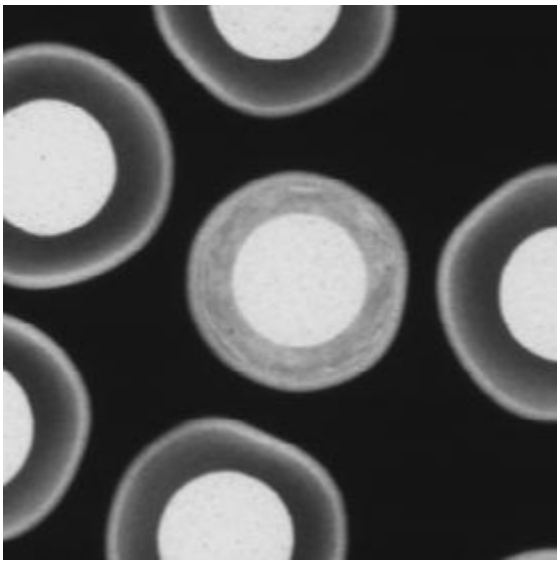

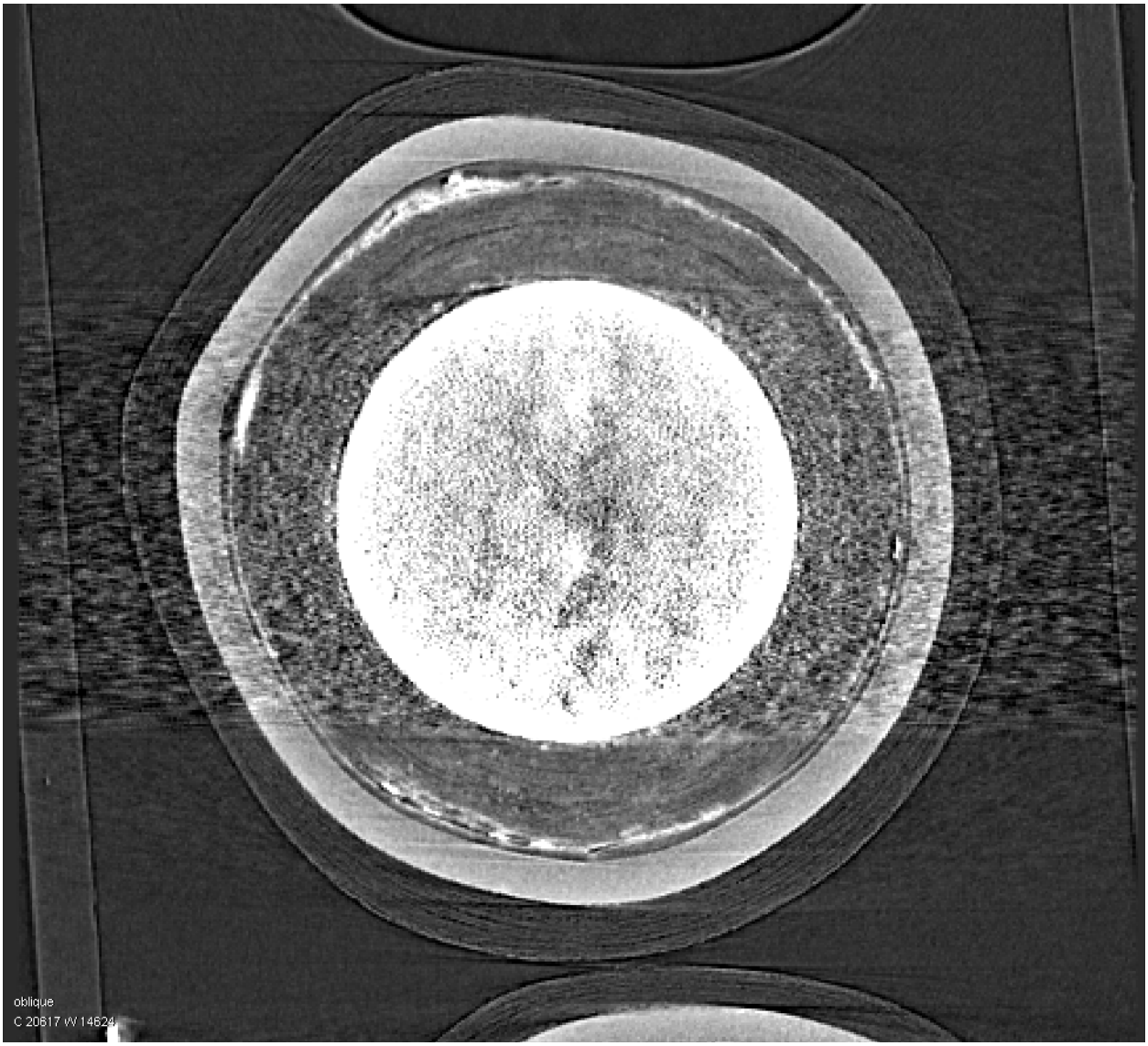
oblique
C 20617 W 14624

A10. Particles from sample NP-C1504 of BWXT coating batch J52R-16-98005

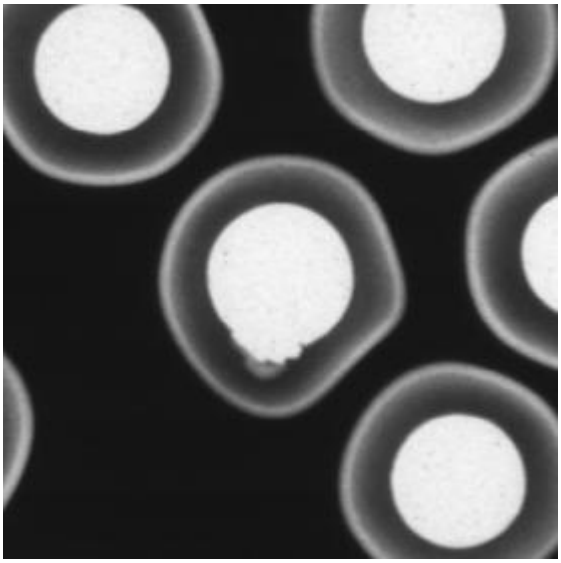

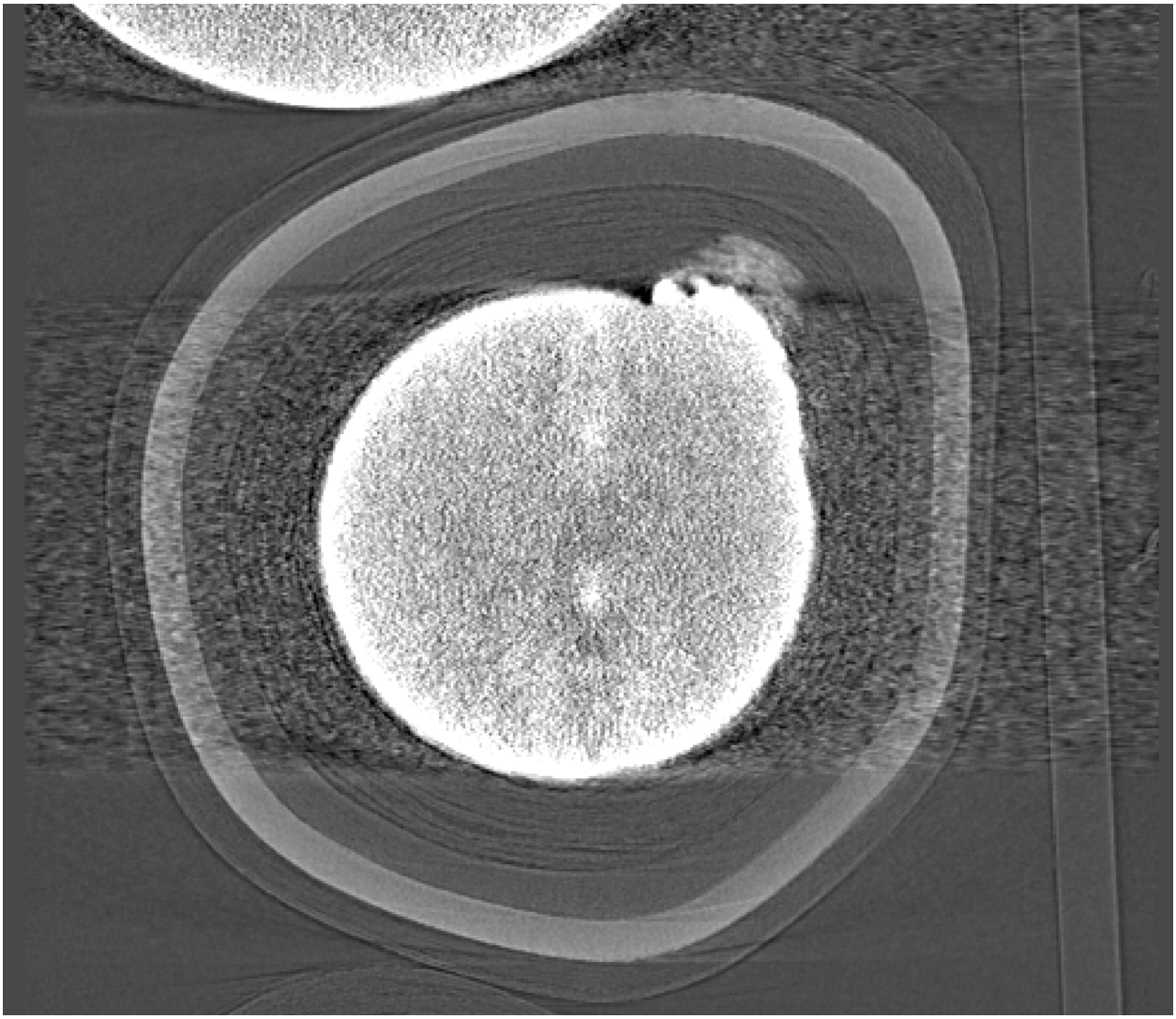

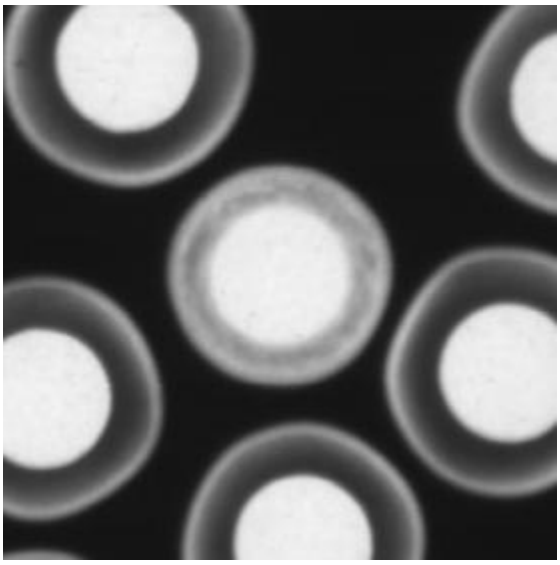

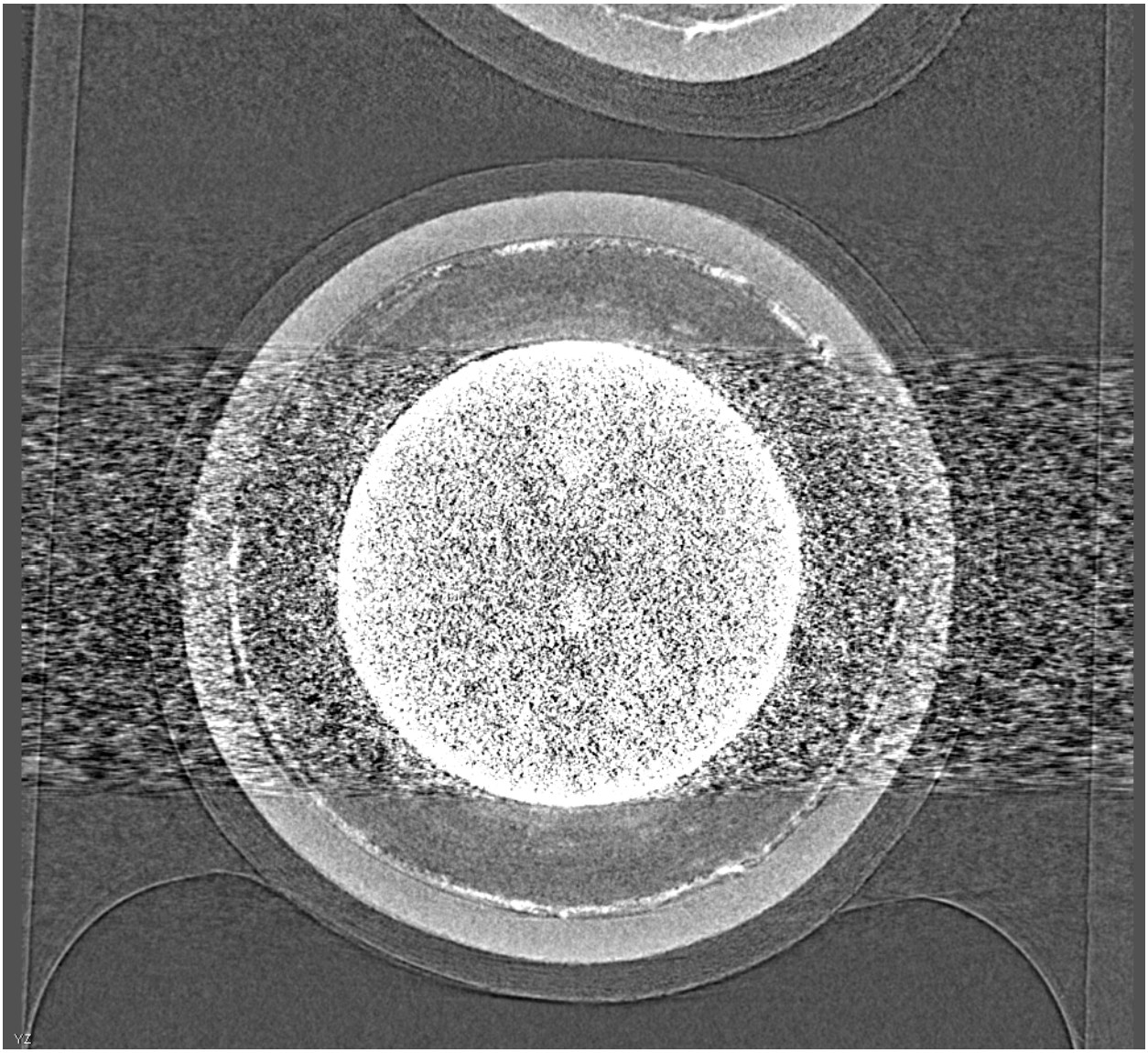
YZ

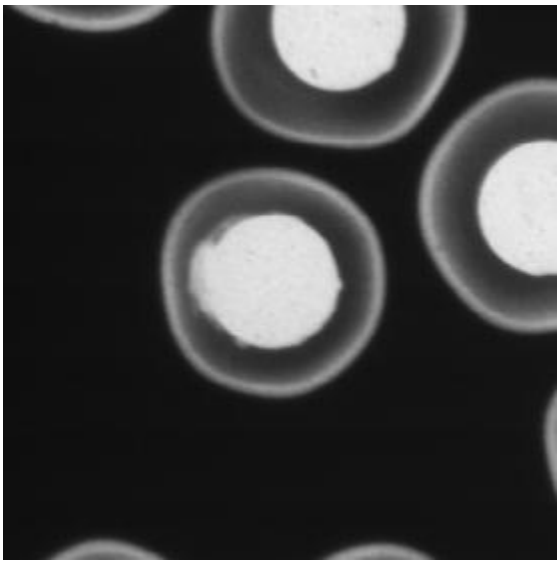

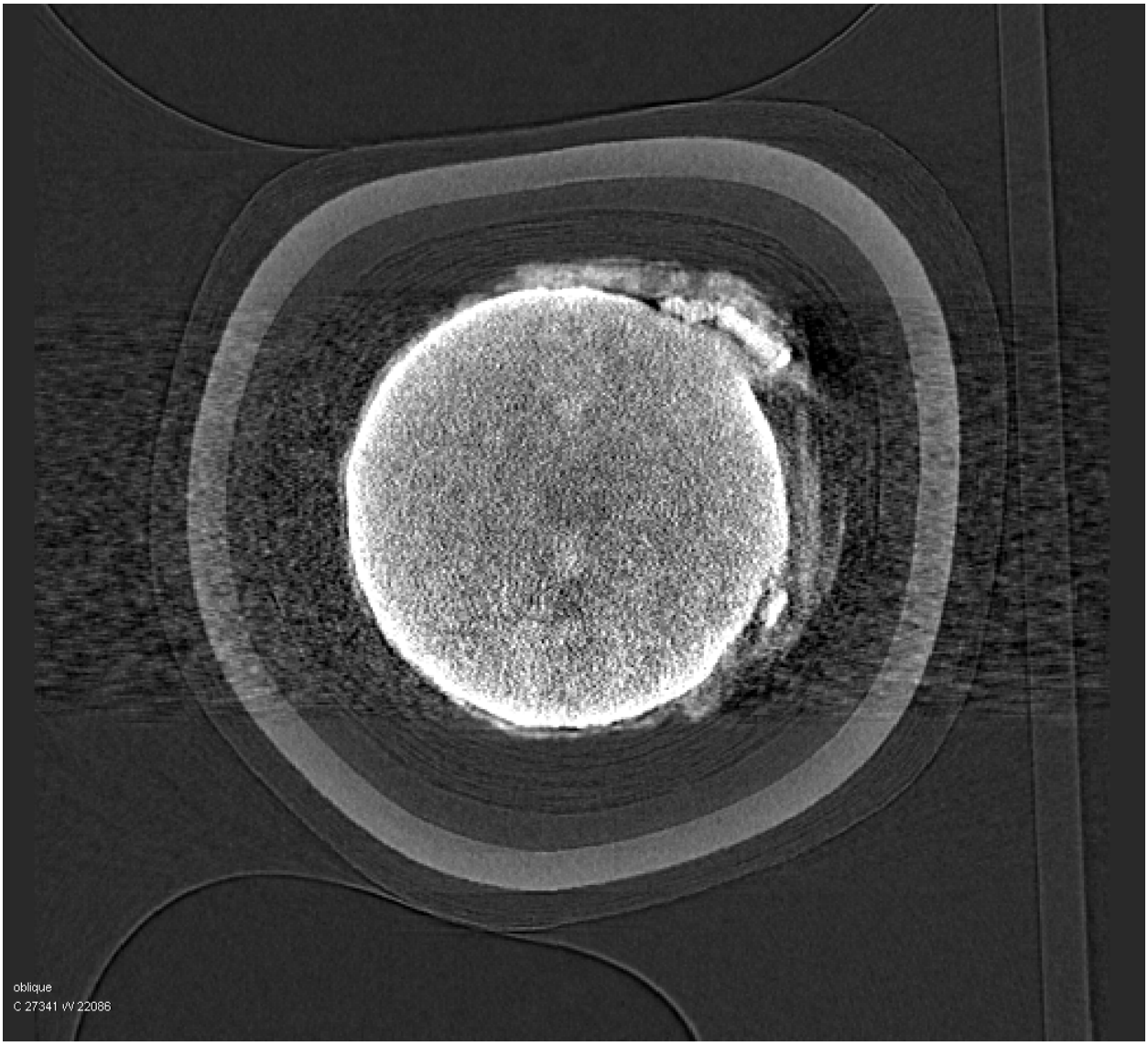
oblique
C 27341 W 22086

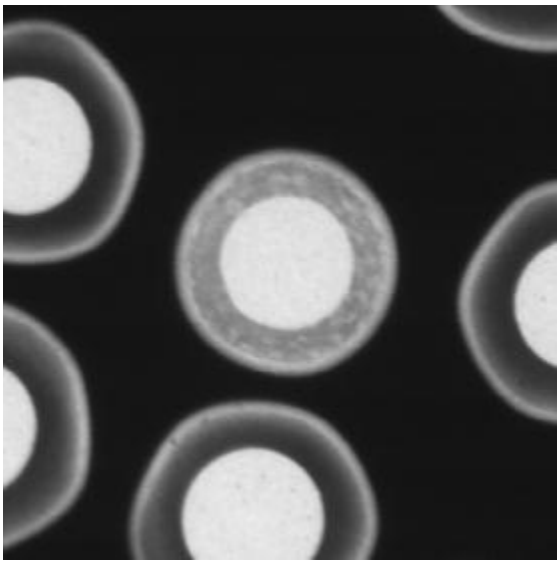

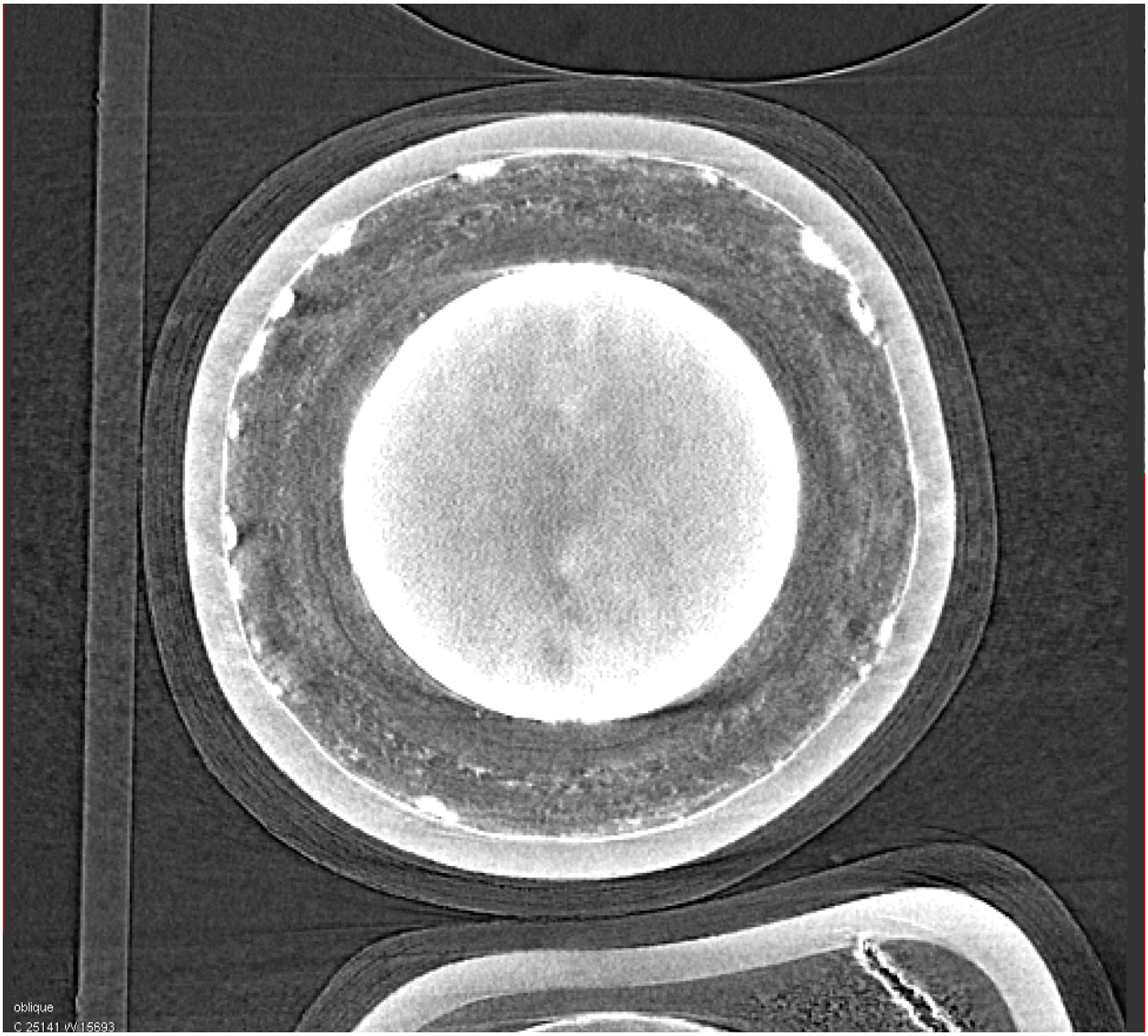
oblique
C 25141 W 15893

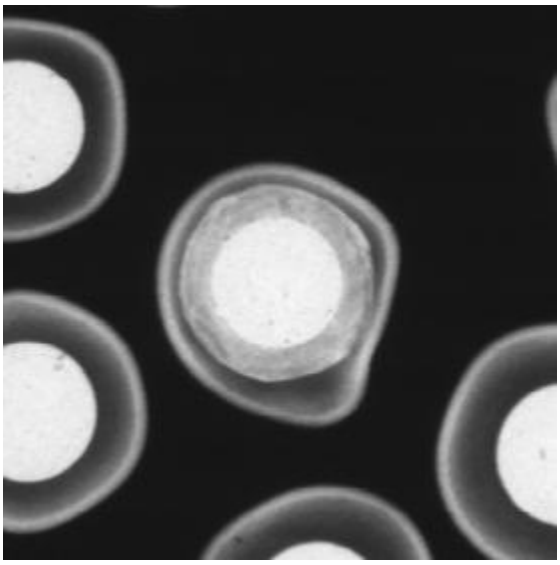

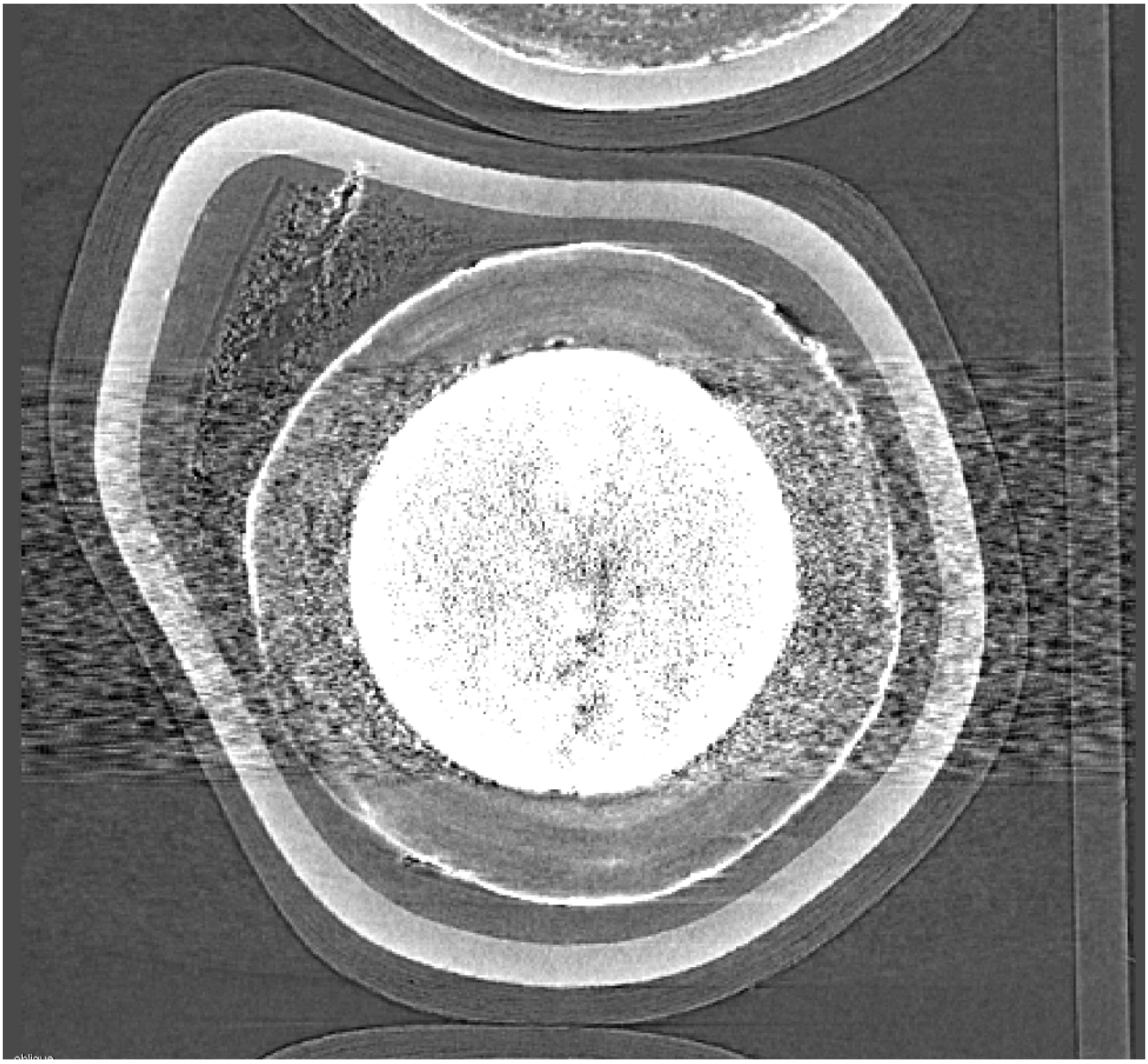

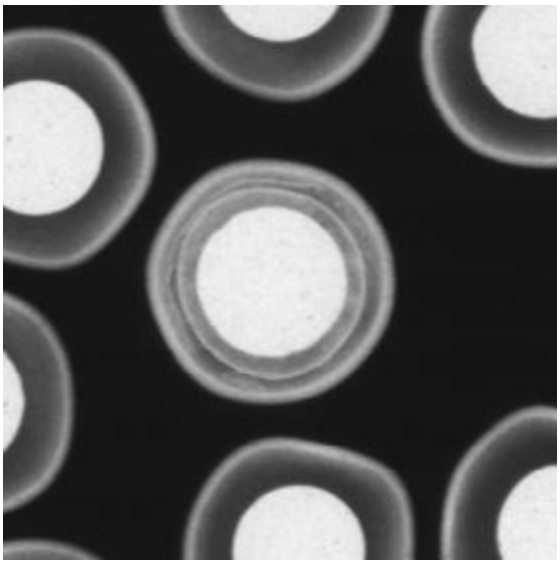

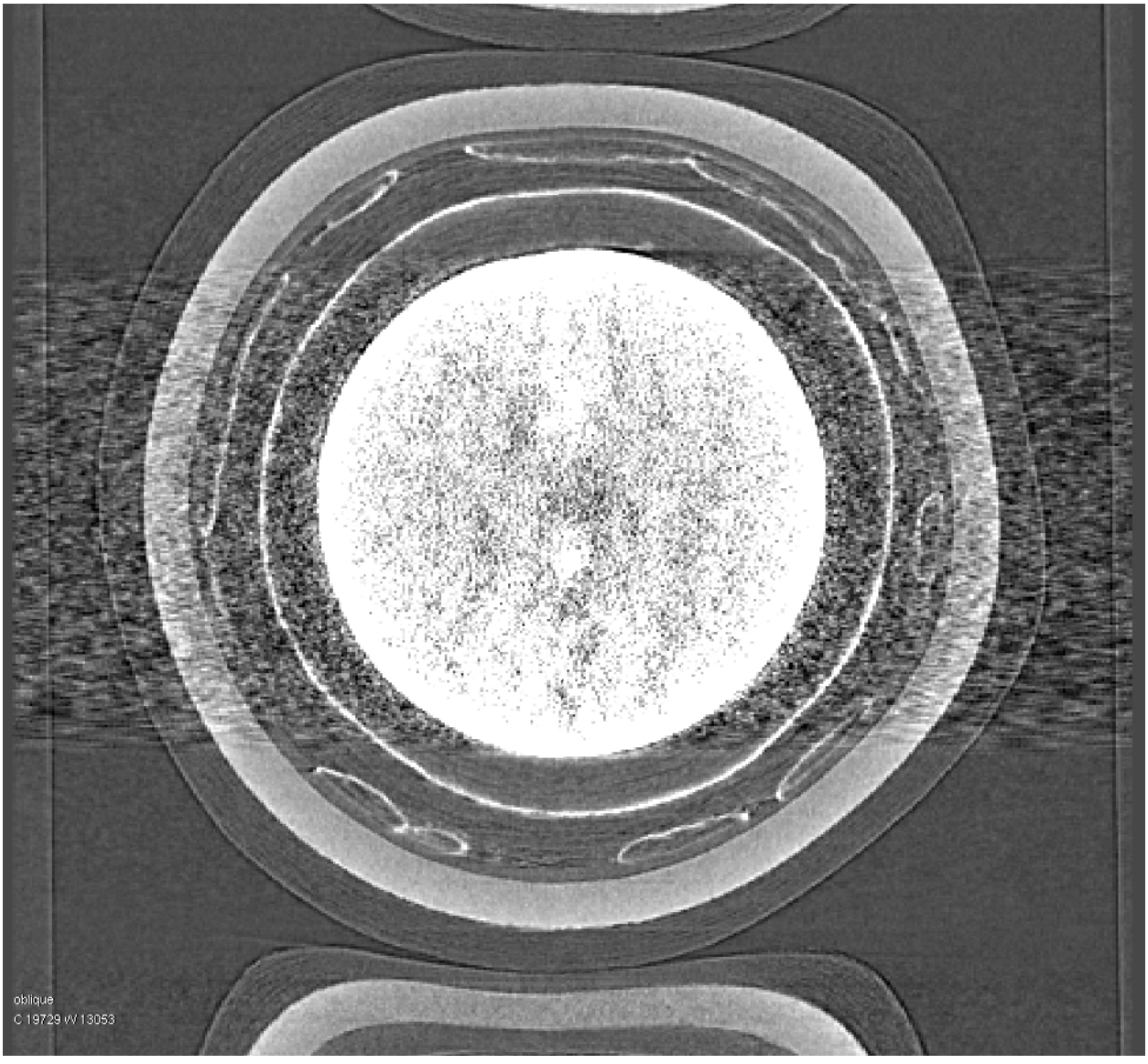
oblique
C 19729 W 13053